THE REACTIVITY OF FERRIC (HYDR)OXIDES TOWARDS DISSOLVED SULPHIDE

Dissertation zur Erlangung des Grades
Doktor der Naturwissenschaften
(Dr. rer. nat.)
an der Fakultät Biologie/Chemie/Geowissenschaften
der Universität Bayreuth

vorgelegt von

Katrin Hellige
Geb. am 25.05.1978 in Dortmund

Die Arbeiten zur vorliegenden Dissertation wurden im Zeitraum von April 2006 bis Dezember 2010 am Lehrstuhl für Hydrologie der Universität Bayreuth unter der Betreuung von Prof. Dr. Stefan Peiffer durchgeführt.

Vollständiger Abdruck der von der Fakultät für Biologie, Chemie und Geowissenschaften der Universität Bayreuth genehmigten Dissertation zur Erlangung des akademischen Grades eines Doktors in den Naturwissenschaften (Dr. rer. nat.).

Einreichung der Dissertation: 15.12.2010
Zulassung durch die Prüfungskommission: 22.12.2010
Wissenschaftliches Kolloquium: 30.05.2011

Amtierender Dekan:
Prof. Dr. Stephan Clemens

Prüfungsausschuss:
Prof. Dr. Stefan Peiffer (Erstgutachter)
Prof. Dr. Stefan Haderlein (Zweitgutachter)
Prof. Dr. Egbert Matzner (Vorsitz)
Prof. Dr. Britta Planer-Friedrich
Prof. Dr. Jürgen Senker

Abstract

Ferric (hydr)oxides are ubiquitous with different characteristics such as stability, reactivity and surface properties. They play an important role in redox reactions in many environments such as soils, marine sediments, lakes, and ground water. Under anoxic conditions, ferric (hydr)oxides are reduced by dissolved sulphide or by microorganisms. The reductive dissolution of ferric (hydr)oxides generates Fe(II) which may precipitate as iron hydroxide, adsorb to the ferric (hydr)oxide surfaces and transform the ferric (hydr)oxides into more stable minerals, or precipitate as iron sulphide. During the reductive dissolution adsorbed species like arsenic may be released from the oxide surfaces to solution. Furthermore, the generation of ferrous iron in ground water systems, their transport through the groundwater-surface water interface, and subsequent iron oxidation and precipitation contribute to the acidification of lakes or sediments as a result of both mining activities and natural processes. Alternatively, the oxidation of iron sulphides due to mining activities and natural events leads to the production of acidity and concentrations of (toxic) metals in ground and surface water. Hence, the redox reactions between dissolved sulphide and ferric (hydr)oxides are of fundamental importance for the elemental cycles of sulphur and iron and in particular for the carbon and electron flow in groundwater, soil, and lake systems. The overall chemical pathway of the reactions and their kinetics are reasonably understood. There is less knowledge on the transient stages and the electron transfer processes during the reactions which involve the formation of amorphous or disordered, as well as, nucleation of (metastable) crystalline phases at the reacting interface as a function of time. Furthermore, the interaction between dissolved sulphide and ferric (hydr)oxides can be regard as a key reaction ultimately leading to pyrite formation in both marine and freshwater sediments. However, the knowledge on the pathways and on the controlling factors of pyrite formation is still limited.

Therefore this work focused on anoxic abiotic kinetic batch and flow-through experiments with various ferric (hydr)oxides and dissolved sulphide at pH 4 and pH 7. Transmission electrode microscopy, X-ray diffraction, Mössbauer spectroscopy, and wet chemistry were used to explore the nanocrystalline products which formed over time during the reaction. Furthermore, these experiments should be contribute to the elucidation of the role of Fe^{2+} regarding the iron sulphide formation and the transformation of Fe(III) oxides.

The electron transfer reaction between dissolved sulphide and ferric (hydr)oxides and the deeper insight into the processes occurring at the ferric (hydr)oxides surfaces were investigated in chapter 2 and 3. Batch experiments with dissolved sulphide and ferrihydrite, lepidocrocite, and goethite were performed under well-defined conditions at pH 7 and at room temperature in a glove box with a special emphasis on the characterization of nanocrystalline products by TEM, XRD, and Mössbauer spectroscopy forming at different time steps over a reaction time of 14 days. The iron species such as dissolved Fe(II), Fe(II) extractable with 0.5 N HCl, and total iron were determined by wet chemistry extraction as well as the sulphur species dissolved S(-II) and S(0). The temporal evolution of the chemical species and the solid phases indicate that the reaction progress was highly dynamic.

Chapter 2 comprised the results of the reductive dissolution of lepidocrocite by dissolved sulphide. The reaction could be divided into 3 phases with (i) fast consumption of dissolved sulphide, formation of mackinawite onto the lepidocrocite surface and S(0) (0-15 min), (ii) consumption of mackinawite due to the formation of magnetite and S(0) while acid extractable Fe(II) slightly increased (15-120 min). TEM measurements revealed the occurrence of a mackinawite rim covering the lepidocrocite crystals that was separated from the lepidocrocite surface by an interfacial magnetite layer. The magnetite layer can be seen as an intermediate stage linking the two reactions: The reaction between lepidocrocite and mackinawite and the diffusion of electrons in deeper regions of the lepidocrocite bulk crystal. In the third phase of reaction S(0) and acid extractable Fe(II) decreased due to pyrite formation accompanied with traces of magnetite (2-14 days). TEM measurements indicated that mackinawite was completely dissolved and the precipitation of pyrite occurred dislocated from the lepidocrocite surface. The absence of dissolved sulphide under these conditions suggest that excess Fe(II) is involved in the formation of polysulphides which are key precursors during pyrite formation.

Chapter 3 includes the results of batch experiments with the same set-up and analysis with ferrihydrite and goethite as described in chapter 2. The objective was to investigate their transformation by Fe(II) and the formation of pyrite in sulphide-rich systems at pH 7 in regard to their reactivity kinetics, intermediate phases, and the final products. The similarities and differences between the ferric (hydr)oxides: ferrihydrite, lepidocrocite, and goethite were explored as well. Wet chemistry analysis showed the same tripartite reaction for all Fe(III) (hydr)oxides like in chapter 2. The mineral reactivity decreased in the order of ferrihydrite ~ lepidocrocite > goethite. Although the surface site concentration was different for ferrihydrite and lepidocrocite, both oxides showed similar reaction kinetics. Alternatively, lepidocrocite

and goethite had the same reaction pathway but different reaction kinetics. The FeS consisted of mackinawite for lepidocrocite and goethite, while only amorphous FeS was formed in the experimental solution of ferrihydrite. Ferrihydrite was completely reduced as identified by wet chemistry and Mössbauer spectroscopy, while the TEM measurements showed a well-developed ferrihydrite structure. After 2 weeks of reaction ferrihydrite was transformed completely via a dissolution-precipitation process into the more stable minerals: magnetite, hematite, and pyrite. This process involved redox reactions, including the partial re-oxidation of Fe(II) and reduction of S(0). The host minerals remained in the experimental solutions with lepidocrocite and goethite, and only pyrite was detected as a new mineral. Small amounts of goethite were transformed to hematite while the pyrite formation in the experimental solution with lepidocrocite was accompanied by traces of magnetite. The differences in secondary mineralization for the observed ferric (hydr)oxides depend on the amount of excess-Fe(II). The production of excess-Fe(II) differed for each mineral and decreased in the sequence ferrihydrite > lepidocrocite > goethite. As the amount of excess-Fe(II) exceeded the concentration of surface sites in each experiment, the excess-Fe(II) had to be located into the bulk phase of each oxide.

Summarized, the differences of excess-Fe(II) concentration depend on electron transfer properties and the ability of accommodation of Fe(II) within the bulk oxide of each mineral. Furthermore, the excess of Fe(II) stimulate the secondary mineralization and the pyrite formation. Whether the pyrite formation occurs via a reaction of FeS with dissolved Fe(II) or requires solid Fe(II) containing cluster is unclear.

In chapter 4, the reaction kinetic of dissolved sulphide and ferric (hydr)oxides were studied under abiotic, anoxic, and flow-through conditions at pH 4 and 7 and at room temperature. Various synthetic Fe(III) (hydr)oxides with a broad range of crystallinity and different surface and bulk properties were used in order to assess how variations in these properties influence the kinetics of chemical Fe(III) (hydr)oxide reduction. The products in solution were analyzed periodically over approximately 6 hours. The mineral reactivity decreased in the order of ferrihydrite > lepidocrocite > goethite and can be described by a second rate law. The reaction between the ferric (hydr)oxides and dissolved sulphide were faster at pH 7 compared to that at pH 4. Furthermore, these experiments showed, as well as, the batch experiments, that the formation of Fe(II) and S(0) was decoupled. In the presence of ferrihydrite and lepidocrocite the generated Fe(II) due to the reaction with dissolved sulphide adsorbed to their surfaces and was accompanied by an electron transfer which led to the formation of excess-Fe(II). These

processes seem to be accelerating the reductive dissolution of ferrihydrite and lepidocrocite by dissolved sulphide. Goethite behaved differ: the adsorption of Fe(II) onto the goethite surface occurred without an electron transfer. These Fe(II) dynamics have a profound influence of the redox potential of the reaction suspension and in turn, affect the semiconducting properties of the Fe(III) solids. Thus, the generated Fe(II) controls the reductive dissolution of various ferric (hydr)oxides by dissolved sulphide.

Zusammenfassung

Durch die Oxidation von gelöstem Fe(II), das durch Verwitterungsprozesse freigesetzt wird, sind Eisen(hydr)oxide in Böden und Sedimenten weit verbreitet. Sie besitzen unterschiedliche Eigenschaften bezogen auf Stabilität, Reaktivität und Oberflächen. Daher übernehmen sie eine wichtige Rolle bei Redoxreaktionen in vielen Umweltsystemen wie in Böden, marinen Sedimenten, Seen und Grundwasserleitern. Unter anoxischen Bedingungen werden Eisen(hydr)oxide mittels Sulfid oder Mikroorganismen reduziert und aufgelöst. Diese Reaktion generiert Fe(II), dass entweder als Eisenhydroxid gefällt wird, an der Eisen(hydr)oxid-Oberfläche adsorbiert und so das Eisen(hydr)oxid in stabilere Eisenmineralphasen transformiert oder Fe(II) reagiert mit Sulfid zu Eisensulfid. Aber auch die reverse Reaktion, die Oxidation von Eisensulfiden durch Bergbauaktivitäten oder durch natürliche Prozesse ist von großer Bedeutung, da sie zur Säureproduktion im Grund- und Oberflächenwasser beiträgt. Durch ihre hohe Oberfläche sind sie außerdem effiziente Adsorber für Schwermetalle wie Arsen, die durch die reduktive Auflösung der Eisen(hydr)oxide in Lösung gehen. Daher beeinflussen die Redoxreaktionen zwischen gelöstem Sulfid und Eisen(hydr)oxid nicht nur den Schwefel- und Eisen-Kreislauf, sondern auch den Kohlenstoff- und Elektronen-Fluss im Grundwasser, Boden und See. Die chemischen Reaktionspfade und die Kinetik dieser Reaktionen sind dabei einigermaßen verstanden, jedoch nicht die Elektronentransferprozesse, die maßgebenden Reaktionsbeeinflussenden Faktoren und die Bildung amorpher wie auch nano-kristalliner Phasen auf der Eisen(hydr)oxid-Oberfläche als Funktion der Zeit. Des Weiteren ist die Pyritbildung in Umweltsystemen, in denen Eisen, Schwefel oder FeS konstant oder periodisch abgereichert sind noch nicht vollständig verstanden.
Deshalb konzentriert sich diese Arbeit auf die Kinetik verschiedener Eisen(hydr)oxide in Gegenwart von gelöstem Sulfid unter anoxischen und abiotischen Bedingungen. Die Edukte und Produkte sowohl fester als auch gelöster Phasen werden durch TEM, Mössbauer Spektroskopie, XRD und nasschemische Analytik charakterisiert. Zudem soll die Rolle des Fe^{2+} bezüglich der Bildung von Eisensulfid und der Transformation von Fe(III) Oxiden untersucht werden.

Der Elektronentransfer zwischen gelöstem Sulfid und verschiedener Eisen(hydr)oxide und die Prozesse auf der Eisen(hydr)oxid-Oberfläche wurden in Kapitel 2 und 3 untersucht. Dazu wurden Batch-Experimente mit gelöstem Sulfid und Ferrihydrit, Lepidokrokit und Goethit

unter gut definierten Bedingungen bei pH 7 und Raumtemperatur in der Glovebox durchgeführt. Die Reaktionen wurden über einen Zeitraum von 14 Tagen untersucht. Der Schwerpunkt lag auf der Charakterisierung von nano-kristallinen Produkten, die sich zu unterschiedlichen Zeitpunkten auf der Oxidoberfläche gebildet haben. Die Charakterisierung erfolgte unter Anwendung von TEM, XRD und Mössbauer Spektroskopie. Auch wurden sowohl die Eisenspezies (gelöstes Fe(II), Säure-extrahierbares Fe(II), Fe gesamt) als auch die Schwefelspezies (gelöstes S(-II), S(0)) durch nasschemische Extraktionen bestimmt. Die zeitliche Entwicklung der chemischen Spezies und der festen Phasen zeigten, dass der Reaktionsverlauf sehr dynamisch war.

Kapitel 2 beinhaltet die Ergebnisse der reduktiven Auflösung von Lepidokrokit durch gelöstes Sulfid. Die Reaktion konnte in 3 Phasen geteilt werden mit (i) schneller Verbrauch von gelöstem Sulfid, Bildung von Mackinawit auf der Lepidokrokitoberfläche und S(0) (0-15 min), (ii) Verbrauch von Mackinawit durch die Bildung von Magnetit und S(0) während die Konzentration von HCl-extrahierbares Fe(II) nur schwach zunimmt (15-120 min). TEM Untersuchungen zeigten folgende räumliche Sequenz: Lepidokrokit, Magnetit, Mackinawit. Magnetit ist hier ein steady-state Produkt zweier Entgegengesetzter Reaktionen; zum einen die Reaktion zwischen der Lepidokrokitoberfläche und des Mackinawits und zum anderen die „Diffusion von Fe^{2+}“ (Elektronen) in tiefere Bereiche des Bulk-Kristalls. In der dritten Phase wird S(0) und HCl-extrahierbaren Fe(II) durch die Pyrit- und Magnetitbildung wieder verbraucht (2-14 Tage). TEM Analysen zeigten, dass Mackinawit vollständig in Fe und S gelöst wurde und sich Pyrit in Abwesenheit von gelöstem Sulfid gebildet hat. Vermutlich hat sich der Pyrit durch die Reaktion mit Polysulfiden und dem überschüssigem Fe(II) gebildet. Die TEM Untersuchungen zeigten außerdem, dass die Pyritbildung von der Mackinawitbildung kinetisch entkoppelt ist. Der Magnetit in der letzten Phase ist ein Beiprodukt der Pyritbildung.

Aufgrund der vorangegangenen Ergebnisse wurden in Kapitel 3 die Eisen(hydr)oxide Ferrihydrit und Goethit unter Verwendung des gleichen Set-ups und Analyse wie in Kapitel 2 beschrieben untersucht. Dabei lag der Schwerpunkt auf Ähnlichkeiten und Unterschiede bezogen auf die Reaktionsraten, der Zwischenprodukte und der Endprodukte von Ferrihydrit, Goehtit und Lepidokrokit. Die nasschemische Analyse zeigte ebenfalls eine dreigeteilte Reaktion für alle Fe(III) (hydr)Oxide wie in Kapitel 2 beschrieben. Die Mineralreaktivität verringerte sich in der Reihenfolge Ferrihydrit ~ Lepidokrokit > Goethit. Obwohl die Oberflächenkonzentration von Ferrihydrit und Lepidokrokit unterschiedlich war, zeigten sie beide eine ähnliche Reaktionskinetik während der Reaktionsweg unterschiedlich war.

Lepidokrokit und Goethit haben einen ähnlichen Reaktionsweg, aber eine unterschiedliche Reaktionskinetik. Bei Lepidokrokit und Goethit bestand FeS aus Mackinawit während sich bei Ferrihydrit nur amorphes FeS gebildet hat. Ferrihydrit wurde komplett reduziert (nasschemische Analytik und Mössbauer Spektroskopie) während TEM Analysen noch eine gut ausgebildete Ferrihydritstruktur zeigte. Nach 2 Wochen Reaktion ist Ferrihydrit komplett durch Lösungs- und Fällungsprozesse durch die stabileren Minerale Magnetit, Hämatit und Pyrit ersetzt worden. Die damit verbundenen Redoxreaktionen beinhalten die teilweise Re-Oxidation von Fe(II) und die Reduktion von S(0). Für Lepidokrokit und Goethit ist das Startmineral erhalten geblieben und nur Pyrit konnte als neues Mineral entdeckt werden. Kleine Bereiche von Goethit wurden in Hämatit transformiert während bei Lepidokrokit zwischen den Pyritkristallen auch Magnetit gefunden wurde. Die Mineralneubildung wird von der Fe(II) Bildung beeinflusst. Alle drei untersuchten Fe(III) (hydr)Oxide zeigten die Bildung von überschüssigem Fe(II), die in folgender Reihenfolge abnahm Ferrihydrit > Lepidokrokit > Goethit. Da die Konzentration von überschüssigem Fe(II) in jedem Experiment größer war als die Konzentration der Oberflächenplätze, muss das Fe(II) in die Bulk-Struktur des jeweiligen Fe(III) Oxids eingebaut worden sein.
Die überschüssige Fe(II) Bildung ist dabei abhängig von der Mineralogie der jeweiligen Eisenoxidphase, genauer gesagt von den Elektronentransfereigenschaften und der Fähigkeit Fe(II) in die Bulk-Phase des Oxids einzubauen. Diese Unterschiede in der Fe(II) Konzentration, wie auch die Reaktivität der einzelnen Eisenoxidphasen können die Unterschiede in der Mineralneubildung erklären. Außerdem scheint es, dass die überschüssige Fe(II) Bildung die Pyritbildung stimuliert.

Im vierten Kapitel wurde die Kinetik von gelöstem Sulfid mit Eisen(hydr)oxiden im Durchfluss unter anoxischen und abiotischen Bedingungen bei pH 4 und 7 und bei Raumtemperatur untersucht. Um die Faktoren, die die Kinetik beeinflussen aufzudecken, wurden verschiedene Fe(III) (hydr)Oxide unterschiedlicher Kristallinität und (Oberflächen-) Eigenschaften verwendet. Die Eisen- und Schwefel-Spezies in der Reaktionslösung wurden periodisch über 6 Stunden gemessen. Bei pH 7 verlief die Reduktion der Fe(III) Minerale schneller als bei pH 4 und die Mineralreaktivität nimmt in folgender Reihenfolge ab: Ferrihydrit > Goethit > Lepidokrokit. Die Durchflussexperimente zeigten ebenfalls, dass die Bildung von Fe(II) und S(0) voneinander entkoppelt war. In Gegenwart von Ferrihydrit und Lepidokrokit adsorbiert das durch die Reaktion mit gelöstem Sulfid gebildete Fe(II) an dessen Oberfläche. Durch die Interaktion von Fe(II) mit dem strukturellen Fe(III) wurde

überschüssiges Fe(II) gebildet. Dieser Prozess scheint die reduktive Auflösung von Ferrihydrit und Lepidokrokit durch Sulfid zu beschleunigen. Goethit verhielt sich anders; das adsorbierte Fe(II) auf der Goethitoberfläche reagierte nicht mit der Fe(III) Phase. Diese Fe(II) Dynamik beeinflusst das Redoxpotential der Reaktionssuspension und damit auch die halbleitenden Eigenschaften der Fe(III) Phasen. Die reduktive Auflösung der verschiedenen Eisen(hydr)oxide in Gegenwart von Sulfid wird maßgeblich von dem gebildeten Fe(II) kontrolliert.

Table of Contents

List of Figures

List of Tables

List of Abbreviations

A	Specific surface area
BET	Developed by Bunauer, Emmett and Teller
C	Celsius
$CaCl_2$	Calcium chloride
CoKα	Cobalt potassium radiation
Fe(II)	Ferrous iron
$Fe(II)_{diss}$	Dissolved ferrous iron
$Fe(II)_{HCl}$	Acid extractable ferrous iron
Fe(III)	Ferric iron
Fe_{TOT}	Total iron
$Fe(OH)_3$	Ferrihydrite
$FeS_{amorphous}$	Amorphous iron(II) monosulfide
FeS_{aq}	Iron(II) monosulfide cluster
FeS_m	Mackinawite
FeS_2	Pyrite
Fe_2O_3	Hematite
Fe_3O_4	Magnetite
H^+	Hydrogen, proton
HCl	Hydrochloric acid
HPLC	High performance liquid chromatography
HRTEM	High resolution transmission electron microscopy
HS^-	Hydrogen sulphide anion
H_2S	Hydrogen sulphide
K	Kelvin
k_{intr}	Intrinsic rate constant
$k_{obs\_Fe(II)}$	Observed rate constant for the reductive dissolution of Fe(II)
k_{obs_H2S}	Observed rate constant for the oxidation of sulphide
kV	kilovolt
NaCl	Sodium chloride
$NaNO_3$	Sodium nitrate
NaOH	Sodium hydroxide
N_2	Nitrogen
OH^-	Hydroxide

pH_{pzc}	Point of zero charge
PIPES	Piperazine-N,N'-bis{2-ethanesulfonic acid},dipotassium salt
S(-II)	Sulphide
$S(-II)_{diss}$	Dissolved sulphide
SO_4^{2-}	Sulphate
S_n^{2-}	Polysulphides
S(0)	Elemental sulphur
SEM	Scanning electron microscopy
STEM-EDX	Scanning transmission electron microscopy-energy dispersive X-ray spectroscopy
TEM	Transmission electron microscopy
TEM-EDX	Transmission electron microscopy- energy dispersive X-ray spectroscopy
TOC	Total organic carbon
XRD	X-ray diffraction
α-FeOOH	Goethite
γ-FeOOH	Lepidocrocite

1. General Introduction

1.1. Ferric (hydr)oxides

Ferric (hydr)oxides are ubiquitous and important components of rocks and soils with different characteristics such as stability, reactivity and surface properties (Cornell and Schwertmann, 1996). Such variations in mineral properties result in a continuum of reactivity. The most widespread ferric (hydr)oxides are goethite, lepidocrocite, ferrihydrite, and green rust while the dominant iron oxides are hematite and the mixed-valence iron mineral magnetite. Ferric (hydr)oxides play an important role in abiotic and biotic reactions such as precipitation, sorption in soils, and redox reactions. They are important terminal electron acceptors for the oxidation of organic matter in aquifers (Jacobsen and Postma, 1999), soils and marine sediments (Canfield et al., 1992; Yao and Millero, 1996). Due to their high surface area, iron oxides are able to scavenge reactive species by adsorption and release them again to the overlying water if the ferric (hydr)oxides are dissolved by reductive processes. The dissolution of ferric (hydr)oxides is a surface controlled reaction (Stumm and Sulzberger, 1992) and may be enhanced or inhibited by substances adsorbed to the surface (Biber et al., 1994). Hence, the fate of heavy metals (arsenic), organics, and ligands are strongly associated with a lot of iron (Pedersen et al., 2005). This is one hypothesis for the serious problems with arsenic contaminated ground waters in many areas of the world. Thus, the development of a reduced zone may have significant consequences for the mobility of toxic organic and inorganic chemicals.

In sedimentary environments under anoxic and reducing conditions, ferric (hydr)oxides often may be reduced by microorganisms using organic matter as substrate (Hansel et al., 2004; Lovley et al., 1991; Thamdrup, 2000). Although, in marine environments the most important electron donor for the iron reduction is dissolved sulphide (Canfield et al., 1992; Yao and Millero, 1996). Both reactions, the reduction of ferric (hydr)oxides by microorganisms and by dissolved sulphide generate Fe(II) may precipitate as iron hydroxide, adsorb to the ferric (hydr)oxide surfaces and transform the oxide into more stable minerals, or precipitate as iron sulfide depending on pH (Hansel et al., 2005; Poulton, 2003).

The generation of ferrous iron in anoxic groundwater, their transport through the groundwater-surface water interface, and subsequent iron oxidation and precipitation

contribute to the acidification of lakes or sediments as a result of mining activities (i.e. acid-mine drainage) or as a natural process (i.e. acid-sulfate soils) (Blodau, 2006; Burton et al., 2008; Peine et al., 2000). Such environments are characterized by high amounts of ferric iron and sulphate and due to the low pH by low primary production (Peine et al., 2000). The oxidation of pyrite takes place when the mineral is exposed to water and air (eq. 1).

$$FeS_2 + 3.5\ O_2 + H_2O \rightarrow Fe^{2+} + 2\ SO_4^{2-} + 2\ H^+ \quad (1)$$

The process of pyrite oxidation is complex and involves both chemical and biological mechanisms, while chemical oxidation is fairly slow (Blodau, 2006) and can decrease lake water pH to values as low as pH 2 (Geller et al., 1998).
The ferrous iron from the pyrite oxidation may be subsequently oxidized and precipitated as ferric (hydr)oxides (eq. 2 and 3).

$$Fe^{2+} + 0.25\ O_2 + H^+ \rightarrow Fe^{3+} + 0.5\ H_2O \quad (2)$$

$$Fe^{3+} + 3\ H_2O \leftrightarrow Fe(OH)_3 + 3\ H^+ \quad (3)$$

During the Fe(II) oxidation and their precipitation as ferric (hydr)oxide, protons are released to solution, which leads to acidification of the sediments (eq. 1-3) (Peine et al., 2000). By contrast, during the microbial sulphate reduction (eq. 4) and the further reduction of ferric (hydr)oxides by sulphide (eq. 5) or by microorganisms (eq. 6), protons are consumed. Due to these transformations and precipitations, the alkalinity and pH of the groundwater changed (eq. 1-6).

$$SO_4^{2-} + 2\ <CH_2O> + 2\ H^+ \rightarrow H_2S + 2\ CO_2 + 2\ H_2O \quad (4)$$

$$FeOOH + H_2S + 4\ H^+ \rightarrow Fe^{2+} + S° + 4\ H_2O \quad (5)$$

$$4\ FeOOH + <CH_2O> + 8\ H^+ \rightarrow 4\ Fe^{2+} + CO_2 + 7\ H_2O \quad (6)$$

The strong dependence of the reaction rates of surface-bound S(-II) and/or Fe(II) on the chemical composition of iron-containing minerals indicates that natural abiotic transformation reactions involving such species in the field may vary strongly with (bio)geochemical conditions (Elsner et al., 2004). Therefore, ferric (hydr)oxides have a profound influence on the water chemistry and it is important to elucidate all feasible pathways for ferric (hydr)oxides in natural environments, as well as, their influencing factors.

1.2. Surface complexation model

Many of previous investigations have been focused on the reaction of ferric (hydr)oxides and demonstrated that the reactivity of ferric (hydr)oxides are controlled by sulphide concentration and oxide surface area (Dos Santos Afonso and Stumm, 1992; Peiffer et al., 1992; Poulton et al., 2004). This reaction can be described by the following reaction sequence (Dos Santos Afonso and Stumm, 1992):

(i) Surface complex formation:

$$>Fe^{III}OH + HS^- \underset{k_{-1}}{\overset{k_1}{\leftrightarrow}} >Fe^{III}S^- + H_2O \quad (7)$$

(ii) Electron transfer:

$$>Fe^{III}S^- \underset{k_{-et}}{\overset{k_{et}}{\leftrightarrow}} >Fe^{II}S \quad (8)$$

(iii) Release of the oxidized product:

$$>Fe^{II}S + H_2O \underset{k_{-2}}{\overset{k_2}{\leftrightarrow}} >Fe^{II}OH_2^+ + S^{\bullet -} \quad (9)$$

(iiii) Detachment of Fe(II):

$$>Fe^{II}OH_2^+ \xrightarrow{k_3} \text{new surface site} + Fe^{2+} \quad (10)$$

The adsorption of dissolved sulphide to the iron oxide surface occurs rapidly due to the formation of inner-sphere complexes $>FeS^-$ and >FeSH with the iron oxide surfaces (eq. 7) (Luther, 1990). The electrons are transferred at the iron oxide surface between the initially formed inner-sphere complexes and the bulk Fe(III) (eq. 8) (Dos Santos Afonso and Stumm, 1992). The oxidized $S^{\bullet -}$ is then released to solution to reduce an additional Fe(III) ion and form a higher oxidation state sulphur species such as S(0) (eq. 9). Subsequently the newly formed Fe^{2+} at the oxide surface is released to solution (eq. 10). The limiting step is the

detachment of Fe(II) from the oxide surface, which is necessary to further oxidation of dissolved sulphide.

But during the reductive dissolution of ferric (hydr)oxides by sulphide at pH 7 a large proportion of reductive iron remains at the ferric (hydr)oxides surfaces or is bound to the solid phase due to the formation of FeS and mixed-valence iron oxides (Handler et al., 2009; Jeon et al., 2003; Poulton et al., 2004).

1.3. The reaction of ferric (hydr)oxides with H_2S

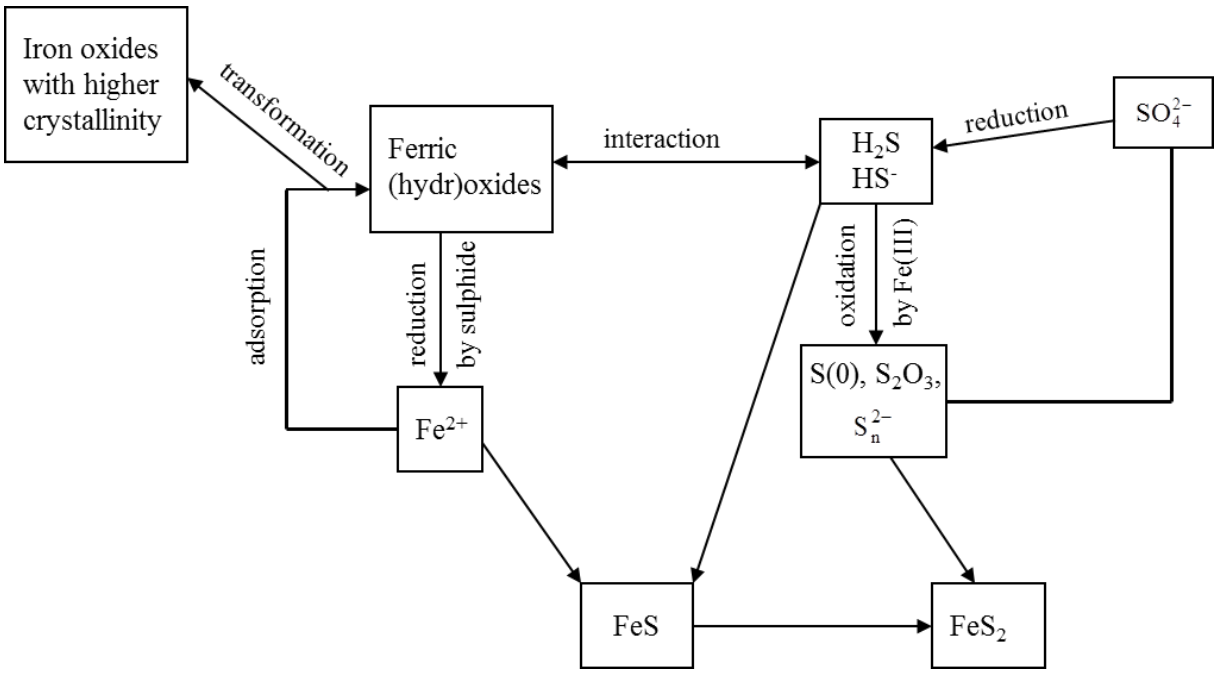

Fig. 1.1. The major pathways for the reaction of ferric (hydr)oxides with dissolved sulphide.

The interaction of H_2S with reactive iron plays a prominent role in natural environments such as marine sediments, freshwater sediments, lakes, soils, and aquifers (Fig. 1.1) (Canfield et al., 1992; Jacobsen and Postma, 1999; Yao and Millero, 1996). During the microbiological oxidation of organic matter, dissolved sulphate may reduce to H_2S in the absence of oxygen (Canfield et al., 1992). H_2S may react further with reactive sedimentary iron and can be oxidized to different sulphur species such as: elemental sulphur, polysulphides, thiosulphate, or sulphate depending on pH (Pyzik and Sommer, 1981). The reduction of ferric (hydr)oxides generates Fe^{2+} in which the nature of the species depends on pH. At circumneutral pH, Fe^{2+} is either bound to the solid phase FeS, which may be further converted to FeS_2 by sulphur species such as S(0) or polysulphides (Rickard, 1974; Rickard, 1975; Rickard and Morse, 2005) or Fe^{2+} is associated to the ferric (hydr)oxides surface which may lead to their

transformation into more stable Fe(III) oxides (Hansel et al., 2005; Liu et al., 2008; Pedersen et al., 2005). The formation of FeS or FeS_2 trap dissolved sulphide and prevent its further oxidation by Fe(III). Thus, the formed Fe(II) and its further reaction to iron sulfides or/and its interaction with the oxide surface have a profound influence on the reaction of ferric (hydr)oxides and dissolved sulphide at circumneutral pH. At acidic pH, the ferric (hydr)oxides surface area is charged positive and only negative charged species can be sorbed.

Several studies in the past years have been focused on the mechanism and kinetics of the reductive dissolution of ferric (hydr)oxides (Larsen and Postma, 2001; Peiffer et al., 1992; Peiffer and Gade, 2007; Postma, 1993; Poulton et al., 2004; Pyzik and Sommer, 1981; Rickard, 1974; Roden, 2003). The reaction mechanism based on the formation of surface complexes (see 1.2.) depending on pH (Dos Santos Afonso and Stumm, 1992) while the reaction rates of ferric (hydr)oxides are influenced by the concentration of dissolved sulphide and solid Fe(III) as well (Dos Santos Afonso and Stumm, 1992; Peiffer et al., 1992; Poulton, 2003; Poulton et al., 2004; Pyzik and Sommer, 1981). Other investigators suggested that not solely the surface properties of the ferric (hydr)oxides control their reductive dissolution by dissolved sulphide, but rather depends on crystal properties (Larsen and Postma, 2001; Postma, 1993; Poulton et al., 2004). Ferric (hydr)oxides with a lower degree of crystal order such as ferrihydrite and lepidocrocite, are more reactive toward dissolved sulphide than more ordered minerals like magnetite, goethite and hematite proposed by Poulton et al. (2004). This assumption implies that the reactivity of the various ferric (hydr)oxides depends on the mineral type.

In nature, the reactivity of ferric (hydr)oxides may be effected by impurities substituted within the mineral structure (Poulton et al., 2004). Poulton et al. (2004) demonstrated that the reactivity for an Al-substituted lepidocrocite decreases with increasing substitution. And also in the presence of sulphate, the reductive dissolution of ferric (hydr)oxides is inhibited and the reaction rates are lower than in the absence of sulphate (Peiffer and Gade, 2007). So, a significant decrease of the reaction rates under acid mine drainage conditions due to the high sulphate concentrations is expected. Furthermore, the comparison of ferric (hydr)oxides reduction rates in nature and the laboratory shows that for natural samples the rate decrease faster than for synthetic ferrihydrite due to the much greater heterogeneity of the ferric (hydr)oxides in natural sediments (Postma, 1993). Comparison of chemical and biotic reduction of ferric (hydr)oxides showed that the abiotic reduction is apparently strongly

influenced by morphologic characteristic while the biotic reduction dependence on the surface area of each mineral regardless of the degree of crystal order (Roden, 2003).

There are many variables which influenced the interaction of ferric (hydr)oxides with dissolved sulphide such as surface properties, dissolved sulphide concentration, crystal properties, adsorbed ions, pH etc. The exact dependence of Fe(III) reduction kinetics on mineral properties including the dynamics of Fe^{2+} and its various species is still discussed in literature. Furthermore, it appears that our understanding of the reaction steps following the electron transfer reaction between sulphide and ferric (hydr)oxides is still incomplete and requires a deeper insight into the processes occurring at the ferric (hydr)oxide surfaces itself.

1.4. Formation of pyrite

The direct homogenous nucleation of pyrite from solution may play only a minor role in low-temperature iron disulfide formation (e.g., salt marshes, epithermal ore deposits) (Schoonen and Banes, 1991a). Hence, here only the pathways of pyrite formation via a FeS precursor are listed.

Iron(II) monosulfides are formed during the reaction of ferrous iron and sulphide in which $FeSH^+$ and $Fe(SH)_2$ act as kinetic intermediates (Rickard et al., 1995). Rickard et al. (1995) proposed the bisulfide pathway for the formation of iron(II) monosulfides for neutral and alkaline mediums and when the sulphide concentration is higher than 10^{-3} M. This pathway includes the formation of $FeSH^+$ complexes and solid $Fe(SH)_2$ and follows the equations:

$$Fe^{2+} + 2\ HS^- \rightarrow Fe(HS)_2 \quad (11)$$

$$Fe(SH)_2 \rightarrow FeS + H_2S \quad (12)$$

The iron(II) monosulphides may further react with sulphur species to pyrite. This conversion is promoted by the oxidation of FeS or of the reduced aqueous sulphur species (Benning L. G. et al., 2000). There are generally three pathways of pyrite formation discussed in the literature, which are (Schoonen, 2004):

$$2\ FeS_{(s)} + 2H^+ \rightarrow FeS_{2(s)} + Fe^{2+} + H_{2(g)} \quad (13)$$

$$FeS_{(s)} + H_2S_{(aq)} \rightarrow FeS_2 + H_2 \quad (14)$$

$$FeS_{(s)} + S(0)_{(s)} \rightarrow FeS_2 \quad (15)$$

All three pathways are dissolution-reprecipitation reactions. The conversion of FeS to FeS_2 can takes place via iron loss (eq. 13), via H_2S (eq. 14), and via S(0) (eq. 15). Usually, intermediate sulphur species are necessary for the oxidation of mackinawite but they are not always present in natural environments (Furukawa and Barnes, 1995). Thus, in the absence of sulphur species the reaction may proceed by iron loss (eq. 13). The conversion of FeS to FeS_2 via Fe^{2+} loss proceeds at an insignificant rate for temperatures below 100°C (Schoonen and Barnes, 1991b).

Benning et al. (2000) conducted experiments below 100°C in reducing sulphide solutions and showed that mackinawite was stable as long as no reactant other than H_2S is provided and suggested that the transformation of iron(II) monosulphide to iron(II) disulphide requires an oxidant other than H_2S or HS^-. Their ageing experiments revealed that pyrite formed at very slow rates in the presence of H_2S or HS^- (eq. 14).

Rickard et al. (1995) proposed the polysulphide pathway for the formation of pyrite which involved the dissolution of FeS, followed by the reaction of Fe(II) and sulphur species resulting in pyrite as the final product. Other investigators prefer the formation of pyrite by S(0) which includes the dissolution of FeS as well (eq. 15) (Wang and Morse, 1995). Though, Schoonen et al. (2004) suggested, that elemental sulphur (eq. 15) is not the true reactant in this process. The hydrolysis of the sulphur or reactions of S° with H_2S creates polysulphide species, which are more likely to be reactants (Luther, 1991; Schoonen and Barnes, 1991b). Schoonen and Barnes (1991b) proposed that the formation of FeS_2 proceeds only at a significant rate if intermediate sulphur species like polysulphides are present. Wilkin and Barnes (1996) identified, that only polysulfide species or colloidal elemental sulphur solutions generated pyrite. The polysulfide pathway is the most prominent pathway which is discussed in the literature (Luther, 1991; Rickard et al., 1995; Wilkin and Barnes, 1996).

The conversion of FeS to FeS_2 via polysulphides can be described by the following reaction sequence where $[FeS\text{-}S_n]^{2-}$ is a reaction intermediate (Luther, 1991; Rickard and Morse, 2005):

$$FeS_{(aq)} + S_n^{2-} \rightarrow [FeS\text{-}S_n]^{2-} \quad (16)$$

$$[FeS\text{-}S_n]^{2-} \rightarrow FeS_2 + S_{n-1}^{2-} \quad (17)$$

$$S(0) + S_{n-1}^{2-} \rightarrow S_n^{2-} \quad (18)$$

which yields in total

$$FeS_{(s)} + S(0)_{(s)} \rightarrow FeS_2 \quad (19)$$

Previous studies showed that FeS clusters ($FeS_{(aq)}$) are a key component in the pyrite formation (Rickard and Morse, 2005) and that the pyrite formation is inhibited if the formation of $FeS_{(aq)}$ is suppressed (Rickard et al., 2001).
$FeS_{(aq)}$ which were formed by the dissolution of mackinawite (FeS_m), followed by further oxidation to FeS_2 (Luther, 1991; Rickard, 2006; Rickard et al., 2001):

$$FeS_m \rightarrow FeS_{(aq)} \quad (20)$$

$FeS_{(aq)}$ structure is similar to that of mackinawite while their stoichiometry range from Fe_2S_2 to $Fe_{150}S_{150}$ (Rickard and Morse, 2005). Their formation from FeS_m is pH dependent and the $FeS_{(aq)}$ is not protonated (Rickard, 2006). Rickard and Morse (2005) pointed out that a solution consists only of $FeS_{(aq)}$ is clear, not black. Furthermore, iron and sulphur are transported via $FeS_{(aq)}$ to the site of pyrite formation (Rickard and Morse, 2005).
Schoonen and Barnes (1991a) indicated that pyrite may be grown directly from solution when the solution is supersaturated with respect to pyrite due to the dissolution of mackinawite (FeS). Hence, mackinawite is not a direct precursor to pyrite, but pyrite is formed from dissolved phases which may be sourced in mackinawite (Rickard and Morse, 2005).

But in many natural environments (e.g. tidal inundation of coastal plains, movement of the capillary fringe in ground waters) pyrite formation occurs even in the absence of dissolved sulphide. The pyrite formation mechanisms in these environments are still unknown.

1.5. Objectives of the dissertation

The interaction of dissolved sulphide and ferric (hydr)oxides occurs in groundwater systems, soils, and lakes and may exert a major role for the sulphur and iron cycle and in particular for the carbon and electron flow. The extent of the reaction depends on mineral reactivity and is controlled by the formation of surface complexes. To elucidate these processes, it is of importance to understand the reactions occurring at the mineral-sulphide interfaces. The overall goal of this project is to established a generalized kinetic model for the abiotic anaerobic H_2S oxidation by ferric (hydr)oxides in the pH range of 4 to 7. The specific

objectives here are (i) determination of the reaction rate coefficients of various iron (hydr)oxides toward dissolved sulphide with regard to different pH's, (ii) identify the processes occurring at the ferric (hydr)oxide surfaces itself by chemical analysis, spectroscopy and microscopy measurements, (iii) elucidate the role of Fe^{2+} during the reaction, and (iv) improve our understanding of the pathway of pyrite formation.

The reaction progress of the reductive dissolution of ferric (hydr)oxides towards dissolved sulphide is highly dynamic. Hence, the temporal development of chemical species (Study 1, 2, and 3) is observed while the formation of several phases is determined by microscopic and spectroscopic measurements (Study 1 and 2). Different abiotic and anoxic experiments are conducted under well-defined conditions in the laboratory, always with an excess of ferric (hydr)oxides regarding dissolved sulphide. The following ferric (hydr)oxides ferrihydrite, lepidocrocite and goethite were prepared after Schwertmann and Cornell (2000) for each experiment. Adjacent to the synthesized minerals, also the commercial Fe(III) oxides lepidocrocite (Bayferrox 943) and goethite (Bayferrox 920 Z) purchased by Lanxess Germany GmbH, Leverkusen were used. The properties of these synthesized and commercial ferric (hydr)oxides were characterized by several techniques such as BET (Brunner, Emmett, Teller) gas adsorption with N_2, X-ray diffraction (XRD), scanning electron microscopy (SEM), transmission electron microscopy (TEM), titration experiments (point of zero charge), and total organic carbon (TOC) measurements (Buchholz, 2009).

Chapter 2 and 3 (Study 1 and 2). A valuable insight into the product formation may help to balance electron flow and explain the reactivity patterns from the flow-through experiments (study 3). Therefore the reaction between ferric (hydr)oxides and dissolved sulphide is studied in batch experiments at pH 7 in a glove box by a combination of chemical, microscopic, and spectroscopic analysis. TEM, XRD, Mössbauer spectroscopy, and wet chemistry extraction are used to explore the nanocrystalline phases and reactive sites at different time steps at the ferric (hydr)oxide surfaces. Iron(II) monosulphides and iron(II) disulphides are formed during the reductive dissolution of ferric (hydr)oxides by dissolved sulphide. But due to the interactions of Fe^{2+} with the Fe(III) oxide surfaces, the ferric (hydr)oxides are transformed into higher crystalline Fe(III) oxides as well. These reactions are coexistent and interact with each other. The similarities and differences between the various ferric (hydr)oxides are explored as well. Contrary to previous work (Dos Santos Afonso and Stumm, 1992; Peiffer et al., 1992; Poulton et al., 2004) which studied only the initial (<5h) phases of the reaction, we

have extended the reaction time to 14 days to deepen our understanding into the dynamics of Fe^{2+} and its various species.

Chapter 4 (Study 3). Fluidized bed reactor experiments are conducted to investigated the initial rates of the interaction between dissolved sulphide and ferric (hydr)oxides under flow-through conditions. The overall aim is to get a dataset to obtain a generalized surface speciation model for the reaction of H_2S with ferric (hydr)oxides. The experiments are prepared at pH 4 and 7 at room temperature with an excess of ferric (hydr)oxides in regard to dissolved sulphide. Various synthetic Fe(III) (hydr)oxides with a broad range of crystallinity and different properties are used in order to assess how variations in these properties would be expected to influence the kinetics of chemical Fe(III) oxides reduction. Therefore the products in solution are determined periodically.
The experimental oxidation rate of H_2S normalized to the surface area and with respect to the initial dissolved sulphide concentration follows a second order rate law and can be derived as

$$R_{obs} = \frac{dc(H_2S)}{dt} = k_{obs}\, c(H_2S)\, A \qquad (21)$$

where R_{obs} is the observed oxidation rate of H_2S (mol L^{-1} min^{-1}), k_{obs} is the rate constant of the oxidation of H_2S (L m^{-2} min^{-1}), $c(H_2S)$ is the initial concentration of dissolved sulphide (mol L^{-1}), and A the surface area concentration of ferric (hydr)oxide added (m^2 L^{-1}).

1.7. References

Benning L. G., Wilkin R. T. and Barnes H. L., 2000. Reaction pathways in the Fe-S system below 100°C. *Chemical Geology*, **167**: 25-51.

Biber, M.V., Afonso, M.D. and Stumm, W., 1994. The Coordination Chemistry of Weathering .4. Inhibition of the Dissolution of Oxide Minerals. *Geochimica Et Cosmochimica Acta*, **58(9)**: 1999-2010.

Blodau, C., 2006. A review of acidity generation and consumption in acidic coal mine lakes and their watersheds. *Science of the Total Environment*, **369(1-3)**: 307-332.

Buchholz, A., 2009. *Redox reactions and phase transformation processes at iron mineral surfaces studied by compound specific isotope analysis.* Dissertation Thesis, Eberhard Karls Universität Tübingen, Tübingen, 145 pp.

Burton, E.D., Bush, R.T., Sullivan, L.A. and Mitchell, D.R.G., 2008. Schwertmannite transformation to goethite via the Fe(II) pathway: Reaction rates and implications for iron-sulfide formation. *Geochimica Et Cosmochimica Acta*, **72(18)**: 4551-4564.

Canfield, D.E., Raiswell, R. and Bottrell, S., 1992. The reactivity of sedimentary iron minerals toward sulphide. *American Journal of Science*, **292**: 659-683.

Cornell, R.M. and Schwertmann, U., 1996. *The iron oxides: Structure, Properties, Reactions, Occurence and Uses.* Wiley-VCH Verlag GmbH, Weinheim, New York, Basel, Cambridge, Tokyo, 573 pp.

Dos Santos Afonso, M. and Stumm, W., 1992. Reductive Dissolution of iron(III) (hydr)oxides by hydrogen sulfide. *Langmuir*, **8**: 1671-1675.

Elsner, M., Schwarzenbach, R.P. and Haderlein, S.B., 2004. Reactivity of Fe(II)-bearing minerals toward reductive transformation of organic contaminants. *Environmental Science & Technology*, **38(3)**: 799-807.

Furukawa, Y. and Barnes, H.L., 1995. *Reactions forming pyrite from precipitated amorphous ferrous sulfide.* In: M.A. Vairavamurthy and M.A.A. Schoonen (Editors), Geochemical Transformations of Sedimentary Sulfur. Acs Symposium Series. Amer Chemical Soc, Washington, pp. 194-205.

Geller, W., Klapper, H. and Schultze, M., 1998. *Natural and antropogenic sulfuric acidification of lakes.* In: W. Geller, H. Klapper and W. Salomons (Editors), Acidic Mining Lakes. Springer, pp. 3-14.

Handler, R.M., Beard, B.L., Johnson, C.M. and Scherer, M.M., 2009. Atom Exchange between Aqueous Fe(II) and Goethite: An Fe Isotope Tracer Study. *Environmental Science & Technology*, **43(4)**: 1102-1107.

Hansel, C.M., Benner, S.G., Nico, P. and Fendorf, S., 2004. Structural constraints of ferric (hydr)oxides on dissimilatory iron reduction and the fate of Fe(II). *Geochim. Cosmochim. Acta*, **68(15)**: 3217-3229.

Hansel, C.M., Benner, S.G. and Fendorf, S., 2005. Competing Fe(II)-induced mineralization pathways of ferrihydrite. *Environ. Sci. Technol.*, **39**: 7147-7153.

Jacobsen, R. and Postma, D., 1999. Redox zoning, rates of sulfate reduction and interactions with Fe-reduction and methanogenesis in a shallow sandy aquifer, Romo, Denmark. *Geochim. Cosmochim. Acta*, **63(1)**: 137-151.

Jeon, B.H., Dempsey, B.A. and Burgos, W.D., 2003. Kinetics and Mechanisms for Reactions of Fe(II) with Iron (III) Oxides. *Envion. Sci. Technol.*, **37**: 3309-3315.

Larsen, O. and Postma, D., 2001. Kinetics of reductive bulk dissolution of lepidocrocite, ferrihydrite, and goethite. *Geochimica Et Cosmochimica Acta*, **65(9)**: 1367-1379.

Liu, H., Guo, H., Li, P. and Wei, Y., 2008. The transformation of ferrihydrite in the presence of trace Fe(II): The effect of the anionic media. *Journal of Solid State Chemistry*, **181**: 2666-2671.

Lovley, D.R., Phillips, E.J.P. and Lonergan, D.J., 1991. Enzymatic Versus Nonenzymatic Mechanisms for Fe(III) Reduction in Aquatic Sediments. *Environmental Science & Technology*, **25(6)**: 1062-1067.

Luther, G.W.I., 1990. *The frontier-molecular-orbital theory approach in geochemical processes.* In: Stumm W. (Editor), Aquatic Chemical Kinetics: Reaction Rates of Processes in Natural Waters, pp. 173-198.

Luther, I.G.W., 1991. Pyrite synthesis via polysulfide compounds. *Geochemica et Cosmochemica Acta*, **55**: 2839-2849.

Pedersen, H.D., Postma, D., Jakobsen, R. and Larsen, O., 2005. Fast transformation of iron oxyhydroxides by the catalytic action of aqueous Fe(II). *Geochimica Et Cosmochimica Acta*, **69(16)**: 3967-3977.

Peiffer, S., Dos Santos Afonso, M., Wehrli, B. and Gächter, R., 1992. Kinetics and mechanism of the reaction of H_2S with lepidocrocite. *Environ. Sci. Technol.*, **26(12)**: 2408-2413.

Peiffer, S. and Gade, W., 2007. Reactivity of ferric oxides toward H_2S at low pH *Environ. Sci. Technol.*, **41**: 3159-3164.

Peine, A., Küsel, K., Tritschler, A. and Peiffer, S., 2000. Electron flow in an iron-rich acidic sediment - evidence for an acidity-driven iron cycle. *Limnol. Oceanogr.*, **45(5)**: 1077-1087.

Postma, D., 1993. The Reactivity of Iron-Oxides in Sediments - a Kinetic Approach. *Geochimica Et Cosmochimica Acta*, **57(21-22)**: 5027-5034.

Poulton, S.W., 2003. Sulfide oxidation and iron dissolution kinetics during the reaction of dissolved sulfide with ferrihydrite *Chemical Geology*, **202**: 79-94.

Poulton, S.W., Krom, D.M. and Raiswell, R., 2004. A revised scheme for the reactivity of iron (oxyhydr)oxide minerals towards dissolved sulfide. *Geochim. Cosmochim. Acta*, **68(18)**: 3703-3715.

Pyzik, A.J. and Sommer, S.E., 1981. Sedimentary iron monosulphides: kinetics and mechanism of formation. *Geochim. Cosmochim. Acta*, **45**: 687-698.

Rickard, D., 1974. Kinetics and mechanism of the sulfidation of goethite. *American Journal of Science*, **274**: 941-952.

Rickard, D., 1975. Kinetics and Mechanism of Pyrite Formation at Low Temperatures. *American Jounal of Science*, **275**: 636-652.

Rickard, D., Schoonen, M.A.A. and Luther, G.W., 1995. *Chemistry of iron sulfides in sedimentary environments.* In: M.A. Vairavamurthy and M.A.A. Schoonen (Editors), Geochemical Transformations of Sedimentary Sulfur. Acs Symposium Series. Amer Chemical Soc, Washington, pp. 168-193.

Rickard, D., Butler, I.B. and Oldroyd, A., 2001. A novel iron sulphide mineral switch and its implications for Earth and planetary science. *Earth and Planetary Science Letters*, **189(1-2)**: 85-91.

Rickard, D.T. and Morse, J.W., 2005. Acid volatile sulfide (AVS). *Mar. Chem.*, **97(3-4)**: 141-197.

Rickard, D., 2006. The solubility of FeS. *Geochimica Et Cosmochimica Acta*, **70(23)**: 5779-5789.

Roden, E.E., 2003. Fe(III) oxide reactivity toward biological versus chemical reduction. *Environ. Sci. Technol.*, **37(7)**: 1319-1324.

Schoonen, M.A.A. and Barnes, H.L., 1991a. Reactions Forming Pyrite and Marcasite from Solution .1. Nucleation of FeS_2 Below 100-Degrees-C. *Geochimica Et Cosmochimica Acta*, **55(6)**: 1495-1504.

Schoonen, M.A.A. and Barnes, H.L., 1991b. Reactions Forming Pyrite and Marcasite from Solution .2. Via Fes Precursors Below 100-Degrees-C. *Geochimica Et Cosmochimica Acta*, **55(6)**: 1505-1514.

Schoonen, M.A.A., 2004. *Mechanisms of sedimentary pyrite formation* In: Amend J.P., Edwards K.J. and Lyons T. W. (Editors), Sulfur Biogeochemistry - Past and Present. Geological Society of America Special Paper 379, pp. 117-134.

Schwertmann U. and Cornell R. M., 2000. *Iron oxides in the laboratory: Preparation and characterization.* Wiley-VCH Verlag GmbH, Weinheim, New York, Basel, Cambridge, Tokyo, 188 pp.

Stumm, W. and Sulzberger, B., 1992. The Cycling of Iron in Natural Environments - Considerations Based on Laboratory Studies of Heterogeneous Redox Processes. *Geochimica Et Cosmochimica Acta*, **56(8)**: 3233-3257.

Thamdrup, B., 2000. *Bacterial manganese and iron reduction in aquatic sediments*, Advances in Microbial Ecology, Vol 16. Advances in Microbial Ecology. Kluwer Academic / Plenum Publ, New York, pp. 41-84.

Wang, F. and Morse, J.W., 1995. Pyrite formation under conditions approximating those in anoxic sediments: I. Pathways and morphology. *Marine Chemistry*, **52**: 99-121.

Wilkin, R.T. and Barnes, H.L., 1996. Pyrite formation by reactions of iron monosulfides with dissolved inorganic and organic sulfur species. *Geochimica Et Cosmochimica Acta*, **60(21)**: 4167-4179.

Yao, W. and Millero, F.J., 1996. Oxidation of hydrogen sulfide by hydrous Fe(III) oxides in seawater. *Mar. Chem.*, **52**: 1-16.

2. Pathways of ferrous iron mineral formation upon sulfidation of lepidocrocite surfaces

Submitted to Geochimica et Cosmochimica Acta

Katrin Hellige[1], Kilian Pollok[2], Philip Larese-Casanova[3], Thilo Behrends[4] and Stefan Peiffer[1]

[1]Department of Hydrology, University of Bayreuth, Universitätsstraße 30, D-95445 Bayreuth, Germany

[2]Bayerisches Geoinstitut, University of Bayreuth, Universitätsstraße 30, D-95445 Bayreuth, Germany

[3]Department of Geology and Geophysics, University of Yale, P.O. Box 208109, New Haven, CT 06520-8109 USA

[4]Department of Earth Sciences, Geochemistry, Utrecht University, P.O. Box 80021, 3508 TA Utrecht, The Netherlands

2.1. Abstract

The interaction between S(-II) and ferric oxides exerts a major control for the sulphur and iron cycle and in particular for the carbon and electron flow in many aquatic systems. It is regarded to be a key reaction leading ultimately to pyrite formation, the pathways still remaining unresolved. We have studied the reaction between lepidocrocite (γ-FeOOH, 21-42 mmol L^{-1}) and dissolved S(-II) (3-9 mmol L^{-1}) in batch experiments at pH 7 in a glove box using TEM, XRD, Mössbauer spectroscopy, and wet chemistry extraction to explore the nanocrystalline products forming at different time steps in close contact to the lepidocrocite surface. S(0) and acid extractable Fe(II) ($Fe(II)_{HCl}$) were the main products detected by wet chemistry extraction. The reaction could be divided into three steps: a rapid (< 15 min) consumption of dissolved S(-II), formation of S(0) and the build-up of an $Fe(II)_{HCl}$ pool. Then in the absence of dissolved S(-II) concentrations of S(0) and $Fe(II)_{HCl}$ increased only slightly. TEM measurements revealed the occurrence of a mackinawite rim covering the lepidocrocite crystals and being separated from the lepidocrocite surface by an interfacial magnetite layer that can be regarded as a steady state product of the interaction between lepidocrocite and mackinawite. A significant fraction of Fe(II) was formed in excess to FeS within the first two hours. The amount of this fraction increased with decreasing ratio between dissolved S(-II) concentration and the concentration of surface sites, which we attributed to a kinetic decoupling of S(-II) oxidation and Fe(II) detachment from the lepidocrocite surface. At low ratios, S(-II) seems to transfer electrons to lepidocrocite faster then stoichiometric amounts of FeS could. After 2 days $Fe(II)_{HCl}$ and S(0) started to decrease resulting in pyrite formation accompanied by traces of magnetite. TEM measurements indicated that mackinawite completely dissolved and precipitation of pyrite occurred dislocated from the lepidocrocite surface. The absence of dissolved sulphide under these conditions suggest that excess Fe(II) is involved in the formation of polysulphides which are key precursors during pyrite formation. We propose that the occurrence of excess Fe(II) is a common phenomenon particularly in low sulphide – high iron environments attributing significant reactivity to ferric (hydr)oxides.

Keywords: ferric (hydr)oxides reductive dissolution, dissolved S(-II), ferrous iron, lepidocrocite, pyrite formation, magnetite, electron transfer

2.2. Introduction

The interaction between H_2S and iron (hydr)oxides plays a prominent role in many environments like marine sediments, lakes, soils or aquifers. In the absence of oxygen, dissolved sulphate can be reduced to H_2S during the biological oxidation of organic matter and react further with sedimentary iron (Canfield et al., 1992) to generate S(0) and FeS (Peiffer, 1994; Poulton et al., 2004; Rickard, 1974; Rickard, 1975). FeS and S(0) are regarded to be the most important reactants in the formation of pyrite (Rickard and Morse, 2005; Schoonen, 2004; Wang and Morse, 1995; Wilkin and Barnes, 1996).

It has been recognised that the formation of FeS and FeS_2 is kinetically decoupled (Rickard, 1975). FeS formation can be directly linked to the sulfidation of ferric (hydr)oxides (Poulton, 2003; Poulton et al., 2004; Pyzik and Sommer, 1981; Rickard, 1975). This reaction is regarded to be controlled by the formation of a reactive surface complex (Dos Santos Afonso and Stumm, 1992; Peiffer et al., 1992) and shows a strong pH dependency which was attributed to surface speciation of sorbed S(-II) atoms (Peiffer et al., 1992; Yao and Millero, 1996). The rate of the sulfidation of lepidocrocite has a maximum value at near-neutral pH (Peiffer et al., 1992). In contrast, pyrite formation is regarded to be preceded by the dissolution of FeS and kinetically controlled by the degree of supersaturation and the occurrence of reactive sulphide species (Luther, 1991; Rickard, 2006; Rickard et al., 2001; Rickard and Morse, 2005; Schoonen and Barnes, 1991b).

Aside from the formation of iron sulphides, Poulton et al. (2003, 2004) found that a large fraction of ferrous iron could be attributed neither to FeS nor to any other sulphide phase. These authors described this Fe(II) as being bound to the surface and extractable with HCl but not exchangeable with $CaCl_2$. The nature, identity and morphology of this species is still unclear. Other researchers who performed Fe(II) adsorption experiments were not able to completely retrieve surface associated Fe(II) through wet chemical extraction and interpret this effect by incorporation of Fe^{2+} into the bulk phase (Larese-Casanova and Scherer, 2007; Rosso et al., 2010; Silvester et al., 2005; Williams and Scherer, 2004). At excess Fe(II) concentrations transformation of the ferric iron (hydr)oxide sorbent (e.g. lepidocrocite or ferrihydrite) to magnetite occurs (Hansel et al., 2005; Tamaura et al., 1983).

It appears that our understanding of the reaction steps following the electron transfer reaction between sulphide and ferric (hydr)oxides is still incomplete and requires a deeper insight into the processes occurring at the iron (hydr)oxides` surfaces itself. In this study we have studied the reaction between sulphide and lepidocrocite at circumneutral pH and followed the reaction

progress using wet chemical extraction techniques. These analyses were supported by X-ray diffraction, Mössbauer spectroscopy and transmission electron microscopy to identify the products. Contrary to previous work (Dos Santos Afonso and Stumm, 1992; Peiffer et al., 1992; Poulton et al., 2004) which studied only the initial (<5h) rates, we have extended the reaction time to 14 days to deepen our understanding into the dynamics of Fe^{2+} and its various species.

2.3. Materials and methods

All solutions were prepared with distilled water and bubbled with N_2 to remove oxygen. All reagents were of analytical grade.

2.3.1. Lepidocrocite

Synthetic lepidocrocite Bayferrox 943 was purchased from Lanxess (Leverkusen, Germany). To remove ions like sulphate from the surface, an aliquot of 1 mol L^{-1} was suspended in 0.01 mol L^{-1} $NaNO_3$ and the pH was adjusted to 10 with NaOH. After 4 days of shaking the lepidocrocite suspension was washed by centrifuging, decanting, and resuspending in deoinized water and centrifuging again. After reaching a conduction value of <20 µS cm^{-1} the lepidocrocite was freeze-dried.

The synthetic lepidocrocite was characterized using X-ray diffractometry (XRD), scanning electron microscopy (SEM), and transmission electron microscopy (TEM). XRD and TEM measurements showed pure lepidocrocite with a minor goethite impurity. The particle size ranges between 0.2-0.4 µm. Multi-point BET (Brunauer, Emmett and Teller) gas adsorption with N_2 (Gemini 2375 Surface Area Analyzer) yielded a surface area of 17.34 m^2 g^{-1}.

2.3.2. Experimental Set-up

Kinetic batch experiments with excess lepidocrocite and dissolved sulphide were conducted at pH 7, at a constant ionic strength (I = 0.1 M NaCl), and at room temperature. All reactions took place in a 500-ml closed glass vessel installed in an anoxic glove box and containing ports for sampling and removals, pH electrode and HCl addition within. The suspensions were gently stirred with a Teflon-coated stirring bar at a constant rate. The pH value was kept constant by adding deoxygenated HCl (0.5 mol L^{-1}) with an automated pH-stat device. HCl addition stopped automatically by the system itself when the pH dropped below 7 towards the end of the experiments.

The reaction solution was prepared by mixing 50 mL of solution I (0.1 mol L^{-1} NaCl) containing between 1.3 and 2.5 g L^{-1} lepidocrocite with 450 ml of solution II (0.1 mol L^{-1} NaCl) to which aliquots of Na_2S*9H_2O (0.5 mol L^{-1}) and HCl (0.5 mol L^{-1}) were added to establish a pH of 7. The initial solution conditions and the consumption of acid are shown in table 1. The sulphide concentration was determined before each run. The following species were determined during the reaction and after 1-2 hours, 24 hours, 1 week and 2 weeks: dissolved Fe(II) and S(-II), Fe(II) extractable with 0.5 N HCl, S(0), and total iron. Furthermore samples were analyzed by XRD, Mössbauer spectroscopy and TEM to trace changes in the solid phase assemblage over a period of 2 weeks.

2.3.3. Sampling and analysis

Iron species. Dissolved Fe(II) ($Fe(II)_{diss}$) was determined after filtration (0.45 µm) using the phenanthroline method Tamura (1974). Total extractable iron was determined after dissolution in 6 N HCl and heating at 60°C for 3 days. HCl extractable solid phase bound Fe(II) ($Fe(II)_{HCl}$) was extracted with 0.5 N HCl for 1 hour, filtered and the Fe(II) was determined in the filtrate as above. Samples were purged with N_2 to remove dissolved sulphide.

Sulphur species. Dissolved sulphide ($S(-II)_{diss}$) was determined photometrically by the methylene blue method (Fonselius, 1999) after filtration. Total elemental sulphur (S(0)) was measured by high performance liquid chromatography (HPLC, Beckman) combined with UV detection (Detector 168, Beckman) after extraction of 300 µL of unfiltered sample suspended in 1200 µL methanol (modified after Ferdelman et al., 1991). After 1 h equilibration time the suspension was filtered (0.2 µm) and the filtrate was stored at -20°C until analysis. Total dissolved sulphur (not further specified) was measured by ICP-OES.

Mössbauer spectroscopy. 30 mL of the suspension was centrifuged outside of the glove box within closed centrifuge tubes. After centrifugation the supernatant was decanted in the glove box and the solid phase was dried under a nitrogen stream for 1 minute. After drying, the solid phase was put on a membrane filter paper (13 mm diameter and 0.45 µm) and was sealed between two layers of Kapton tape (polyimide tape with very low oxygen permeability). The samples were placed in a sealed crimp vial and stored at 4°C until measurement. Mössbauer spectra were collected with a WissEl Mössbauer gamma-ray spectrometer and a Janis closed-cycle helium gas cryostat that allowed for sample temperatures down to 4.2 K. A Co-57 gamma-ray source was used with a constant acceleration drive system operated in transmission mode. Spectra were calibrated against a

spectrum of alpha-Fe(0) foil at room temperature. Data acquisition times were usually about 12-20 hours per spectrum. Spectral fitting was performed using Recoil® software (University of Ottawa, Canada) and Voigt-based spectral lines.

X-ray diffraction. XRD patterns were collected with a Bruker-D8 with GADDS system (Bruker AXS GmbH, Karlsruhe) with CoKα radiation focused to a 300 micron spot size. The samples were scanned from 5 to 75° CoKα using step size of 0.1°. The sample preparation was the same as described for Mössbauer spectroscopy.

Transmission electron microscopy. Solids retrieved from the reacting suspension were analyzed by a Philips CM 20-FEG TEM, operating at 200 kV. In order to limit oxidation in air during sample preparation the suspension was first sampled in gas-tight vials. A drop of solution was then taken with a syringe and put onto a Lacey carbon-coated copper grid. The grid was immediately transferred to the TEM holder and inserted into the high vacuum of the TEM. The short exposure of the sample to air was limited to 1-2 minutes at maximum with this procedure. The chemical composition and the distribution of elements were determined by energy-dispersive X-ray spectroscopy (Thermo Noran Ge detector).

TEM was performed on the reaction products of run 10, 13, 14, and 15 (Table 1) at different reaction times as well as on the lepidocrocite starting material. All of the experimental runs were analyzed after 2 h and run 10, 14, and 15 also after 336 h (except run 13). Additional TEM measurements have been made for run 14 after 24, 48, 72, and 168 h. It is important to note that the TEM samples cannot be stored for repeated analyses because of the oxidation of run products after removal from the instrument vacuum. Anoxic storage may cause further reactions of the nanocrystalline run products and has not been applied.

Conventional and high-resolution imaging as well as selected area electron diffraction (SAED) and EDX microanalysis were used to identify phases and to constrain their chemical composition and textural relationships. SAED patterns from both a high number of crystals leading to polycrystalline ring patterns and from individual crystals producing spot patterns that represent two-dimensional section of the reciprocal lattice have been produced and indexed. In addition, d-values of various phases were determined directly from high resolution images as well as from calculated diffraction patterns produced by fast Fourier transform (FFT) of selected areas.

Table 2.1. Initial conditions for each run. All runs were conducted at pH 7 and the chemical species was analyzed. TEM measurements were performed in run 10, 13, 14, and 15, Mössbauer spectroscopy and XRD were only for run 10.

Run no.	Runtime	Lepidocrocite concentration	Surface area	Surface sites[a]	Initial sulphide concentration	H^+ consumption during pH reaction[b]	H^+ consumption during pH adjustment[c]
	(hours)	(mmol L^{-1})	(m^2 L^{-1})	(mmol L^{-1})	(mmol L^{-1})	(mmol L^{-1})	(mmol L^{-1})
6	3	14	21.6	0.14	9	2.7	13.9
7	1.5	21.8	33.6	0.21	7.8	2.5	13.1
8	1.5	16.8	25.9	0.16	8.8	2.8	13.7
9	1.5	27.5	42.4	0.27	8.3	2.8	12.9
10	336	26.6	41.1	0.26	7.2	2.9	9.8
13	7	25.6	39.5	0.25	6.7	2.9	10.9
14	336	27.2	42	0.26	7.4	3	10.
15	336	20.5	31.6	0.20	3.7	1.3	5.1

[a] Concentration of surface sites was calculated based on a value of $6.3*10^{-6}$ mol m^{-2} for all minerals (Peiffer and Gade, 2007)
[b] H^+ consumption after addition of lepidocrocite
[c] H^+ consumption in order to adjust the pH in the sulphide solution before the addition of lepidocrocite

2.4. Results

2.4.1. Chemical speciation during the reaction

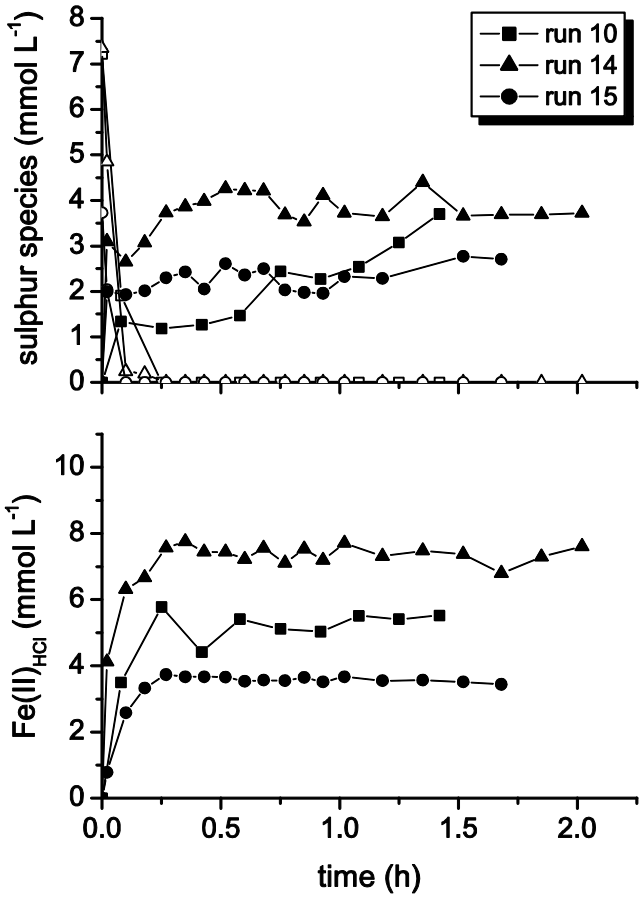

Fig. 2.1. Evolution of sulphur with □ Δ ○ = dissolved sulphide and ■▲● = elemental sulphur (top) and acid extractable Fe(II) as ■▲● (bottom) during the first two hours of reaction for run 10, 14, and 15.

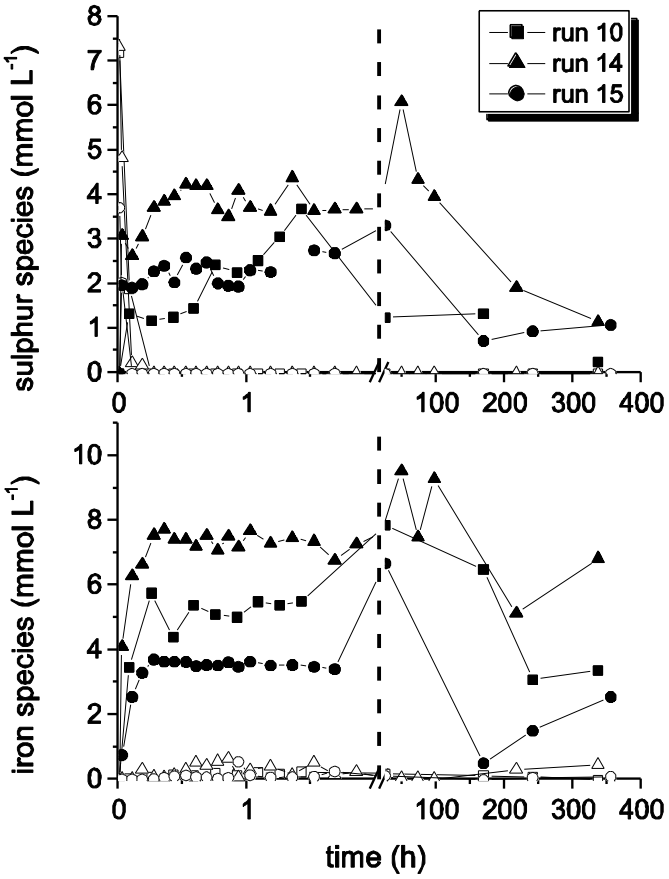

Fig. 2.2. Evolution of sulphur with □ Δ ○ = dissolved sulphide and ■▲● = elemental sulphur (top) and iron species with □ Δ ○ = dissolved Fe(II) and ■▲● = acid extractable Fe(II) (bottom) during two weeks of reaction for run 10, 14, and 15. Note, that the initial sulphide concentration in run 10 and 14 was double the concentration in run 15 (Table 2.1).

Dissolved sulphide was consumed completely in the first 15 minutes after addition of lepidocrocite (Fig. 2.1). Optically, a change of the lepidocrocite colour from orange to black was visible immediately after it was added to the sulphide solution. The main products of the reaction between lepidocrocite and dissolved sulphide were S(0) and acid extractable Fe(II) (Fig. 2.1). Only low concentrations of dissolved Fe(II) were measured (0.01-0.66 mmol L^{-1}) (Fig. 2.2). Initially, the formation of S(0) and $Fe(II)_{HCl}$ was fast and after 10 minutes the concentration of both species increased slowly for S(0) up to 2.5-4.5 mmol L^{-1} and for $Fe(II)_{HCl}$ up to approximately 4-8 mmol L^{-1} (Fig. 1). The concentration of S(0) dropped to 1-2 mmol L^{-1} after 1 week and decreased further to 0.3-1.2 mmol L^{-1} towards the end (Fig. 2.2). The concentration of $Fe(II)_{HCl}$ had a maximum after 48 hours and then decreased to 3-7 mmol L^{-1} (Fig. 2.2).

The initial sulphide concentration in run 10 and 14 was double the concentration in run 15 (Table 2.1).

Similar observations were made in previous studies (Peiffer et al., 1992; Poulton, 2003; Poulton et al., 2004; Pyzik and Sommer, 1981; Rickard, 1974) where S(0) was the dominant

oxidized sulphur product and a large proportion of Fe(II) was bound to the solid phase as FeS or remained at the oxide surface.

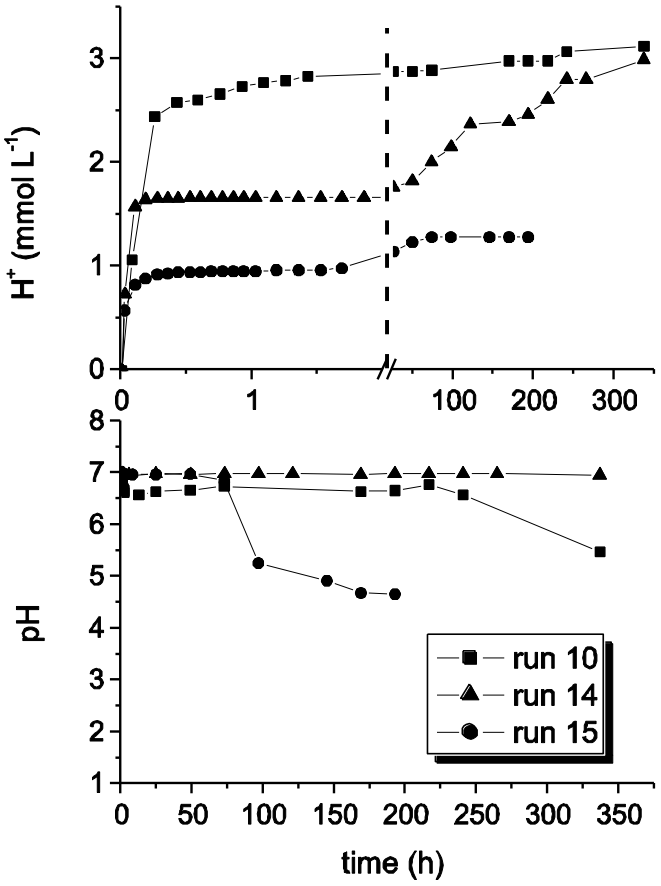

Fig. 2.3. pH progress (bottom) and H^+ consumption (top) during the reaction between lepidocrocite and dissolved sulphide for run 10, 14, and 15.

Within the first 24 hours 1.2-2.9 mmol L^{-1} of H^+ were consumed, while in the following time the consumption increased slowly to a value of 1.3-3.1 mmol L^{-1} H^+ (Fig 2.3). The fast consumption of dissolved sulphide coincides with a fast consumption of H^+, and once dissolved sulphide has been consumed completely, H^+ consumption declined to a slower rate. Most of the added H^+ appeared to be consumed for the reaction between sulphide and Fe(III) at the lepidocrocite surface. After 10 days of reaction the pH started to decrease and after 2 weeks the pH was 7, 5.5, and 4.5 for run 14, run 10, and run 15, respectively. Towards the end of the experiments after 14 days, the black coloration of the suspension disappeared and the suspensions turned into greyish-yellow.

Overall, the reaction progress can be divided into three steps (Fig. 2.1, 2.2). The first is an initial fast reaction (< 15 min) in which dissolved sulphide was consumed upon formation of

$Fe(II)_{HCl}$ and S(0). Then, in a second phase, the concentration of $Fe(II)_{HCl}$ and S(0) slightly increased. In a third step, both $Fe(II)_{HCl}$ and S(0) were consumed.

2.4.2. Spectroscopical and microscopical results

2.4.2.1. Mössbauer spectroscopy

Mössbauer spectra were measured at 4.2 K to identify lepidocrocite transformation products (Fig. 2.4, run 10). Model parameters are listed in Table 2.2.

Table 2.2. Model parameters for 4.2 K Mössbauer spectra of lepidocrocite reacted with sulphide in Fig. 2.4.

Sample time	Lepidocrocite								FeS_2		
	I^a (mm s^{-1})	$X^{2\,b}$	<CS>^{c} (mm s^{-1})	<QS>^{d} (mm s^{-1})	<H>^{e} T	# of comp.^{f}	$H_p{}^g$ T	Abundance (%)	<CS> (mm s^{-1})	<QS> (mm s^{-1})	Abundance (%)
1 hr	0.11	1.4	0.5	0.04	44.8	2	45.4	100			
1 d	0.11	2.0	0.5	0.04	43.7	3	45.5	100			
1 wk	0.11	1.3	0.5	0.04	43.9	3	45.5	98.2	0.42	0.6	1.8
2 wk	0.11	2.0	0.5	0.03	44.4	2	45.4	93.4	0.4	0.65	6.6
Mineral standards											
Lepidocrocite, 4.2 K			0.5	0.02	44.9	1	44.9				
Pyrite, 77K									0.36	0.64	
Pyrite, 4.2 K									0.43	0.66	
Marcasite, 80 K									0.37	0.5	

[a]Lorenztian half-width at half-maximum.
[b]Reduced chi-squared goodness of fit value.
[c]Average center shift.
[d]Average quadrupole splitting.
[e]Average hyperfine magnetic field.
[f]Number of Voigt-based components used to model the hyperfine magnetic field.
[g]Most probable hyperfine magnetic field value.
[g]At an analysis temperature of 77 K, the spectrum contained an Fe(II) doublet with <CS> = 1.32 mm s^{-1}, <QS> = 2.92 mm s^{-1} and an Fe(III) doublet with <CS> = 0.48 mm s^{-1}, <QS> = 0.76 mm s^{-1}. Here, <QS> refers to the average quadrupole splitting distribution.
[h] At an analysis temperature of 77 K, the spectrum contained two Fe(II) doublets that resembled the paired Fe(II) octahedra (<CS> = 1.34 mm s^{-1}, <QS> = 3.29 mm s^{-1}) and the isolated Fe(II) octahedra (<CS> = 1.30 mm s^{-1}, <QS> = 2.56 mm s^{-1}) in vivianite. An Fe(III) doublet was also observed with (<CS> = 0.55 mm s^{-1}, <QS> = 0.55 mm s^{-1}. Here, <QS> refers to the average quadrupole splitting distribution.

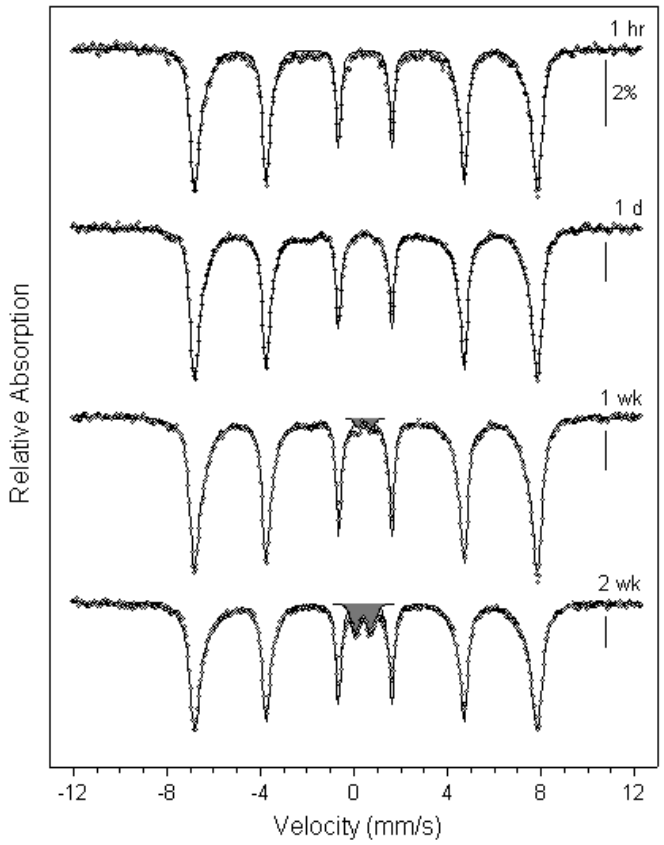

Fig. 2.4. Mössbauer spectrum of lepidocrocite reacted with sulphide after 1 hour, 1 day, 1 week, and 2 weeks (run 10). White shaded sextets are lepidocrocite, and gray shaded doublets are FeS_2. All spectra were collected at a temperature of 4.2 K. The scale bar represents a length of 2% absorption for each spectrum. Solution conditions are listed in Table 2.1, and model parameters are listed in Table 2.2.

In all samples, a six-line signal (sextet) was identified as lepidocrocite based on model parameters that were consistent with an oxidation state of Fe(III) in a high-spin octahedral configuration similar to synthetic lepidocrocite in its antiferromagnetic state. The lepidocrocite was the dominant signal in all samples, but after a week a second signal emerged in the form of a paramagnetic doublet and increased with time (Fig. 2.4). We eliminated the possibility of this signal being an iron (hydr)oxide phase because no crystalline iron (hydr)oxides are paramagnetic at 4.2 K. Pyrite and marcasite share the same unit cell formula (FeS_2) and have low-spin octahedral Fe(II) configurations with paired d-orbital electrons that allow the minerals to remain paramagnetic at 4.2 K. On this basis, the paramagnetic doublet indicates that 1.8 % of the initial added lepidocrocite was transformed into FeS_2 after 1 week and 6.6 % after 2 weeks (Table 2.2).

No other iron phases than lepidocrocite and FeS_2 were observed by Mössbauer spectroscopy. Spectra collected at 77 K also confirmed the presence of lepidocrocite but did not discern the overlapping iron sulphide doublets (data not shown).

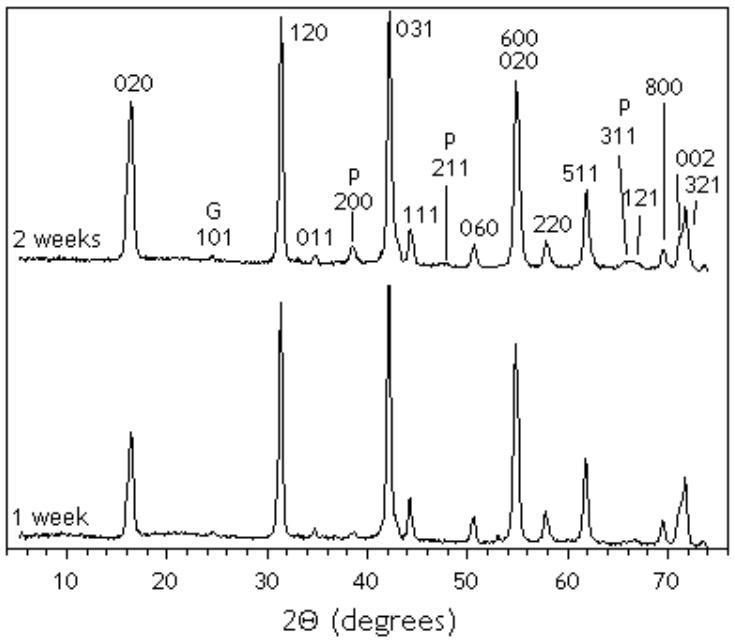

Fig. 2.5. X–ray diffractograms illustrating the formation of FeS_2 during the reaction between lepidocrocite and dissolved sulphide after 1 and 2 weeks (top) and the typical mineral peaks with regard to their intensity (bottom) (run 10).

The XRD results are shown in Fig. 5. The samples were taken after 1 week and 2 weeks of reaction. The characteristic reflections for unreacted lepidocrocite were apparent (Ewing, 1935). XRD measurements confirmed the formation of FeS_2 (pyrite) with XRD peaks at 38.8°, 47.4°, and 65.5°, respectively (Fig. 2.5). Both XRD and Mössbauer spectroscopy demonstrated that the FeS_2 signal increased with time. The characteristic reflections for magnetite and marcasite were not distinctly observed, although the 34.8° reflection might indicate magnetite (in addition to lepidocrocite) and the 38.5° reflection might include marcasite (in addition to pyrite).

2.4.2.2. Transmission electron microscopy

TEM was performed at different reaction times to localize and identify nanocrystalline reaction products. At 2 and 24 hours of reaction rims of 10-20 nm thickness are observed at the surface of all lepidocrocite crystals (Fig. 2.6a). High-resolution TEM reveals that these rims consists of mackinawite (tetragonal FeS) nanocrystals showing (001) lattice fringes with a spacing of 5.0 to 5.2 Å. (111) planes (d_{111} = 2.3 Å) have been frequently observed as well (Fig. 2.6b). Fig. 6c shows intersecting (001) and (101) planes of a mackinawite nanocrystal consistent with a [010] zone axis orientation. A set of continuous lattice fringes represents a mackinawite single crystal and allows to estimate the particle size. The thin tabular crystals are usually about 2 to 10 nm in size and elongated to the c-axis. However, the particle outline is often poorly defined. The same appearance has been reported by Ohfuji and Rickard (2006)

and Burton et al. (2009) for freshly-prepared nanocrystalline synthetic mackinawite and biologically-formed sedimentary mackinawite, respectively. The spotted contrast on the lepidocrocite grains (Fig. 2.6a) was first attributed to the dehydration of the crystals during observation. However, a careful inspection of a large number of grains revealed that the contrast is omnipresent and not related to beam damage indicating mackinawite nanocrystals covering the entire surface of lepidocrocite.

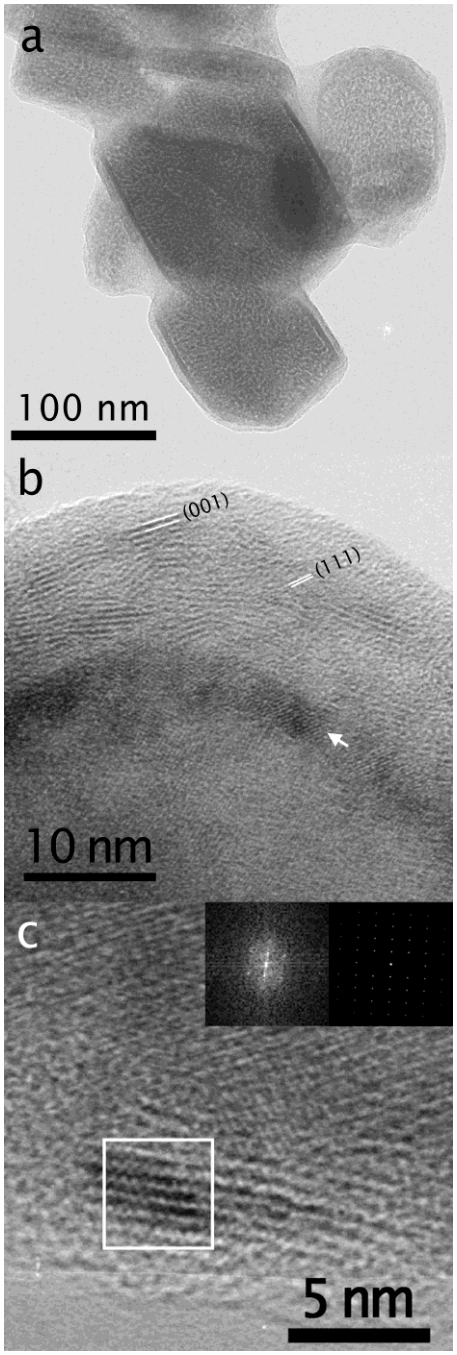

Fig. 2.6. Bright field (a) and high resolution (b,c) TEM images of lepidocrocite crystals with sulphur-rich rims after 2 hours of reaction. The spotted contrast on lepidocrocite grains in (a) is due to nanocrystalline mackinawite. In (b) characteristic (001) and (111) lattice fringes of mackinawite were visible in the outer rim. A continuous intermediate layer (arrow) shows fringes matching d_{220} of magnetite/maghemite. This layer can also notice in (a). A nanocrystal of

mackinawite in [010] zone axis orientation is shown in (c) together with its calculated FFT and a simulated diffraction pattern as inset.

The observations were consistent with scanning TEM-EDX maps taken which show a sulphur and iron signal from mackinawite in the rims and iron, oxygen and a low amount of sulphur at the lepidocrocite grains (Fig. 2.7).

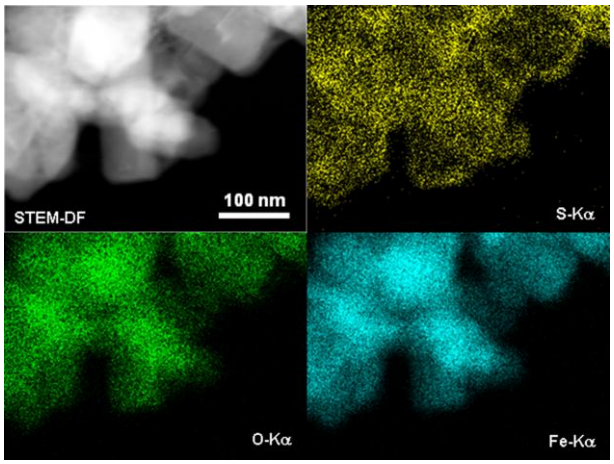

Fig. 2.7. Dark-field STEM image (upper left) and EDX maps of S Kα (upper right), O Kα (lower left), and Fe Kα (lower right) after 24 hours of reaction. Sulphur was enriched at the rims of the lepidocrocite crystals. Variations in counts of oxygen and iron are well correlated and mainly due to thickness differences which are caused by stacked crystals.

The sulphur signal indicates a thin mackinawite layer on the upper and lower surface of lepidocrocite. Between the sulphur-rich rim and the lepidocrocite crystal an additional layer with a thickness of less than 10 nm was observed in the bright-field and high resolution image (Fig. 2.6a,b). The d-spacing in this continuous layer is 2.96 Å with constant orientation to lepidocrocite which strongly argues against mackinawite. The only iron oxides or hydroxide which fits to the observed lattice spacing are the (220) d-spacings of magnetite or maghemite. A reaction with ferrous iron as well as dehydroxylation with lepidocrocite can lead to magnetite/maghemite formation (Cornell and Schwertmann, 1996) which might be favoured by the structural similarities of lepidocrocite structural unit to the inverse spinel structure (Cudennec and Lecerf, 2005). The spinel layer was observed in a number of crystals, but a quick formation due to the electron beam during TEM observation cannot be ruled out completely.

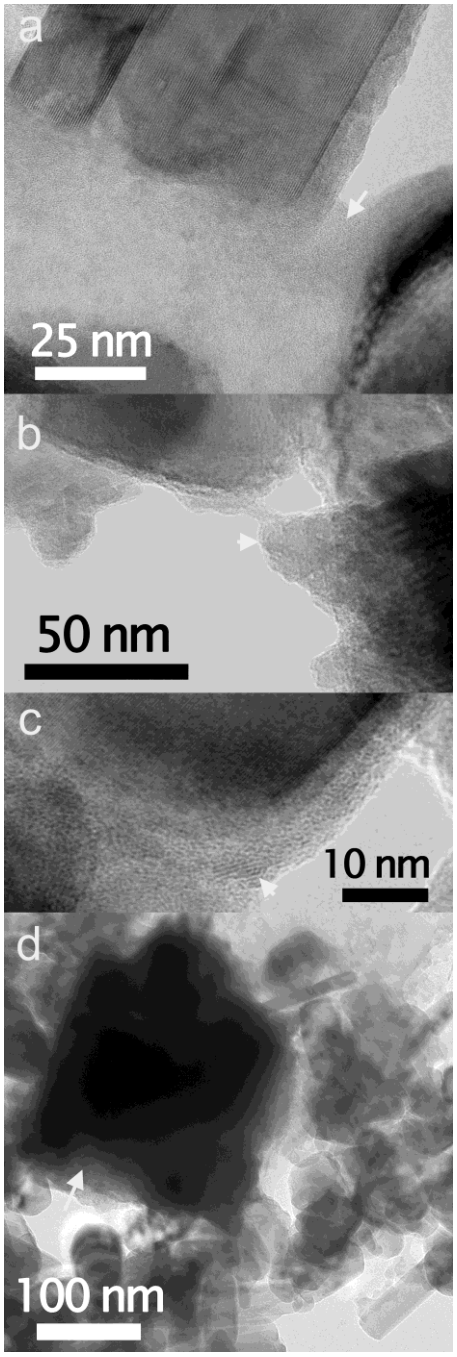

Fig. 2.8. A temporal sequence of the conversion of mackinawite to pyrite at 72 hours (a), 1 (b,c) and 2 weeks (d). The high resolution TEM image after 72 hours (a) shows a slightly corrugated mackinawite rim on lepidocrocite. Additionally, amorphous areas form between the grains which consisted of Fe and S with variable stoichiometry (arrow). After 168 hours (b,c) pyrite starts to form (arrow in (b)) while only relicts of mackinawite can be found (arrow in (c)). At 336 hours, pyrite grains (arrow) with a diameter of 200-500 nm are present. Some magnetite grains could be identified between the pyrite crystals.

Fig. 2.8 shows a temporal sequence of the conversion of mackinawite to pyrite at 72 hours, 1 and 2 weeks. The mackinawite rims get gradually thinner and more corrugated with time. After 72 hours amorphous regions composed of iron and sulphur in variable concentration can be found between lepidocrocite grains (Fig. 2.8a). After 1 week pyrite crystals were formed

on the expense of the amorphous films and the mackinawite rims (Fig. 2.8b,c). The pyrite grains reach diameters between 200 and 500 nm after 2 weeks and commonly show striking cubic or octahedral outlines and have been identified by both SAED and EDX analyses (Fig. 2.8d, Fig. 2.9). Essentially, high resolution images reveal that the grains are composed of smaller cubic building blocks which point to a formation by oriented aggregation. Mackinawite cannot be found after 2 weeks. The lepidocrocite grain size has not significantly changed (lepidocrocite was in large excess to sulphide) and show no sulphur attached to the surface which remains corrugated. In addition to pyrite, some magnetite grains similar in size and shape could be identified by STEM-EDX and electron diffraction as well.

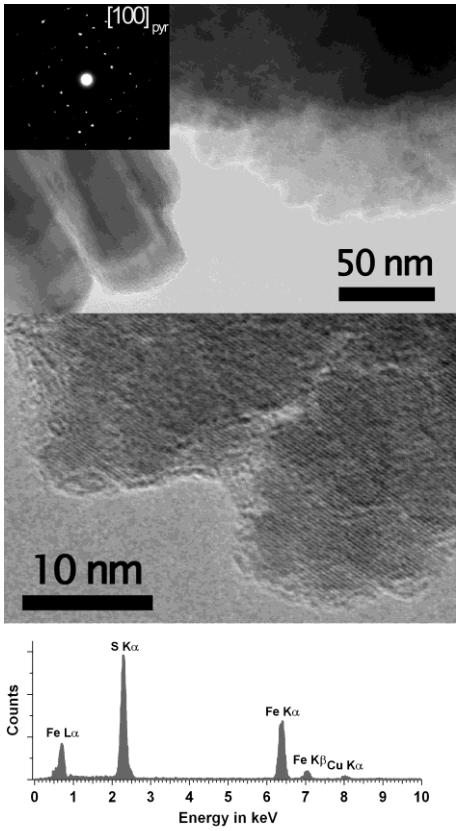

Fig. 2.9. High resolution images, electron diffraction pattern and EDX spectra of pyrite. Note the aggregative nature of the grain consisting of cubic building blocks. Slight misorientations were also reflected in the diffraction pattern.

2.5. Discussion

2.5.1. Redox processes at the lepidocrocite surfaces

Fast consumption of surface bound sulphide in the initial phase can account for the quantitative consumption of dissolved sulphide within the first 15 minutes of reaction. According to the proposed mechanism for the reaction between sulphide and ferric (hydr)oxides (Dos Santos Afonso and Stumm, 1992) the electron transfer from sulphide to

Fe(III) is preceded by the formation of the inner-sphere surface complexes ≡FeS$^-$ and ≡FeSH (Luther, 1990). The rate of the reaction is pH dependent and the oxidation rate of the reactive surface species ≡FeHS has a maximum at pH 7 (Peiffer et al., 1992).

The second phase is characterized by the occurrence of FeS as confirmed by TEM analyses made after 2 h. The concentration of FeS at this time step can be estimated based on the mass balance of sulfur (eq.1)

$$c(FeS) = c(S(-II))_{added} - c(S(0)) \quad (1)$$

where $c(S(-II))_{added}$ is the concentration of initially added S(-II). This calculation is based on the assumption that S(0) is the dominant product of S(-II) oxidation under these conditions (Poulton et al., 2004) and that the formed FeS is quantitatively recovered in the HCl extract. TEM analyses reveal that the FeS phase in the sulphur rich rims surrounding the lepidocrocite particles has mackinawite structure. Well crystalline mackinawite does not completely dissolve during in 0.5 N HCl extraction (Rickard and Morse, 2005) but it is very likely that the dissolution of the thin FeS layers observed is sufficiently fast to be completed during the extraction with 0.5 N HCl.

It appears, however, that the concentration of $Fe(II)_{HCl}$ exceeds that of FeS in this reaction phase (cf. Table 2.3). Hence, a fraction of acid extractable Fe(II) is formed which is not bound to FeS.

The amount of this excess Fe(II) ($Fe(II)_{excess}$) can be defined as the difference between $Fe(II)_{HCl}$ and the amount of FeS (eq. 2)

$$c(Fe(II)_{excess}) = c(Fe(II)_{HCl}) - c(FeS) \quad (2)$$

Table 2.3. Concentrations of products after 2 hours of the reaction of H_2S with lepidocrocite.

Run no.	$S(-II)_{added}$ (mmol L^{-1})	S(0) (mmol L^{-1})	$Fe(II)_{HCl}$ (mmol L^{-1})	H^+ (mmol L^{-1})	$FeS_{calculated}$ eq. 1 (mmol L^{-1})	$Fe(II)_{excess}$ eq. 2 (mmol L^{-1})
6	9.0	3.0	5.5	2.6	6	-0.5
7	7.8	2.0	6.0	2.5	5.8	0.2
8	8.8	2.0	6.5	2.8	6.8	-0.3
9	8.3	2.0	7.0	2.8	6.3	0.7
10	7.2	3.7	5.5	2.8	3.5	2.0
13	6.7	4.0	8.0	2.0	2.7	5.3
14	7.4	4.0	7.5	1.7	3.4	4.1
15	3.7	2.7	3.7	1.0	1	2.7

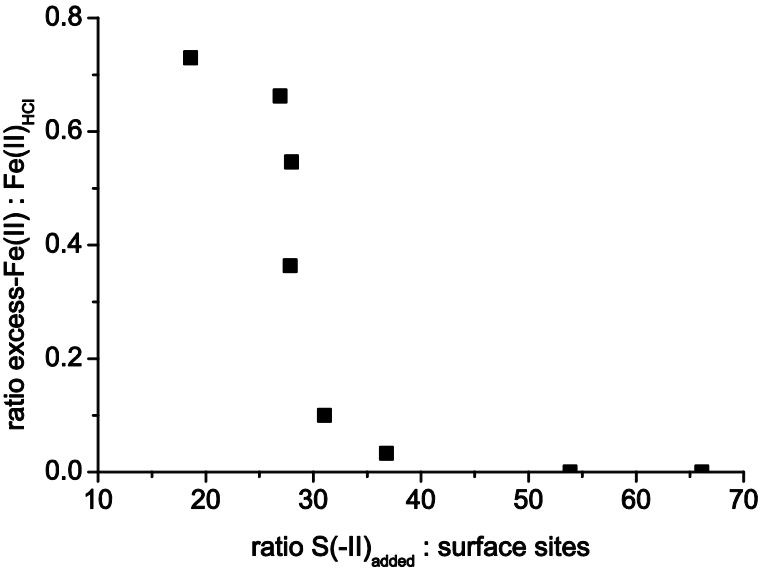

Fig. 2.10. Fraction of excess Fe(II) of HCl extractable Fe(II) as a function of the ratio between the concentration of initial S(-II) and of the lepidocrocite surface sites after 2 h.

The fraction of $Fe(II)_{excess}$ formed during Fe(III) reduction seems to depend on the ratio between the concentration of initial S(-II) and that of the surface sites of lepidocrocite (S(-II):SS-ratio, Fig. 2.10), so that a general stoichiometry for the turnover after 2 h can be written as

$$(1.5\text{-}x)\ H_2S + FeOOH \rightarrow x\ Fe^{2+}_{excess} + (1\text{-}x)\ FeS + 0.5\ S° + 2x\ OH^- + 2(1\text{-}x)\ H_2O \qquad (3)$$

The variable x ($0 < x < 1$) represents the fraction of reduced Fe(II) which is not bound in FeS. This fraction decreases with increasing initial S(-II):SS-ratio (Fig. 2.10). Note that also negative values exist for $Fe(II)_{excess}$ as a result of the mass balance in eqs. (1) and (2) indicating the range of error. We have set negative fractions in Fig. 2.10 equivalent to zero. We propose that the reason for this pattern is related to the decoupling of the kinetics of sulphide oxidation, Fe(III) reduction and FeS formation.

According to the proposed mechanism for reductive dissolution of iron (hydr)oxides by sulphide, the oxidation rate of dissolved sulphide is proportional to the concentration of reactive surface complexes (Peiffer et al, 1992) while detachment of Fe(II) from the surface is considered the rate limiting step for the reductive dissolution of ferric (hydr)oxides (Dos Santos Afonso et al, 1992). Given the high affinity of sulphide to the ferric (hydr)oxide surface (Dos Santos Afonso et al, 1992) it can be assumed that in all our experiments full surface coverage with HS^- is rapidly obtained and its oxidation operates at the maximum rate.

Under conditions where the initial sulphide concentration is low relative to the amount of reactive sites (low ratios in Figure 2.10) the consumption of the sulphide pool is fast. Since detachment of Fe(II) is slow relative to the consumption of sulphide the build-up of significant amounts of FeS is not possible. A disproportionation seems to occur between the electrons transfered and the generation of Fe(II) to be available for FeS formation as reflected by the high fraction of excess Fe(II). In other words, S(-II) seems to transfer electrons to lepidocrocite faster under these conditions then stoichiometric amounts of FeS could form.
In contrast, at high S(-II):SS-ratios, the detachment rate of Fe^{2+} is seemingly high enough to channel Fe^{2+} into FeS formation from the remaining S(-II) pool. The fraction of $Fe(II)_{excess}$ under these conditions approaches zero.
The presence of large amounts of $Fe(II)_{excess}$ indicates that transfer of Fe^{2+} from the surface into solution is not required for the continuation of Fe(III) reduction. This can be explained by a mechanism in which electrons, that are generated by the oxidation of S(-II) at the particle surface, are transported into the lepidocrocite bulk phase.

Formation of Fe^{2+} in the bulk phase is supported by the observation that the calculated concentrations of $Fe(II)_{excess}$ (Table 2.3) exceed the estimated concentration of reactive sites at the lepidocrocite surface by far. Concentrations of dissolved Fe(II) are relatively low so that a considerable fraction of $Fe(II)_{excess}$ is solid-phase Fe(II) which does not occur adsorbed onto the lepidocrocite surface. This solid-phase Fe(II) is apparently incorporated inside the bulk phase. Poulton et al. (2003, 2004) studied the reaction of several iron oxides with sulfide at circumneutral pH and also report the formation of solid-phase Fe(II) which is not FeS nor can it be extracted from the surface by 1 M $CaCl_2$ solution. They refer to this pool of Fe(II) as surface-Fe(II) without further specification.

Formation of Fe^{2+} within the iron oxide bulk phase can be explained by a displacement of electrons from the mineral surface into the mineral's interior. Proposed mechanisms for the reaction of S(-II) with iron oxides (Dos Santos Alfonso and Stumm, 1992; Peiffer et al., 1992) conform with the idea that the first step of the reaction is the adsorption of S(-II) onto the oxide surface followed by electron transfer between sulphide and iron. Thermodynamic calculations (Luther, 2010) suggest, that two electrons are transferred simultaneously and S(-II) is directly oxidized to S(0) while other proposed mechanisms involve a sequence of one-electron transfer steps by assuming intermediate formation of a $S^{\bullet-}$ radical. Irrespective of the detailed mechanism of the redox reaction at the surface, many studies demonstrate that electrons can be transferred from surface bound Fe(II) into the iron oxide bulk (Hiemstra and

van Riemsdijk, 2007; Burton et al., 2008; Catalano et al., 2010; Larese-Casanova and Scherer, 2007; Williams and Scherer, 2004). It has been proposed that the oxidized Fe^{2+}, now Fe^{3+}, becomes incorporated into a Fe^{3+} containing layer similar in structure to the bulk oxide (Williams and Scherer, 2004) and results in growth of the ferric (hydr)oxide (Handler et al., 2009). The electron is regarded to be injected into the oxide structure but the exact fate is unknown. It is assumed that the electron moves through the crystal lattice and reduces another bulk Fe^{3+} which can be released into solution (Catalano et al., 2010; Handler et al., 2009) or can be accumulated inside the bulk structure (Hansel et al., 2004).

HRTEM analysis reveals the occurrence of magnetite at the interface between mackinawite and the lepidocrocite surface (Fig. 2.6.). Interaction between Fe(II) and ferric hydroxides can stimulate the formation of magnetite (Hansel et al., 2005; Jeon et al., 2003; Jeon et al., 2001; Tamaura et al., 1983; Tronc et al., 1992) which is the thermodynamically stable product in a system containing Fe(II) and lepidocrocite. However, magnetite formation at the FeS – lepidocrocite interface appears to be only a transient phenomenon. After 48 hours no magnetite could be detected anymore (data not shown).

Nevertheless, the observed interfacial nanocrystalline magnetite layer indicates a functional relationship between lepidocrocite and the surface attached FeS. The occurrence of magnetite may be connected to a reaction between these two phases as reflected in the time evolution of $Fe(II)_{HCl}$ and S(0) during the second phase of the reaction. After 48 h measured S(0) and $Fe(II)_{HCl}$ concentrations are in most experiments higher than those determined at the end of the first phase when dissolved sulphide is consumed. This implies that concentrations of $Fe(II)_{excess}$ increase at the expense of FeS. We therefore propose that interfacial FeS in contact with lepidocrocite can also transfer electrons to the ferric (hydr)oxide in a similar way as adsorbed sulphide. Magnetite in this case reflects the steady-state product of this interaction.

The possibility of $Fe(II)_{excess}$ production upon the reaction of FeS with lepidocrocite is in agreement with the observed disappearance of the mackinawite rims at the lepidocrocite surfaces after 72 h (Fig. 2.8a), which seems to be accompanied by the generation of the amorphous material composed of not further identifiable iron and sulphur species separated from the lepidocrocite particles. Both, disaggregation of amorphous FeS and generation of $Fe(II)_{excess}$ in the second phase of the reaction can thus be assumed to contribute to the generation of precursors for pyrite formation in the third phase.

2.5.2. Implications for the pathway of pyrite formation

The products of the first two phases of the reaction are thermodynamically metastable and evolve further into more stable products during the third phase of the reaction. Based on thermodynamic considerations, pyrite and magnetite are the most stable minerals under the experimental conditions. Hence, the observed formation of pyrite and magnetite at the expense of FeS, $Fe(II)_{excess}$, and S(0) towards the end of the experiments (Fig. 8d) is consistent with thermodynamic predictions. The interaction between these components can be represented by the stoichiometry:

$$FeS + S(0) + Fe^{2+}_{excess} + 2\ FeOOH \rightarrow FeS_2 + Fe_3O_4 + 2\ H^+ \qquad (4)$$

This reaction accounts for the decrease in S(0) and pH as well as for the decrease in $Fe(II)_{HCl}$ concentration after 48 h of reaction (Fig 2.2), because magnetite and pyrite only marginally dissolve during 0.5 HCl extraction (Rickard and Morse, 2005). Although formation of pyrite is thermodynamically favored, pyrite formation upon the reaction of S(-II) with iron (hydr)oxides within 14 days has not been reported so far and FeS does not readily transform into pyrite (Rickard and Morse, 2005).

Occurrence of pyrite was first observed after 168 hours and was preceded by disappearance of mackinawite (Fig. 2.8). Typically, dissolution of FeS is regarded to be the initial step in a pyrite formation pathway proposed by Wang and Morse (1995) according to which Fe(II) reacts with polysulfide species to ultimately generate pyrite (Luther, 1991; Rickard et al., 1995; Wilkin and Barnes, 1996). It has been argued, however, that FeS is not any more of a precursor mineral as any other Fe phase to generate pyrite (Rickard & Luther, 2007) and it can be expected that basically all ingredients for pyrite formation are occurring in the suspensions.

We observed the onset of dissolution of mackinawite after 72 hours (Fig. 2.8) of reaction when also the concentration of S(0) and $Fe(II)_{HCl}$ started to decrease (Fig. 2.2).

Previous studies have shown that $FeS_{(aq)}$ is a key component in pyrite formation (Rickard et al., 1999; Rickard and Morse, 2005) and that pyrite formation is inhibited by suppression of $FeS_{(aq)}$ formation (Rickard et al., 2001). Formation of FeS clusters is typically related to dissolution of mackinawite (FeS_m) (Luther, 1991; Rickard, 2006; Rickard et al., 2001). The conversion of $FeS_{(aq)}$ to FeS_2 is postulated to occur via reaction with polysulphides (Luther, 1991):

$$FeS_{(aq)} + S_n^{2-} \rightarrow [FeS\text{-}S_n]^{2-} \rightarrow FeS_2 + S_{n-1}^{2-} \quad (5)$$

where $[FeS\text{-}S_n]^{2-}$ is an intermediate product.

Schoonen and Barnes (1991a) suggest that pyrite may grow directly from solution when the solution is supersaturated with respect to pyrite after dissolution of FeS. This is consistent with our observation that pyrite particles form spatially separated from the lepidocrocite surfaces (Fig. 2.8d). However, the nucleation of FeS_2 proceeds at a significant rate only, if intermediate sulphur species like polysulphides are present (Schoonen and Barnes, 1991b). Hence, the proposed mechanisms for pyrite formation have in common that polysulphides are involved in the process and the question arises how polysulphides might contribute to pyrite formation in the reaction of lepidocrocite with S(-II).

The accepted pathway for polysulphide formation is the dissolution of S(0) by dissolved sulphide (Hartler et al, 1967), the rate of which seems to be 2nd order with respect to dissolved sulphide in the absence of polysulphides and 1st order in their presence (Hartler et al, 1967). The activity of dissolved sulphide in our experimental systems needs to be controlled by the solubility of the remaining FeS and will be low. Moreover, S(-II) dissolving from FeS will tend to react in a competitive reaction with lepidocrocite so that one can assume that the polysulphide generation rate through this pathway and subsequently the overall pyrite formation rate would be low. We therefore propose that, through an additional pathway, the disappearance of $Fe(II)_{excess}$ during the third reaction phase could possibly contribute to polysulphide formation.

Magnetite, the expected product of $Fe(II)_{excess}$ reacting with lepidocrocite, could be detected by TEM analysis as separate entities not associated with the lepidocrocite crystals, but the magnetite concentrations in the solids were so low that they were not detectable by Mössbauer spectroscopy or XRD implying that part of the $Fe(II)_{excess}$ is consumed through another process. Formation of polysulphides by the reduction of S(0) with $Fe(II)_{excess}$ could provide an explanation for the concurrent disappearance of the two species. Production of $Fe(II)_{excess}$ in the first two reaction phases is driven by the presence of S(-II) or FeS at the lepidocrocite surface as described through reactions (eq. 1-3). Once, the pool of surface bound S(-II) is exhausted the driving force for $Fe(II)_{excess}$ generation is exhausted likewise. Under these circumstances, partial reduction of S(0) by $Fe(II)_{excess}$ leading to the formation of polysulphides

$$2\ Fe^{2+}{}_{excess} + S_n + 2\ H_2O \rightarrow FeOOH + S_n^{2-} + 4\ H^+ \quad (6)$$

might be thermodynamically feasible if the polysulphides are, in turn, directly consumed in the formation of pyrite as described through reaction (5).

According to this reaction model, the occurrence of $Fe(II)_{excess}$ acts as an intermediate storage of electrons created during the conversion of lepidocrocite into pyrite upon reaction with S(-II). Chemical reduction of elemental sulphur typically requires a strongly reducing reagent, such as Cr^{2+}, and it may therefore be hypothesized that the redox potential of the stored electrons is rather low compared to that of any other Fe(II) species. According to our model, the built up of this stock of electrons thus facilitates the formation of polysulphides in the third phase of the reaction and by this accounts for the formation of pyrite. However, direct evidence for the proposed mechanism of polysulphide formation from $Fe(II)_{excess}$ is lacking and requires further investigation.

2.6. Implications for sedimentary processes

This study has provided novel insights into the dynamic redox processes occurring at the surface and in the vicinity of the lepidocrocite crystals upon reaction with dissolved sulphide. The major initial product of these interactions is mackinawite forming at the surface of the lepidocrocite crystals within minutes. We were able to demonstrate that complete conversion of S(-II) to pyrite at room temperature occurred within 2 weeks, a time period that is much shorter than formation rates previously observed in FeS aging experiments with sulphur species such as S(0), polysulphides, or dissolved sulphide (Rickard and Morse, 2005; Schoonen and Barnes, 1991a; Schoonen 2004). In this study, pyrite formed much faster than expected for abiotic reactions in the absence of dissolved sulphide and matches the time scale of pyrite formation in salt marsh sediments and subtidal sediments where the pyrite formation occurs within 2 days (Howarth, 1979; Howarth and Jörgensen, 1984).

We propose that the rapid conversion observed in our study is related to the close interaction between FeS and the ferric (hydr)oxide surface that serves as an oxidant for FeS. The electrons appeared to be transferred between lepidocrocite and mackinawite through magnetite as an interfacial layer and to eventually lead to disaggregation of mackinawite being followed by generation of polysulphides even in the absence of dissolved sulphide. This step seems to be essential, since it allows for the physical separation of the location of pyrite precipitation from that of FeS as being postulated in several previous experimental and field

observations (Raiswell et al., 1993). In this study we were able to prove the spatial dislocation through the HRTEM images made.

In a broader sense, dissolved sulphide has two functions during the interaction with lepidocrocite: it generates Fe(II) (respectively excess electrons) driving the transformation of this mineral and it is a sulphide source for FeS formation at the surface generating a highly reactive redox interface. The extent of FeS and/or Fe(II) formation, however, seems to depend on the ratio between dissolved sulphide and the amount of surface sites available. At low S(-II):SS ratios, the concentration of dissolved sulphide is low relative to the concentration of reactive surface sites which matches conditions in freshwater or groundwater systems. It may be hypothesized that excess reactive Fe surface sites in the presence of sulphide may create highly reactive excess Fe(II) and thus affect the reactivity of ferric (hydr)oxides. In this study, we have proposed a pathway to generate polysulphides through reduction of S(0). This concept may be even extended to contaminants that undergo abiotic reduction at the surface of ferric (hydr)oxides to which Fe^{2+} is adsorbed (e. g. Pecher et al., 2002; Elsner et al., 2004).

In contrast, high S(-II):SS ratios reflect the conditions in marine systems. According to the results derived in this work, the formation of excess Fe(II) would be suppressed by the fast formation of FeS and its further conversion into pyrite in these systems. This consideration implies the hypothesis that the pathways of pyrite formation through reaction of sulphide with ferric (hydr)oxides are different between fresh and ground water systems and marine environments because the mechanism of polysulphide generation is different.

The question arises, whether the observation made in this work can be generalized in regard to other ferric (hydr)oxides, since their reactivity in regard to Fe^{2+} is different (Cornell & Schwertmann). The key for understanding the kinetics of pyrite formation under sedimentary conditions but also in ground-water systems is therefore related to the understanding of the formation pathways of FeS and polysulphide as related to the specific ferric (hydr)oxides.

2.7. Acknowledgements

This research was supported by the Deutsche Forschungsgemeinschaft (DFG). The project was part of the DFG Research Unit 580 “Electron Transfer Processes in Anoxic Aquifers” (PE 438/11-2). KP was supported by grant 03G0718A from the R&D-Programme GEOTECHNOLOGIEN funded by the German Ministry of Education and Research (BMBF) (publication no. GEOTECH- XXXX). We thank the staff members of the Department of Hydrology, University of Bayreuth for help and support. Furthermore, we thank Prof. Stefan

Haderlein and Prof. Andreas Kappler, University of Tübingen, for using their Mössbauer spectroscopic instrument.

We would like to thank three anonymous reviewers for their helpful comments on an earlier version of this paper.

2.8. References

Burton, E.D., Bush, R.T., Sullivan, L.A. and Mitchell, D.R.G., 2008. Schwertmannite transformation to goethite via the Fe(II) pathway: Reaction rates and implications for iron-sulfide formation. *Geochimica Et Cosmochimica Acta*, **72(18)**: 4551-4564.

Burton, E.D., Bush, R.T., Sullivan, L.A., Hocking, R.K., Mitchell, D.R.G., Johnston, S.G., Fitzpatrick, R.W., Raven, M., McClure, S.m Jang, L.Y., 2009. Iron monosulfide oxidation in natural sediments: Resolving microbially-mediated S transformations using XANES, electron microscopy and selective extractions. Environmental Sciences & Technology **43**: 3128-3134.

Canfield D. E., Raiswell R. and Bottrell S., 1992. The reactivity of sedimentary iron minerals toward sulphide. *American Journal of Science*, **292**: 659-683.

Catalano, J.G., Fenter, P., Park, C., Zhang, Z. and Rosso, K.M., 2010. Structure and oxidation state of hematite surfaces reacted with aqueous Fe(II) at acidic and neutral pH. *Geochimica Et Cosmochimica Acta*, **74(5)**: 1498-1512.

Cornell, R.M. and Schwertmann, U., 1996. The iron oxides. *VCH*, 573 pp.

Coughlin, B.R. and Stone, A.T., 1995. Nonreversible Adsorption of Divalent Metal-Ions (Mn-Ii, Co-Ii Ni-Ii Cu-Ii and Pb-Ii) onto Goethite - Effects of Acidification, Fe-Ii Addition, and Picolinic-Acid Addition. *Environmental Science & Technology*, **29(9)**: 2445-2455.

Cudennec, Y. and Lecerf, A., 2005. Topotactic transformations of goethite and lepidocrocite into hematite and maghemite. *Solid State Sciences*, **7(5)**: 520-529.

Cutting, R.S., Coker, V.S., Fellowes, J.W., Lloyd, J.R. and Vaughan, D.J., 2009. Mineralogical and morphological constraints on the reduction of Fe(III) minerals by Geobacter sulfurreducens. *Geochimica Et Cosmochimica Acta*, **73(14)**: 4004-4022.

Dos Santos Afonso, M. and Stumm, W., 1992. Reductive Dissolution of iron(III) (hydr)oxides by hydrogen sulfide. *Langmuir*, **8**: 1671-1675.

Elsner M., Schwarzenbach R. P., Haderlein S. B. (2004): Reactivity of Fe(II) bearing minerals toward reductive transformation of organic contaminants. *Environ. Sci. Technol.*, **38**: 799-807

Ewing, F.J., 1935. The crystal structure of lepidocrocite. *Journal of Chemical Physics*, **3**: 420-424.

Fonselius S., Dyrssen D. and Yhlen B., 1999. Determination of hydrogen sulphide. In: Grasshoff K., Kremling K. and Ehrhardt M. (Editors), *Methods of Seawater Analysis*.

Wiley-VCH, Weinheim, New York, Chichester, Brisbane, Singapore, Toronto, pp. 91-108.

Handler, R.M., Beard, B.L., Johnson, C.M. and Scherer, M.M., 2009. Atom Exchange between Aqueous Fe(II) and Goethite: An Fe Isotope Tracer Study. *Environmental Science & Technology*, **43(4)**: 1102-1107.

Hansel, C.M., Benner, S.G. and Fendorf, S., 2005. Competing Fe(II)-induced mineralization pathways of ferrihydrite. *Environ. Sci. Technol.*, **39**: 7147-7153.

Hansel, C.M., Benner, S.G., Nico, P. and Fendorf, S., 2004. Structural constraints of ferric (hydr)oxides on dissimilatory iron reduction and the fate of Fe(II). *Geochim. Cosmochim. Acta*, **68(15)**: 3217-3229.

Hartler, N., Libert, J., Teder A., 1967. Rate of Sulphur Dissolution in Aqueous Sodium Sulfide. *Ind. Eng. Chem. Process Des. Dev.*, **6 (4)**: 398–406.

Hiemstra, T. and van Riemsdijk, W.H., 2007. Adsorption and surface oxidation of Fe(II) on metal (hydr)oxides. *Geochim. Cosmochim Atcta*, **71(24)**: 5913-5933.

Howarth, R. W., Jörgensen, B. B., 1984. Formation of ^{35}S-labelled elemental sulfur and pyrite in coastal marine sediments (Limfjorden and Kysing Fjord, Denmark) during short term $^{35}SO_4^{2-}$-reduction measurements. Geochim. Cosmochim. Acta **48**: 1807-1818.

Howarth, R. W., 1979. Pyrite: Its rapid formation in a salt marsh and its importance in ecosystem metabolism. Science **203**: 49-51.

Jeon, B.H., Dempsey, B.A. and Burgos, W.D., 2003. Kinetics and Mechanisms for Reactions of Fe(II) with Iron (III) Oxides. *Envion. Sci. Technol.*, **37**: 3309-3315.

Jeon, B.H., Dempsey, B.A., Burgos, W.D. and Royer, R.A., 2001. Reactions of ferrous iron with hematite. *Colloids and Surfaces a-Physicochemical and Engineering Aspects*, **191(1-2)**: 41-55.

Larese-Casanova, P. and Scherer, M.M., 2007. Fe(II) sorption on hematite: New insights based on spectroscopic measurements. *Environ. Sci. Technol.*, **41**: 471-477.

Luther, G.W, 1990. The frontier-molecular-orbital theory approach in geochemical processes. In: Stumm W. (Editor), *Aquatic Chemical Kinetics: Reaction Rates of Processes in Natural Waters*, pp. 173-198.

Luther, G.W., 1991. Pyrite synthesis via polysulfide compounds. *Geochemica et Cosmochemica Acta*, **55**: 2839-2849.

Luther, G.W., 2010. The role of one- and two-electron transfer reactions in forming thermodynamically unstable intermediated as barriers in multi-electron redox reactions. *Aquatic Geochemistry*, **16(3)**: 395-420.

Ohfuji, H. and Rickard, D., 2006. High resolution transmission electron microscopic study of synthetic nanocrystalline mackinawite. *Earth and Planetary Science Letters*, **241(1-2)**: 227-233.

Pecher K., Haderlein S. B., Schwarzenbach R. P. (2002): Reduction of polyhalogenated methanes by surface-bound Fe(II) in aqeuous suspensions of iron oxides. *Environ. Sci. Technol.*, **36**: 1734-1741

Peiffer, S., 1994. Reaction of H_2S with Ferric Oxides - Some Conceptual Ideas on Its Significance for Sediment-Water Interactions. In: L.A. Baker (Editor), *Environmental Chemistry of Lakes and Reservoirs*. Advances in Chemistry Series. Amer Chemical Soc, Washington, pp. 371-390.

Peiffer, S., Dos Santos Afonso, M., Wehrli, B. and Gächter, R., 1992. Kinetics and mechanism of the reaction of H_2S with lepidocrocite. *Environ. Sci. Technol.*, **26(12)**: 2408-2413.

Peiffer, S. and Gade, W., 2007. Reactivity of ferric oxides toward H_2S at low pH *Environ. Sci. Technol.*, **41**: 3159-3164.

Poulton S. W., Krom D. M. and Raiswell R., 2004. A revised scheme for the reactivity of iron (oxyhydr)oxide minerals towards dissolved sulfide. *Geochim. Cosmochim. Acta*, **68(18)**: 3703-3715.

Poulton, S.W., 2003. Sulfide oxidation and iron dissolution kinetics during the reaction of dissolved sulfide with ferrihydrite *Chemical Geology*, **202**: 79-94.

Pyzik, A.J. and Sommer, S.E., 1981. Sedimentary iron monosulphides: kinetics and mechanism of formation. *Geochim. Cosmochim. Acta*, **45**: 687-698.

Raiswell, R., Whaler, K., Dean, S., Coleman, M.L. and Briggs, D.E.G., 1993. A Simple 3-Dimensional Model of Diffusion-with-Precipitation Applied to Localized Pyrite Formation in Framboids, Fossils and Detrital Iron Minerals. *Marine Geology*, **113(1-2)**: 89-100.

Rickard, D., 1974. Kinetics and mechanism of the sulfidation of goethite. *American Journal of Science*, **274**: 941-952.

Rickard, D., 1975. Kinetics and Mechanism of Pyrite Formation at Low Temperatures. *American Jounal of Science*, **275**: 636-652.

Rickard, D., 1995. Kinetics of Fes Precipitation .1. Competing Reaction-Mechanisms. *Geochimica Et Cosmochimica Acta*, **59(21)**: 4367-4379.

Rickard, D., 2006. The solubility of FeS. *Geochimica Et Cosmochimica Acta*, **70(23)**: 5779-5789.

Rickard, D., Butler, I.B. and Oldroyd, A., 2001. A novel iron sulphide mineral switch and its implications for Earth and planetary science. *Earth and Planetary Science Letters*, **189(1-2)**: 85-91.

Rickard, D., Oldroyd, A. and Cramp, A., 1999. Voltammetric evidence for soluble FeS complexes in anoxic estuarine muds. *Estuaries*, **22(3A)**: 693-701.

Rickard, D., Schoonen, M.A.A. and Luther, G.W., 1995. Chemistry of iron sulfides in sedimentary environments. In: M.A. Vairavamurthy and M.A.A. Schoonen (Editors), *Geochemical Transformations of Sedimentary Sulfur*. Acs Symposium Series. Amer Chemical Soc, Washington, pp. 168-193.

Rickard, D.T. and Morse, J.W., 2005. Acid volatile sulfide (AVS). *Mar. Chem.*, **97(3-4)**: 141-197.

Rosso, K.M., Yanina, S.V., Gorski, C.A., Larese-Casanova, P. and Scherer, M.M., 2010. Connecting Observations of Hematite (alpha-Fe2O3) Growth Catalyzed by Fe(II). *Environmental Science & Technology*, **44(1)**: 61-67.

Schoonen, M.A.A., 2004. Mechanisms of sedimentary pyrite formation In: Amend J.P., Edwards K.J. and Lyons T. W. (Editors), *Sulfur Biogeochemistry - Past and Present.* Geological Society of America Special Paper 379, pp. 117-134.

Schoonen, M.A.A. and Barnes, H.L., 1991a. Reactions Forming Pyrite and Marcasite from Solution .1. Nucleation of Fes2 Below 100-Degrees-C. *Geochimica Et Cosmochimica Acta*, **55(6)**: 1495-1504.

Schoonen, M.A.A. and Barnes, H.L., 1991b. Reactions Forming Pyrite and Marcasite from Solution .2. Via Fes Precursors Below 100-Degrees-C. *Geochimica Et Cosmochimica Acta*, **55(6)**: 1505-1514.

Silvester, E. et al., 2005. Redox potential measurements and Mossbauer spectrometry of Fe-II adsorbed onto Fe-III (oxyhydr)oxides. *Geochimica Et Cosmochimica Acta*, **69(20)**: 4801-4815.

Stumm, W. and Sulzberger, B., 1992. The Cycling of Iron in Natural Environments - Considerations Based on Laboratory Studies of Heterogeneous Redox Processes. *Geochimica Et Cosmochimica Acta*, **56(8)**: 3233-3257.

Tamaura, Y., Ito, K. and Katsura, T., 1983. Transformation of □-FeO(OH) to Fe_3O□ by Adsorption of Iron(II) Ion on γ-FeO(OH). *J. Chem. Soc. Dalton Trans.* **(2)**: 189-194.

Tamura H., Goto K., Yotsuyanagai T. and M., N., 1974. Spectrophotometric determination of iron(II) with 1,10-phenanthroline in the presence of large amounts of iron(III). *Talanta*, **21**: 314-318.

Tronc, E., Belleville, P., Jolivet, J.P. and Livage, J., 1992. Transformation of Ferric Hydroxide into Spinel by Fe(Ii) Adsorption. *Langmuir*, **8(1)**: 313-319.

Wang, F. and Morse, J.W., 1995. Pyrite formation under conditions approximating those in anoxic sediments: I. Pathways and morphology. *Marine Chemistry,* **52**: 99-121.

Wilkin, R.T. and Barnes, H.L., 1996. Pyrite formation by reactions of iron monosulfides with dissolved inorganic and organic sulfur species. *Geochimica Et Cosmochimica Acta,* **60(21)**: 4167-4179.

Williams, A.G.B. and Scherer, M.M., 2004. Spectroscopic evidence for Fe(II)-Fe(III) electron transfer at the iron oxide - water interface *Envion. Sci. Technol.,* **38**: 4782-4790.

Yao, W. and Millero, F.J., 1996. Oxidation of hydrogen sulfide by hydrous Fe(III) oxides in seawater. *Mar. Chem.,* **52**: 1-16.

3. The influence of structural properties of ferric (hydr)oxides 6-line ferrihydrite, lepidocrocite, and goethite on reaction pathways with sulphide

Planned submission to Geochimica et Cosmochimica Acta

Katrin Hellige[1], Kilian Pollok[2], Philip Larese-Casanova[3], Thilo Behrends[4] and Stefan Peiffer[1]

[1]Department of Hydrology, University of Bayreuth, Universitätsstraße 30, D-95445 Bayreuth, Germany

[2]Bayerisches Geoinstitut, University of Bayreuth, Universitätsstraße 30, D-95445 Bayreuth, Germany

[3]Department of Geology and Geophysics, University of Yale, P.O. Box 208109, New Haven, CT 06520-8109 USA

[4]Department of Earth Sciences, Geochemistry, Utrecht University, P.O. Box 80021, 3508 TA Utrecht, The Netherlands

3.1. Abstract

The reductive dissolution of ferric (hydr)oxides in sulphide-rich systems is a complex process, including the interaction of Fe(II) and S(-II) with the oxide surface, electron transfer, the formation of nanocrystalline minerals onto the oxide surface, transformation to secondary minerals, and the formation of iron sulphides. These reactions are influenced by structural properties of the various ferric (hydr)oxides. To elucidate the dynamics of these surface reactions we conducted batch experiments in a glove box at pH 7 using various ferric (hydr)oxides (ferrihydrite, lepidocrocite, and goethite) and dissolved sulphide. The nanocrystalline products forming at different time steps in close contact to the ferric (hydr)oxides surface were explored over 2 weeks by wet chemistry analysis, TEM, and Mössbauer spectroscopy.

Wet chemistry showed that dissolved sulphide was consumed rapidly and S(0) and $Fe(II)_{HCl}$ were the main products in each experimental solution. But the formation of S(0) and Fe(II) was decoupled and the most of Fe(II) was not bound in FeS but rather associated with the oxide surface whereby, electrons may transferred between the structural Fe(III) and the surface bound Fe(II). These electron transfers led to the formation of excess-Fe(II) which amounts depending on electron transfer properties and the adsorption properties of the Fe(III) solid phases. As the amount of excess-Fe(II) exceeded the concentration of surface sites, a large proportion had to be located in the bulk phase of the oxide. The ability to form excess-Fe(II) and to accommodate Fe(II) in the bulk phase increased in the order goethite > lepidocrocite > ferrihydrite which agrees to the order of the specific surface area.

After two weeks we observed the formation of secondary minerals and pyrite in all experiments as a result of excess-Fe(II) formation. Ferrihydrite was transformed completely via dissolution-precipitation processes into more stable minerals such as magnetite, hematite, pyrite, and into minor amounts of goethite. In the experimental solution with lepidocrocite and goethite the host mineral remained and we detected only pyrite as new mineral. Small amounts of goethite were transformed to hematite while the pyrite formation in the experimental solution with lepidocrocite was accompanied by traces of magnetite.

We proposed that the sequence of mineral transformations and the pyrite formation are promoted by excess-Fe(II), whereby the excess-Fe(II) formation is more facilitate for ferrihydrite and lepidocrocite due to a higher specific surface area compared to goethite.

Keywords: ferric (hydr)oxides reduction, dissolved sulphide, ferrous iron, ferrihydrite, lepidocrocite, goethite, pyrite formation, magnetite, electron transfer

3.2. Introduction

Ferric (hydr)oxides are ubiquitous with different characteristics such as stability, reactivity and surface properties (Cornell and Schwertmann, 1996). Under anoxic conditions ferric (hydr)oxides are reduce by dissolved sulphide (Dos Santos Afonso and Stumm, 1992; Peiffer, 1994; Peiffer et al., 1992; Peiffer and Gade, 2007; Poulton et al., 2004; Pyzik and Sommer, 1981) or by microbes (Canfield et al., 1992; Hansel et al., 2003; Hansel et al., 2004) which generated soluble Fe^{2+} at acidic pH. At higher pH the generated Fe^{2+} is often bound to FeS which is prevalent the final product of the reductive dissolution of ferric (hydr)oxides by dissolved sulphide at circumneutral pH (Rickard, 1974; Rickard, 1975). This implies that two parallel pathways exist for the consumption of dissolved sulphide which are (i) oxidation by Fe(III) and (ii) precipitation with Fe^{2+} at circumneutral pH. Furthermore, during the reduction of ferric (hydr)oxides most of the adsorbed species such as arsenic will be released from the oxide surfaces to solution (Pedersen, 2006). Hence, the fate of Fe(II) have a direct influence on the biogeochemical cycling of Fe and is associated with nutrients and contaminants. In addition, at higher pH Fe(II) may adsorbed to the Fe(III) (hydr)oxide surfaces and react with them resulting in their transformation. This reaction which is usually explained by electron transfer from adsorbed Fe(II) to structural Fe(III) (Jeon et al., 2003; Jeon et al., 2001; Pedersen et al., 2005; Tronc et al., 1992; Williams and Scherer, 2004), is primary controlled by Fe(II) concentration (Hansel et al., 2005; Hansel et al., 2004; Jeon et al., 2003; Jeon et al., 2001; Liu et al., 2009; Liu et al., 2005).

The reductive dissolution of ferric (hydr)oxides by dissolved sulphide is a surface controlled process proposed by Dos Santos Afonso and Stumm (1992). After the reduction of Fe(III) at the ferric (hydr)oxide surface, the reaction can only proceed after surface bound Fe(II) is released into solution and a new surface site is exposed. According to this mechanism reductive dissolution of Fe(III) (hydr)oxides by dissolved sulphide at circum neutral pH is expected to accompanied by FeS precipitation. Poulton et al. (2004) investigated the reaction of various ferric (hydr)oxides with dissolved sulphide at pH 7.5 and observed the accumulation of acid extractable Fe(II) which is neither in the form of FeS nor exchangeable with other cations. They consider this fraction of acid extractable Fe(II) as “surface bound” but the amount of Fe(II) in this pool exceeds the number of sites at the Fe(II) oxide surface several times so that a considerable part of this Fe(II) has to be located in the bulk phase. In the following, we will refer to the pool of acid extractable Fe(II) which is not bound in FeS as “excess-Fe(II)”.

In a previous study we investigated the evolution of the reaction of lepidocrocite with dissolved sulphide at pH 7 over a period of up to 14 days by a combination of chemical analysis, spectroscopic, and microscopic measurements (Hellige et al., 2010). During the reduction of lepidocrocite by dissolved sulphide, S(0) and acid extractable Fe(II) which consisted of FeS and surface-associated Fe(II) were formed which corresponds well to the findings of Poulton et al. (2004). Electron transfer from surface bound Fe(II) to bulk Fe(III) leads to the formation of excess-Fe(II) and the recycled Fe(III) at the surface is available to oxidize an additional S(-II) (Catalano et al., 2010; Handler et al., 2009; Silvester et al., 2005). Due to this mechanism, oxidation of S(-II) can proceed without release of Fe(II) into solution and precipitation of FeS. However, lepidocrocite containing excess-Fe(II) is instable and after complete consumption of aqueous S(-II) the reaction proceeds involving further electron transfer reactions and mineral transformations (Hellige et al., 2010). These mineral transformations include intermediate formation of magnetite, dissolution of FeS and formation of pyrite.

The question is, whether the formation of excess-Fe(II) is a common feature of the reaction of Fe(III) (hydr)oxides with dissolved sulphide. We hypothesize that the extent of excess production of Fe(II) is different for the various ferric (hydr)oxides and depends on their electron transfer properties and their ability to accommodate Fe(II) within the structure. Furthermore, we proposed in the previous study that formation of excess-Fe(II) triggered the sequence of mineral transformations and promoted the formation of pyrite (Hellige et al., 2010). Hence, the evolution of the system after complete consumption of dissolved sulphide and the type and concentrations of secondary Fe minerals being formed is dependent on the amount of excess-Fe(II) and the reactivity of the remaining Fe(III) (hydr)oxide phase. Here, we compare the reductive dissolution of lepidocrocite with those of ferrihydrite and goethite, representing a less stable or more stable iron oxide phase, respectively. We conducted batch experiments with the same set-up and analysis as described in Hellige et al. (2010) to investigate their transformation by Fe(II) and the formation of pyrite in sulphide-rich systems at pH 7 in regard to the reaction rates, intermediate phases, and the final products.

3.3. Materials and methods

All solutions were prepared with distilled water and bubbled with N_2 to remove oxygen from solutions. All reagents were of analytical grade.

3.3.1. Ferric (hydr)oxides

Synthetic 6-line ferrihydrite was prepared after Schwertmann and Cornell (2000). Under rapid stirring 20 g of $Fe(NO_3)_3*9H_2O$ was added to 2 L 75°C hot distilled water. After 12 minutes of stirring, the solution was cooling and dialyses for three days. The final product was freeze dried.

Synthetic lepidocrocite and goethite were purchased from Lanxess (Leverkusen, Germany). The trade names are Bayferrox 920 Z for goethite and Bayferrox 943 for lepidocrocite. To remove ions like sulphate from the iron oxides surface, 1 mol L^{-1} of it was suspended in 0.01 mol L^{-1} $NaNO_3$ and the pH was adjusted to 10 with NaOH. After 4 days of shaking the iron oxides solution was washed and freeze-dried.

The ferric (hydr)oxides were characterized using X-ray diffractometry (XRD), scanning electron microscopy (SEM), and transmission electron microscopy (TEM). XRD and TEM measurements showed lepidocrocite contaminated with goethite with a particle size of 0.2-0.4 µm and pure goethite with a particle size of 0.2-0.9 µm. Surface area was measured by multi-point BET-N_2 (Brunauer, Emmett and Teller) method (Gemini 2375 Surface Area Analyzer). Surface area were determined as 140 m^2 g^{-1} for ferrihydrite, 17.34 m^2 g^{-1} for lepidocrocite and 9.12 m^2 g^{-1} for goethite.

3.3.2. Experimental Set-up

Kinetic batch experiments with 12-45 mmol L^{-1} ferric (hydr)oxide and dissolved sulphide (4-11 mmol L^{-1}) were conducted at pH 7, at a constant ionic strength (I = 0.1 M NaCl), and at room temperature (Hellige et al., 2010). All reactions took place in a 500-mL glass vessel with ports for sampling and removals, pH electrode and HCl addition within anoxic glove box. The solution was stirred with a Teflon-coated stirring bar at constant rate. With an automatic pH-stat device the pH value was kept constant by adding HCl (0.5 mol L^{-1}).

The reaction solution was prepared by mixing 50 mL of solution I (0.1 mol L^{-1} NaCl) containing ferric (hydr)oxide with 450 ml of solution II (0.1 mol L^{-1} NaCl) to which aliquots of Na_2S*9H_2O (0.5 mol L^{-1}) and HCl (0.5 mol L^{-1}). The sulphide concentration was determined before each run. The initial solution conditions and the consumption of acid are shown in Table 3.1.

During the reaction and after 1-2 hours, 24 hours, 1 week and 2 weeks the following species were determined: dissolved Fe(II) and S(-II), Fe(II) extractable with 0.5 N HCl, S(0), and

total iron. Furthermore samples were analyzed by Mössbauer spectroscopy and TEM to trace changes in the solid phase assemblage over a period of 2 weeks.

3.3.3. Sampling and analysis

All samples were taken within the glovebox and were immediately purged with N_2 to dispel H_2S within the glovebox.

Iron species. The iron species total iron (Fe_{TOT}), solid phase bound Fe(II) ($Fe(II)_{HCl}$), and dissolved Fe(II) ($Fe(II)_{diss}$) were determined after addition of HCl using the phenanthroline method of Tamura (1974). Dissolved Fe(II) was measured on filtered (0.45 µm) samples using 0.5 N HCl, while total iron was measured on unfiltered samples using 6 N HCl. After the extraction of the solid phase bound Fe(II) with 0.5 N HCl, the solution was filtered and Fe(II) was determined.

Sulphur species. Dissolved sulphide was determined photometrically by methylene blue method of Fonselius (1999) after filtration. Elemental sulphur content of the solid and aqueous phase was measured by high performance liquid chromatography (HPLC, Beckman) combined with UV detection (Detector 168, Beckman) after extraction with methanol (modified after Ferdelman et al., 1991). Therefore 300 µL of unfiltered sample was suspended in 1200 µL methanol. After 1 h equilibration time the solution was filtered (0.2 µm) and stored at -20°C until analyses.

Mössbauer spectroscopy. 30 mL of the suspension was filtered (membrane filter paper, 13 mm diameter and 0.45 µm) and was sealed between two layers of Kapton tape (polyamide tape with very low oxygen permeability). The samples were placed in an anoxically sealed crimp vial and stored at 4°C until measurement. Mössbauer spectra were collected with a WissEl Mössbauer gamma-ray spectrometer and a Janis closed-cycle helium gas cryostat that allowed for sample temperatures down to 4.2 K. A Co-57 gamma-ray source was used with a constant acceleration drive system operated in transmission mode. Spectra were calibrated against a spectrum of alpha-Fe(0) foil at room temperature. Data acquisition times were usually about 12-20 hours per spectrum. Spectral fitting was performed using Recoil® software (University of Ottawa, Canada) and Voigt-based spectral lines.

Transmission electron microscopy. At different time steps aliquots of the reacting suspension were analyzed by a Philips CM 20-FEG TEM, operating at 200 kV. In order to limit oxidation in air during sample preparation the suspension was first sampled in gas-tight vials. A drop of solution was then taken with a syringe and put onto a Lacey carbon-coated copper grid. The

grid was immediately transferred to the TEM holder and inserted into the high vacuum of the TEM. The short exposure of the sample to air was limited to 1-2 minutes at maximum with this procedure.

The chemical composition and the distribution of elements were determined by energy-dispersive X-ray spectroscopy (Thermo Noran Ge detector).

Table 3.1. Initial conditions for each run. All runs were conducted at pH 7 and the chemical speciation was analyzed. TEM measurements were performed in run 13, 14, 21, 24, 26, and 27. Mössbauer spectroscopy was used for 14, 16, 17, and 24.

Run no.	Mineral	Runtime (hours)	Mineral concentration (mmol L^{-1})	Surface area (m^2 L^{-1})	Surface sites[a] (mmol L^{-1})	Initial sulphide concentration (mmol L^{-1})	H^+ consumption during pH reaction[b] (mmol L^{-1})	H^+ consumption during pH adjustment[c] (mmol L^{-1})
23	Ferrihydrite	1.5	28	362	2.28	7.3	0.4	12.7
24	Ferrihydrite	336	12	155	0.98	7.5	1.6	10.1
25	Ferrihydrite	1	30	388	2.44	8.1	0.3	13.1
9	Lepidocrocite	3	14	21.6	0.14	9	2.9	13.9
11	Lepidocrocite	1.5	21.8	33.6	0.21	7.9	2.5	13.1
12	Lepidocrocite	1.5	16.8	25.9	0.16	8.8	2.8	13.7
13	Lepidocrocite	1.5	27.5	42.4	0.27	8.3	2.8	12.9
14	Lepidocrocite	336	26.6	41.1	0.26	7.2	2.9	9.8
20	Lepidocrocite	7	25.6	39.5	0.25	6.7	2.9	10.9
26	Lepidocrocite	336	27.2	42	0.26	7.4	3	10
27	Lepidocrocite	336	20.5	31.6	0.20	3.7	1.3	5.1
10	Goethite	4	24	19.5	0.12	8.9	2.7	13.8
15	Goethite	19	35	28.4	0.18	8.6	3.5	13.4
16	Goethite	12	45	36.5	0.23	10	3.9	14.2
17	Goethite	168	32	26	0.16	11	4.1	15.1
21	Goethite	336	22	17.9	0.11	6.7	3.2	10.8

[a]Concentration of surface sites was calculated based on a value of $6.3*10^{-6}$ mol m^{-2} for all minerals (Peiffer and Gade, 2007)
[b]H^+ consumption after addition of lepidocrocite
[c]H^+ consumption in order to adjust the pH in the sulphide solution before the addition of lepidocrocite

3.3.4. Equilibrium Thermodynamics

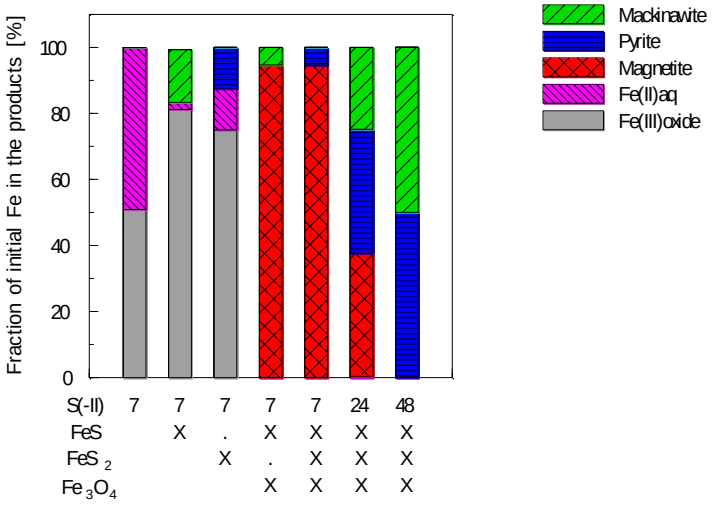

Fig. 3.1. Equilibrium distribution of Fe in the products of the reaction of 28 mM ferrihydrite with $S(-II)_{diss}$ at pH 7 (run 23). The calculations are based on the assumption that S is not oxidized beyond the redox state of elemental sulphur. In the calculations the amount of $S(-II)_{aq}$ was varied and is listed below the bars. Furthermore, different assemblages of solids were taken into considerations in the calculations. Minerals, which were allowed to from in the calculations are indicated by "X" in the table below the graph.

Fig. 3.1 shows the calculated equilibrium distribution of Fe in the products of the reaction with ferrihydrite and different concentrations of dissolved sulphide. These calculations were performed by using MINEQL. The first three scenarios demonstrate, that a larger fraction of Fe(III) can be reduced when the formation of FeS or FeS_2 are kinetically hindered. In the first scenario where no secondary minerals are formed, half of the Fe(III) is supposed to become reduced upon addition of 7 mM S(-II). In contrast, the formation of mackinawite prevents about 64% of the added S(-II) to become oxidized by Fe(III) and, consequently, the fraction of reduced iron is considerably smaller than without mackinawite formation. However, the formation of pyrite is thermodynamically more favourable than mackinawite precipitation and the electron balance requires that the formation of one mol pyrite is accompanied by one extra mol Fe(II). Hence, the fraction of Fe(II) is larger when pyrite is formed compared to the formation of mackinawite. After complete oxidation of S(-II) the system proceeds towards an energetically more favourable state by forming FeS or FeS_2, then a part of the Fe(II) is expected to become re-oxidized.

Scenarios 4 and 5 demonstrate that the formation of magnetite is energetically more favourable than FeS and FeS_2 precipitation. The amount of excess-Fe(II) which can eventually be accommodated in magnetite is limited by the availability of Fe(III). But increasing initial S(-II)/Fe(III) ratios lead to decreasing fractions of magnetite in favour of

pyrite and mackinawite formation (scenario 6). Hence, when the added amount of $S(-II)_{aq}$ exceeds 16.5% of the initial concentration of Fe(III), mackinawite or pyrite are expected to form together with magnetite.

In conclusion, magnetite formation is the thermodynamically most favourable sink for excess-Fe(II), provided excess-Fe(II) does not exceed 50% of the remaining Fe(III). When larger amounts of excess-Fe(II) are formed, only the formation of pyrite and/or mackinawite is expected. The latter might require partial re-oxidation of Fe(II) if not sufficient reduced sulphur is available for precipitating the required amounts of pyrite and mackinawite.

3.4. Results

3.4.1. Chemical speciation

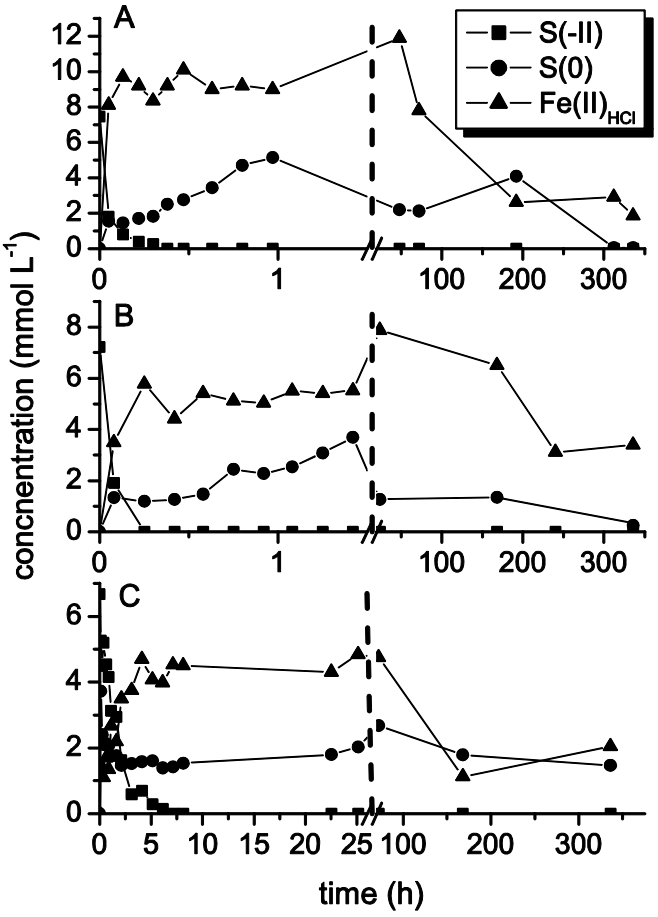

Fig. 3.2. Evolution of sulphur and iron species during the reaction between dissolved sulphide and ferrihydrite (A, run 24), lepidocrocite (B, run 14), and goethite (C, run 21).

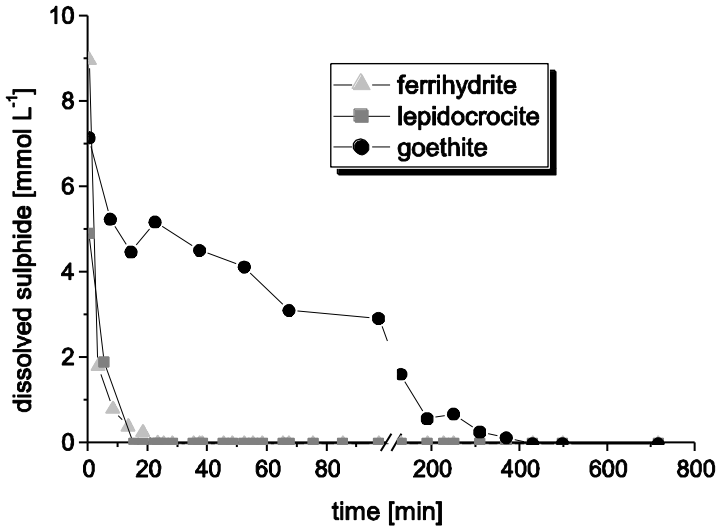

Fig. 3.3. Consumption of sulphide for the various ferric (hydr)oxides over time.

Fig. 3.2 shows the development of the formation of sulfur and iron species during the reaction of dissolved sulphide with the three ferric (hydr)oxides. The initial amounts of dissolved sulphide in the three suspensions were the same while the consumption of dissolved sulphide was different (Fig. 3.3). In the presence of ferrihydrite and lepidocrocite dissolved sulphide was consumed within fewer 30 minutes. In contrast, the reaction was slower when goethite was added and more than 5 hours were required to remove dissolved sulphide. The decrease in S(-II) was accompanied by production of Fe(II) and S(0) (Fig. 3.2). In all cases the concentration of dissolved Fe(II) was of little importance with a maximum concentration of 0.1-0.3 mmol L^{-1} (data not shown). The main amount of the formed Fe^{2+} was extractable with HCl which consisted of dissolved Fe(II), Fe(II)-S solid, and surface-associated Fe(II). In the following, we will refer to the $Fe(II)_{HCl}$ which is not bound in FeS as excess-Fe(II). In experiments with ferrihydrite and lepidocrocite $Fe(II)_{HCl}$ concentrations reached almost instantaneously a level which remained practically constant during the first hour of reaction (Fig. 3.2). Production of $Fe(II)_{HCl}$ followed S(-II) consumption in the experiments with goethite, and was hence slower compared to the reaction with ferrihydrite and lepidocrocite.

The ratio of produced Fe(II) per consumed S(-II) varied between the different minerals (Table 3.2). After the consumption of dissolved sulphide was completed and S(0) concentration reached its maximum value which was for ferrihydrite and lepidocrocite after approximately 1 hour and 5-10 hours for goethite excess-Fe(II) were calculated based on the S mass balance as

$$\text{excess-Fe(II)} = Fe(II)_{HCl}\text{-FeS} = Fe(II)_{HCl}\text{-}(S(-II)_{initial}\text{-}S(0)_{max}) \quad (1)$$

The highest relative concentrations of excess-Fe(II) are found for ferrihydrite (e.g. run 24 about 55 % excess-Fe(II)) while the relative excess-Fe(II) are lower for lepidocrocite and practically zero for goethite (Table 3.2). In all cases the increase of S(0) was slower than the production of Fe(II) which is most pronounced for ferrihydrite (Fig. 3.2).

Table 3.2. The concentrations of products during the reaction of H_2S with the three ferric (hydr)oxides. These values are the maximum concentration for S(0) and $Fe(II)_{HCl}$. Ferrihydrite and lepidocrocite reached the constant level of S(0) and $Fe(II)_{HCl}$ concentration within 1 hour while goethite required 5 to 10 hours.

Run no.	Mineral	$H_2S_{initial}$ (mmol L^{-1})	S(0) (mmol L^{-1})	$Fe(II)_{HCl}$ (mmol L^{-1})	Excess Fe(II) (mmol L^{-1})	Excess $Fe(II)/Fe_{TOT}$ (%)
24	Ferrihydrite	7.5	5.14	8.99	6.63	55.25
25	Ferrihydrite	8.1	2.85	12.92	7.67	25.57
9	Lepidocrocite	9	2.87	6.14	0.01	0.07
11	Lepidocrocite	7.9	1.79	6.55	0.54	2.48
12	Lepidocrocite	8.8	2.42	6.26	-0.12	
13	Lepidocrocite	8.3	1.58	7.22	0.5	1.82
14	Lepidocrocite	7.2	3.7	5.52	2.02	7.59
20	Lepidocrocite	6.7	4.18	8.52	6	23.44
26	Lepidocrocite	7.4	3.72	7.71	4.03	14.81
10	Goethite	8.9	1.58	4.69	-2.63	
15	Goethite	8.6	1.58	3.98	-3.04	
16	Goethite	10	3.14	4.79	-2.07	
17	Goethite	11	1.5	4.98	-4.52	
21	Goethite	6.7	0.29	1.28	-6.7	

In the presence of ferrihydrite the concentration of $Fe(II)_{HCl}$ had a maximum at 12 mmol L^{-1} after 24 hours which implies a complete reduction of the initial amount of ferrihydrite (Fig. 3.2A). But after 2 days, the reaction changed and $Fe(II)_{HCl}$ and S(0) started to decrease for all three minerals (Fig. 3.2). Whereas this decrease is more pronounced for $Fe(II)_{HCl}$ and in particular in the experiments with ferrihydrite.

Optically, all ferric suspensions turned black during the reaction with dissolved sulphide. But after 2 weeks the black coloration of the suspensions disappeared for goethite and lepidocrocite while the ferrihydrite suspension was still black.

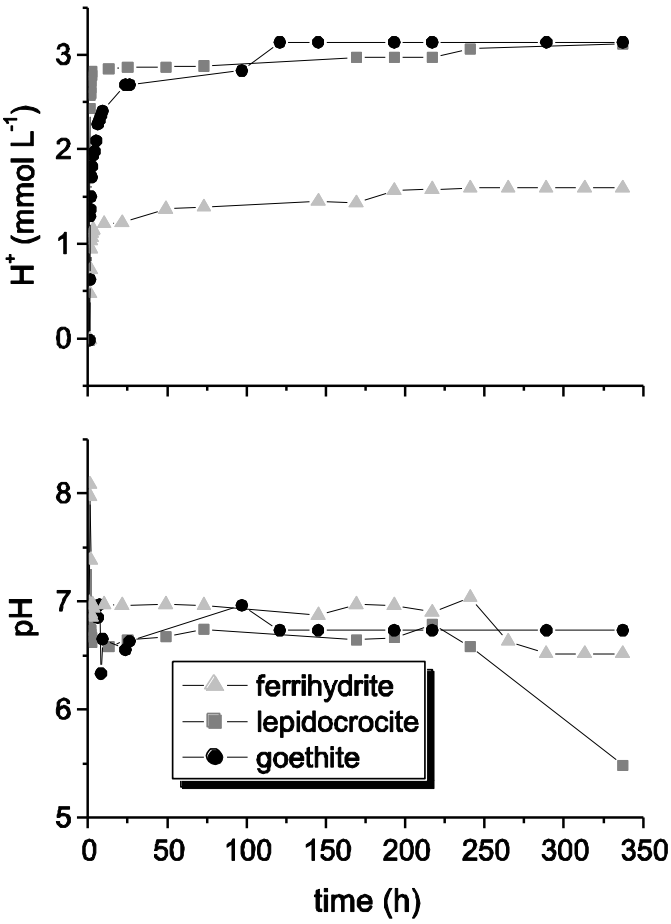

Fig. 3.4. pH progress (bottom) and H^+ consumption (top) during the reaction between ferrihydrite (run 24), lepidocrocite (run 14), and goethite (run 21) and dissolved sulphide.

Fig. 3.4 depicts the pH progress and the consumption of H^+ over 2 weeks reaction of the three ferric (hydr)oxides with dissolved sulphide (Table 3.1). The H^+ consumption was equal for lepidocrocite and goethite; 2.8 mmol L^{-1} H^+ were consumed within the first 24 hours and after 2 weeks 3.2 mmol L^{-1}. Compared to the both ferric oxides, the H^+ consumption in the case of ferrihydrite was lower. Only 1.2 mmol L^{-1} H^+ was consumed after 24 hours and 1.6 mmol L^{-1} H^+ during the 2 weeks of reaction.

The three ferric (hydr)oxides showed the same chemical reaction pattern but the velocity of dissolved sulphide consumption was different. The reactivity decreased in the order ferrihydrite ~ lepidocrocite < goethite with the rate coefficient k_{obs} for the oxidation of dissolved sulphide normalized to the surface area of $1.04*10^{-2}$ m^{-2} min^{-1}, $4.18*10^{-2}$ m^{-2} min^{-1}, and $4.96*10^{-4}$ m^{-2} min^{-1}, respectively (Fig. 3.5). The rate constants k_{obs} were determined by the slope of the logarithm of numbers of the moles of H_2S consumed due to the reaction with ferric (hydr)oxides versus time (Fig. 3.5).

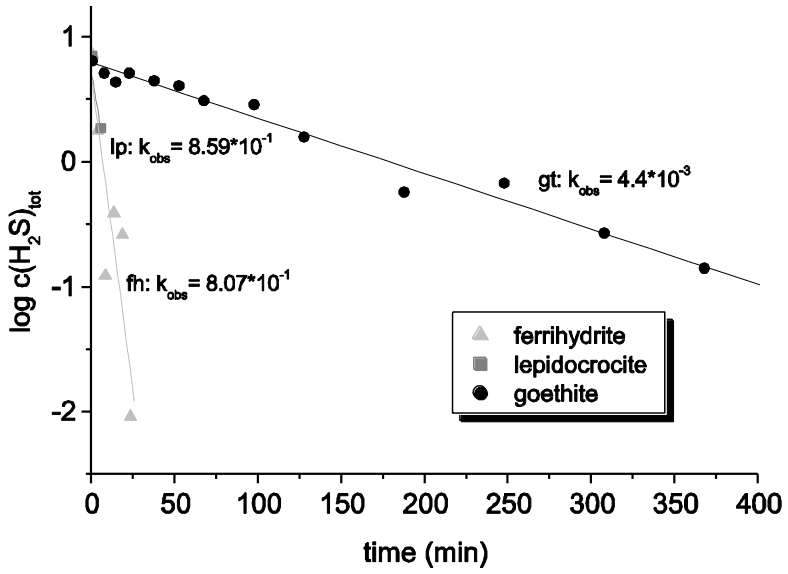

Fig. 3.5. Negative logarithm of number of moles of H_2S, $c(H_2S)$, consumed due to the reaction with ferrihydrite (fh), lepidocrocite (lp), and goethite (gt). k_{obs} is the rate constant for the oxidation of sulphide expressed in min^{-1}.

3.4.2. Spectroscopic and microscopic results

3.4.2.1. Mössbauer Spectroscopy

The Mössbauer spectra obtained at 4.2 K for products from the reduction of ferrihydrite and goethite are shown in Fig. 3.6 and 3.7, respectively. Table 3.3 described the model parameters which were used for the Mössbauer spectroscopy. The model parameters to characterize the experimental solution with lepidocrocite and its Mössbauer spectrum are shown in Hellige et al. (2010).

Table 3.3. Model parameters for 4.2 K Mössbauer spectra of ferrihydrite and goethite reacted with sulphide in Fig. 3.6 and 3.7 respectively.

	Fe(III) sextet								FeS_2		
Sample time	**I[a] (mm s^{-1})**	**X^{2} [b]**	**<CS>[c] (mm s^{-1})**	**<QS>[d] (mm s^{-1})**	**<H>[e] T**	**# of comp.[f]**	**H_p[g] T**	**Abundance (%)**	**<CS> (mm s^{-1})**	**<QS> (mm s^{-1})**	**Abundance (%)**
Ferrihydrite						*Ferrihydrite sextet*					
1 hr	0.11										
1 d	0.11										
1 wk	0.11	4	0.49	-0.11	49.1	2	50.1	70.7	0.41	0.62	29.3
2 wk	0.11	2	0.48	-0.1	48.8	2	49.9	73.6	0.4	0.64	26.4
Goethite						*Goethite sextet*					
1 hr	0.11	1.6	0.49	-0.23	50.6	1	50.6	100			
1 d	0.11	2.9	0.49	-0.23	50.6	1	50.6	100			
1 wk	0.11	2.3	0.49	-0.23	50.6	1	50.6	91.6	0.4	0.64	8.4
2 wk	0.11	1.5	0.49	-0.23	50.6	1	50.6	98	0.4	0.64	2
Mineral standards											
Ferrihydrite, 4.2 K			0.48	-0.02	47.4	2	49.9				
Goethite, 4.2 K			0.48	-0.25	50.6	1	50.6				
Pyrite, 77K									0.36	0.64	
Pyrite, 4.2 K									0.43	0.66	
Marcasite, 80 K									0.37	0.5	

[a]Lorenztian half-width at half-maximum.
[b]Reduced chi-squared goodness of fit value.
[c]Average center shift.
[d]Average quadrupole splitting.
[e]Average hyperfine magnetic field.
[f]Number of Voigt-based components used to model the hyperfine magnetic field.
[g]Most probable hyperfine magnetic field value.

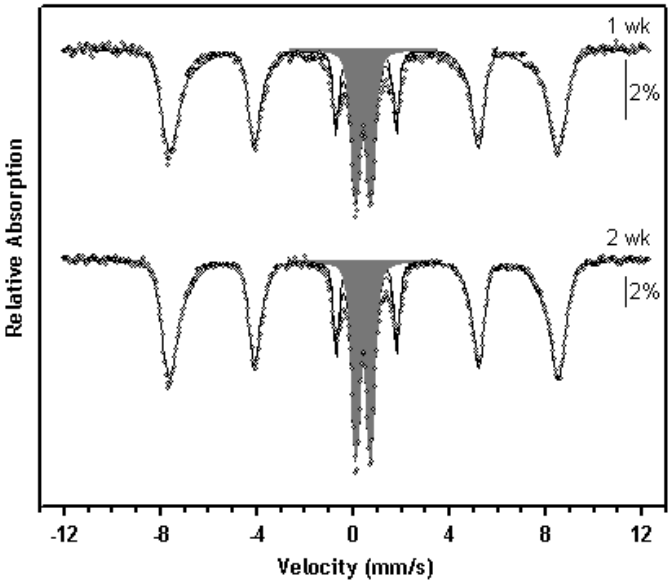

Fig. 3.6. Mössbauer spectra of ferrihydrite reacted with sulphide after 1 week and 2 weeks. White shaded sextets are bulk models for all Fe(III) (hydr)oxides present and may represent a combination of the goethite, hematite, and magnetite observed in TEM spectra. Gray shaded doublets are FeS_2. All spectra were collected at a temperature of 4.2 K. The scale bar represents a length of 2% absorption for each spectrum. Solution conditions are listed in Table 3.1, and model parameters are listed in Table 3.3.

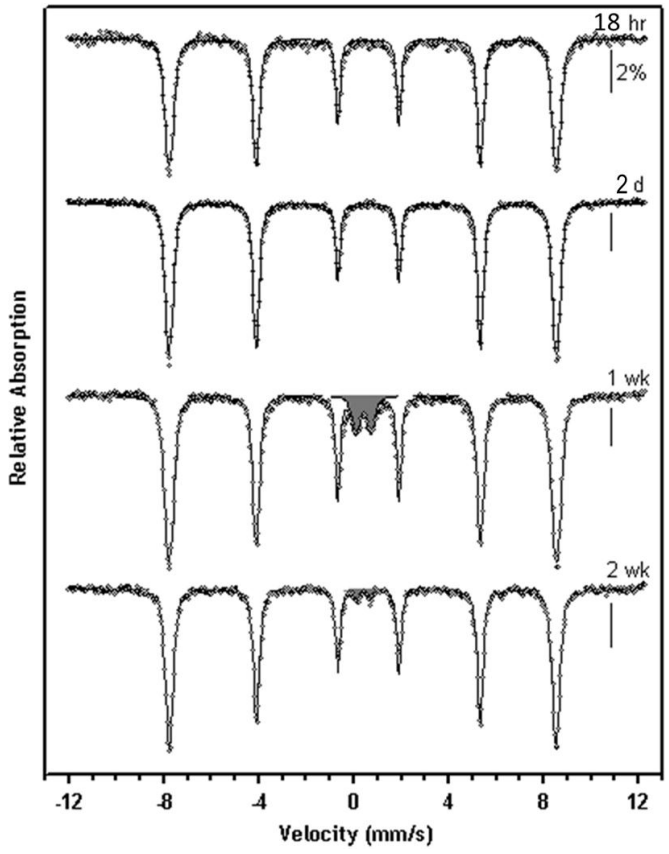

Fig. 3.7. Mössbauer spectra of goethite reacted with sulphide after 18 hours, 2 days, 1 week, and 2 weeks. White shaded sextets are goethite and gray shaded doublets are FeS_2. All spectra were collected at a temperature of 4.2 K. The scale bar represents a length of 2% absorption for each spectrum. Solution conditions are listed in Table 3.1, and model parameters are listed in Table 3.3.

Fig. 3.6 shows the Mössbauer spectra of ferrihydrite during the reaction with dissolved sulphide. For the first two samples no correlation to ferric (hydr)oxides could be made because of a huge noise (sample 1 hour and 24 hours are not shown). This is consistent with the chemical analysis which revealed that the complete amount added ferrihydrite was reduced in the first 2 days as indicated by HCl-extractable Fe(II) (Fig. 3.2A).

After two weeks sextets emerged in the experimental solution with ferrihydrite which were identified as ferric (hydr)oxides such as goethite, hematite, and magnetite (Sample 1 and 2 weeks, Table 3.3). In the experimental solutions with lepidocrocite and goethite, the host minerals were the dominant signal in all samples (Hellige et al., 2010, Fig. 3.7). Over time, a second signal emerged in the form of a paramagnetic doublet which was identified as FeS_2 for the three ferric (hydr)oxides. 26.4 %, 6.6 %, and 2 % of the initially added ferrihydrite, lepidocrocite (Hellige et al., 2010), and goethite, respectively, were converted into FeS_2 (Table 3.3). In the case of goethite the signal decreased with time due to an incomplete sampling (Fig. 3.7, Table 3.3). Not all samples were filterable, so the filtered solids may not be completely representative of the entire solids. After 1 week 8.4 % of the initial added goethite was transformed into FeS_2 and only 2 % after 2 weeks (Table 3.3).

3.4.2.2. TEM Analysis

Fig. 3.8 displays the TEM images of ferrihydrite after 2 hours of reaction with dissolved sulphide. Contrary to wet chemistry and Mössbauer spectroscopy data which implies the complete reduction of Fe(III), TEM images show a well-defined ferrihydrite structure without any changes in morphology of the particles. No differences in electron diffraction pattern were found to those of the initial ferrihydrite. Hence, after 2 hours of reaction no formation of secondary phases were detected and the structure of ferrihydrite seemed to have been preserved. Sulphur was adsorbed evenly on the ferrihydrite surfaces (Fig. 3.8d,e).

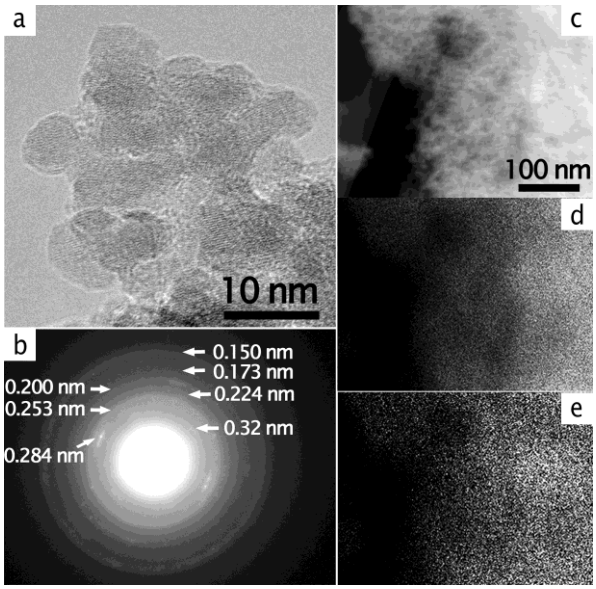

Fig. 3.8. High resoluiton TEM image (a) and electron diffraction pattern (b) of ferrihydrite after 2 hours reaction with dissolved sulphide. Dark-field STEM image (c) and EDX maps of iron [Fe Kα] (d) and sulphur [S Kα] distribution (e) show that sulphur was evenly adsorbed on ferrihydrite.

In experiments with lepidocrocite sulphur-rich rims were formed around the lepidocrocite crystals. Contrary to ferrihydrite the nucleation of mackinawite was revealed in these rims by high resolution TEM images. Additional a thin layer of magnetite could be identified at the interface between the mackinawite and lepidocrocite structure (see Hellige et al., 2010) which disappeared after 2 weeks of reaction.

At the end of the second phase of the reaction (18 hours), the goethite crystals were surrounded with a layer of mackinawite of variable thickness (Fig. 3.9b,c). In contrast to lepidocrocite, no magnetite layer was found at goethite crystals.

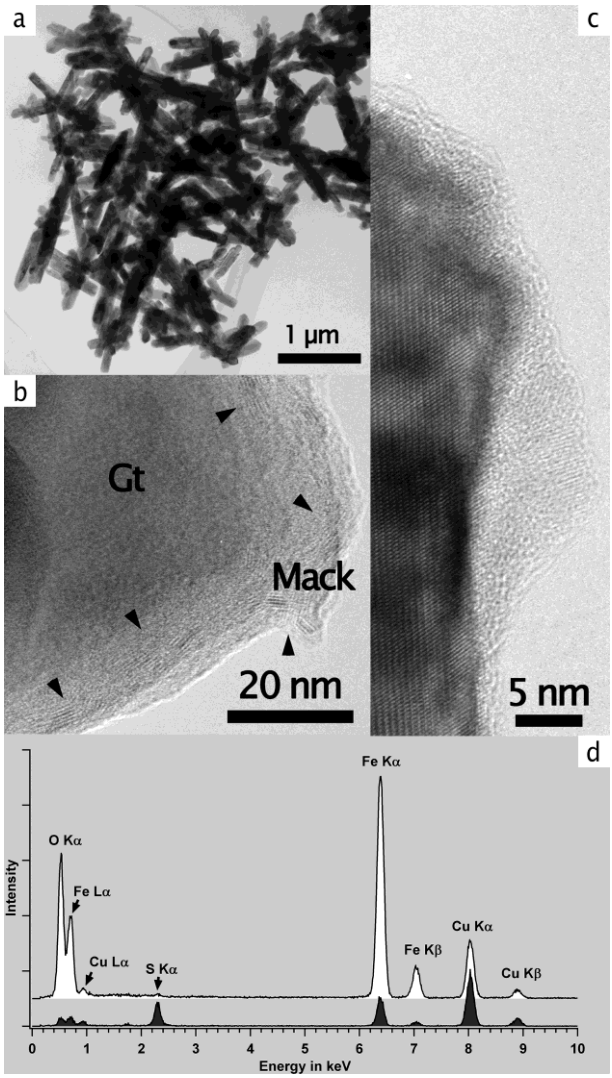

Fig. 3.9. Bright field TEM image (a) of the apparently pristine particle size and morphology of goethite after 18 hours of reaction. High resolution TEM images (b, c) reveal sulphur rich rims on goethite crystals. Lattice fringes in these rims are characteristic for mackinawite (FeS). EDX spectra (d) taken from the rims (black) and in the centre of goethite crystals (white) reveal the formation of iron sulphide with a Fe:S ratio of 1:1 on the goethite surface.

After two weeks of reaction no ferrihydrite crystals could be detected anymore. TEM observations confirmed the complete transformation of ferrihydrite and the formation of new minerals which is consistent with the chemical data and Mössbauer spectra. Table 3.4 shows the d-values of the formed phases due to the reductive dissolution of ferrihydrite which were predominantly magnetite and hematite (Fig. 3.10d,e). Only a minor amount of goethite was observed which may be served as hematite precursor and may be seen as an intermediate stage. In contrast to lepidocrocite and goethite the black coloration of the suspension did not disappear towards the end of reaction which might be due to the nanocrystalline nature of the newly formed iron oxides.

Table 3.4. d values of phases formed by the reaction of ferrihydrite with dissolved sulphide identified by electron diffraction and FFT of HR images.

Pyrite	$(hkl)_{pyrite}$	Hematite	$(hkl)_{hematite}$	Magnetite	$(hkl)_{magnetite}$	Goethite	$(hkl)_{goethite}$
3.12	1 1 1	3.70	0 1 2	4.86	1 1 1	4.18	1 0 1
2.71	2 0 0	2.76	1 04	2.95	2 2 0	2.72	3 0 1
2.42	2 1 0	2.54	1 1 0	2.52	3 1 1	2.56	2 1 0
2.21	2 1 1	2.23	1 1 3	1.48	4 4 0	2.24	2 1 1/1 0 2
1.93	2 2 0	1.79	0 2 4			2.18	4 0 1
1.64	3 1 1	1.71	1 1 6				
1.47	3 1 2	1.46	2 1 4/3 0 0				
1.21	4 2 0						

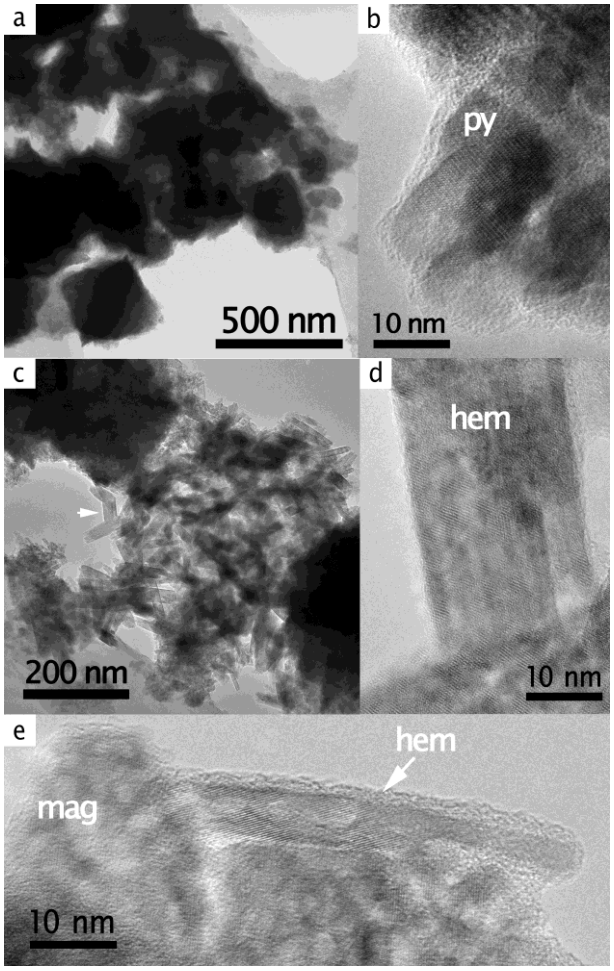

Fig. 3.10. Bright field (a, c) and high resolution (b, d, e) TEM images after 2 weeks of reaction between ferrihydrite and dissolved sulphide. Pyrite crystals are characterized by quadratic outlines and occur separated from ferric oxides (a, c). The aggregates consisted of agglomerated nanocrystalline domains (b). Ferrihydrite was completely transformed into hematite (arrow in c, d, e) and magnetite (e).

We observed the pyrite formation for all three ferric (hydr)oxides (Fig. 3.10a, 3.11a, Hellige et. al, 2010). In all cases the pyrites consisted of nanocrystalline domains and were probably formed by oriented aggregation. The morphology of the aggregated assemblages resembles quadric outlines (black squares) indicating an Ostwald ripening process to attain lower surface energy. These structures were not directly connected to the iron oxide crystals. The EDX

spectra (data not shown) confirm the Fe:S of 1:2 corresponding to pyrite in the black squares. As observed in Hellige et al. (2010) mackinawite becomes dissolved over time in the experimental solution with lepidocrocite and Fe and S accumulated between the lepidocrocite crystals. From these sulphur-rich accumulations were pyrite formed after two weeks accompanied by minor amounts of magnetite which have been found with a similar morphology.

Additionally, small amounts of hematite in the goethite rims with a thickness of ~ 20 nm (Fig. 3.11d) were detected; prevalent at the end of the acicular goethite crystals.

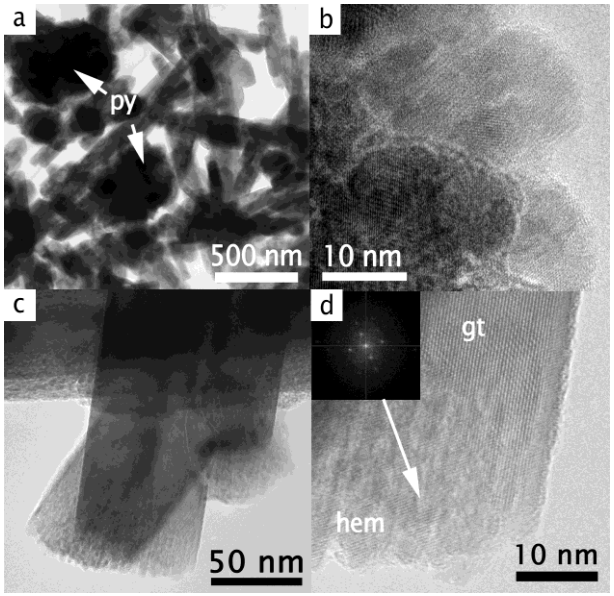

Fig. 3.11. Bright field TEM image (a) showing the distribution of goethite and pyrite after 2 weeks reaction. The pyrite crystals consisted of nanocrystalline aggregates (b). Bright field TEM images (c, d) and FFT electron diffraction pattern (inset in d) revealed that minor amounts of goethite were transformed into hematite, preferred at the end of the acicular goethite crystals.

In conclusion, mineral reactions occurred in experiments with all three oxides during the second phase of the reaction. However, after 2 weeks of reaction the extent of these transformations and the composition of the solids differed. In particular, the formation of other iron oxides and pyrite was less pronounced in experiments with goethite than with lepidocrocite and ferrihydrite, whereas complete transformation into secondary minerals occurred in experiments with ferrihydrite.

3.5. Discussion

As described in Hellige et al. (2010) the reaction progress of the reductive dissolution of lepidocrocite by dissolved sulphide was highly dynamic. Spectroscopic and microscopic data

showed that various phases were formed and disappeared during the reaction with pyrite as the final product. The main products were S(0) and acid extractable Fe(II) which consisted of FeS, surface-associated Fe(II), and dissolved Fe(II). The reaction could be subdivided into three phases with (i) fast consumption of dissolved sulphide, formation of S(0) and mackinawite onto the lepidocrocite surface (0-15 min), (ii) consumption of mackinawite due to the formation of magnetite onto the lepidocrocite surface and S(0) while acid extractable Fe(II) slightly increased (15-120 min), and (iii) decrease of S(0) and acid extractable Fe(II) due to pyrite formation accompanied with traces of magnetite (2-14 days). The magnetite in the first phase was an intermediate product which acted as "electron shuttle" between the lepidocrocite and mackinawite layer while the magnetite in the third phase was a by-product of the pyrite formation. After 2 days of reaction the dissolution of mackinawite started and Fe and S were accumulated between the lepidocrocite crystals and pyrite started to growth. The dissolution of lepidocrocite by dissolved sulphide and the pyrite formation were kinetically decoupled.

In the current study we observed differences in the reaction pathway as expressed by Mössbauer spectroscopy and TEM and differences in the reaction kinetics as expressed by wet chemistry for ferrihydrite, lepidocrocite, and goethite. Therefore we want to compare the oxides and highlight common characteristics and differences in the following.

3.5.1. The order of mineral reactivity

In any experiment the concentration of dissolved sulphide was higher than the number of surface sites which resulted in an incomplete adsorption of sulphide at the oxide surfaces (Table 3.1). Under this condition the oxide surfaces were saturated with respect to dissolved sulphide.

Fig. 3.3 shows that dissolved sulphide was consumed in the first minutes of the reaction for ferrihydrite and lepidocrocite with rate constant k_{obs} of $1.04*10^{-2}$ and $4.18*10^{-2}$ min^{-1} m^{-2}, respectively, while the concentration of surface sites was different for both oxides. In the experimental solution with goethite dissolved sulphide was consumed after 5 hours with a rate constant of $4.96*10^{-4}$ min^{-1} m^{-2}. Fig. 3.5 indicates that lepidocrocite and ferrihydrite have similar reaction kinetics. The reactivity decreases in the order of ferrihydrite ~ lepidocrocite > goethite. Differences in reactivity are related to the variations in crystal degree, particle size, specific surface area or site density. The reactivity increases with increasing surface area. This order is similar to the dissolution order and reverse to the degree of crystallinity (Cornell and

Schwertmann, 1996). The mechanisms and kinetics for the dissolution of ferric (hydr)oxides towards dissolved sulphide have been studied in detail (Canfield et al., 1992; Peiffer et al., 1992; Peiffer and Gade, 2007; Poulton et al., 2004; Pyzik and Sommer, 1981; Rickard, 1974). The easily extractable iron phases ferrihydrite and lepidocrocite are more reactive towards sulphide than the crystalline oxides goethite and hematite (Canfield, 1989; Poulton et al., 2004) which is consistent with our results.

3.5.2. Extent of Fe(II) excess formation

As pointed out above, the reaction progress can be divided into three steps according to Hellige et al. (2010) which includes an initial fast reaction where sulphide was rapidly consumed by a combined fast adsorption and oxidation process that lead to quasi instantaneous Fe(III) reduction and to Fe(II) and S(0) formation. But the generation rate of Fe(II) seems to be higher than the oxidation rate of dissolved sulphide and the sum of Fe(II) phases was more than double the concentration of S(0) for all three ferric (hydr)oxides (Table 3.2, Fig. 3.2). In the previous paper, we explained this phenomenon as a result of S(-II) adsorption which leads initially to the formation of Fe(II) and S(-I) while S(0) is formed in a subsequent second electron transfer reaction or upon disproportionation of two S(-I) by forming S(-II) and S(0) (Hellige et al., 2010). Hence, a part of sulphide was not oxidized to S(0) but rather fixed in FeS (Fig. 3.8, 3.9). The two reactions removing dissolved sulphide, the oxidation to S(0) and FeS precipitation, proceed at different rates. So, the formation of S(0) and Fe(II) is decoupled which is most pronounced when a large proportion of the added dissolved sulphide is removed upon adsorption (Hellige et al., 2010).

But the major fraction of the reduced iron which we refer as excess-Fe(II) might not be accessible for dissolved sulphide to form FeS solids and the rate of Fe(III) reduction exceeds the rate of FeS solid formation except for goethite (Table 3.2). This kinetic effect might lead to the development of a metastable reaction product such as magnetite onto the lepidocrocite surface (Hellige et al., 2010) in which the amount of Fe(II) is larger than expected based on thermodynamic consideration (Fig. 3.1).

The excess production of $Fe(II)_{HCl}$ increases in the sequence goethite > lepidocrocite > ferrihydrite (Table 3.2) and is conform to the results of Hansel et al. (2004). As the amount of $Fe(II)_{HCl}$ exceeds the number of surface sites for each mineral suspension (Table 3.1, 3.2), a proportion of $Fe(II)_{HCl}$ might to be accommodate in the bulk phase (Catalano et al., 2010; Handler et al., 2009; Williams and Scherer, 2004). Apparently, the ability of the three oxides

to form and to accommodate Fe(II) within the bulk phase increases in the order as the excess formation of Fe(II). Additionally, the specific surface area decreases in the order ferrihydrite > lepidocrocite > goethite. This implies that ferrihydrite and lepidocrocite are more favor to S(-II) adsorption and excess-Fe(II) formation due to their higher specific surface areas compared to goethite. Hence, the differences in specific surface area might additionally emphasize the differences between the three ferric (hydr)oxides regarding the tendency to form excess-Fe(II). The modeled chemical equilibriums for different scenarios showed that the major sink for excess-Fe(II) is the formation of magnetite (Fig. 3.1). Except for goethite, the formation of magnetite could be detected which implies that the formation of excess-Fe(II) was higher in the presence of lepidocrocite and ferrihydrite.

Hiemstra and van Riemsdijk (2007) investigated the reactivity of ferrihydrite, lepidocrocite, and goethite regarding the Fe^{2+} adsorption and concluded that the oxidation of adsorbed Fe(II) to the goethite surface is less pronounced compared to Fe(II) at the lepidocrocite surface. This is due to different electron charge distribution in goethite and lepidocrocite. In analogy, this difference can also explain the lower extent of excess-Fe(II) formation during the reductive dissolution of goethite compared to the reaction of lepidocrocite. Furthermore, they found out that the Fe(II) adsorption to lepidocrocite occurs only if the electron transfer is accepted which may explain the formation of magnetite onto the lepidocrocite surface (Hellige et al., 2010). Typically, magnetite formation is regarded to occur at high Fe(II) concentrations (Hansel C. M. et al., 2005) which can be an explanation that we observed no magnetite in the experimental solution with goethite neither with microscopy nor spectroscopy measurements. Another explanation may that the magnetite formation and its consumption due to the interaction of mackinawite with the goethite surfaces occurred at the same rate and so, we were not able to observed magnetite. However, according to Hiemstra and van Riemsdijk (2007) the Fe(II) adsorption to ferrihydrite and goethite surfaces is a combination process of adsorption with and without electron transfer which may explained also why we observed only the formation of amorphous FeS and mackinawite onto the surfaces of ferrihydrite and goethite without a magnetite layer in the initially phase. Compared to goethite, a large amount of magnetite appeared after 14 days of reaction in the experimental solution with ferrihydrite which might be a result of a high production of excess-Fe(II).

Furthermore, they applied the ion adsorption model CD (charge distribution) to analyze the Fe(II) adsorption behavior (Hiemstra and van Riemsdijk, 2007) which uses the Pauling valence bond concept to obtain the CD value of the surface complexes (Hiemstra and VanRiemsdijk, 1996). Possibly, the electron transfer in ferrihydrite cannot be explained by

the CD distribution following Pauling distribution alone. Silvester et al. (2005) reported considerable oxidation of Fe(II) upon adsorption onto ferrihydrite and its incorporation into the bulk oxide. Based on these experimental findings it can be concluded that the ability of ferrihydrite to transfer electron charge and to form bulk Fe(II) can also account for the formation of excess-Fe(II). This may also explain the TEM measurements which showed a well-defined ferrihydrite structure after 2 hours of reaction (Fig. 3.8) while no ferrihydrite structure was observed by Mössbauer spectroscopy. Chemical analysis depicted that the ferrihydrite was almost completely reduced after 2 hours (Fig. 3.2). One explanation for this contradiction could be the exchange of Fe(III) ions through Fe(II) ions due to the reaction with dissolved sulphide while the ferrihydrite structure was preserved. So, we were able to recover all added Fe(III) as $Fe(II)_{HCl}$ and observed the ferrihydrite structure by TEM.

Summarized, the extent of FeS formation depends on the Fe(II) adsorption behaviour of the respective Fe(III) solid phase. Due to the slower formation of FeS in the presence of goethite, the FeS was of higher crystallinity in contrast to that in the experimental solution with ferrihydrite where the FeS was built-up very fast. The crystallinity/stability of FeS increases in the order ferrihydrite > lepidocrocite > goethite. This order is reverse to the order of the formation of excess-Fe(II). It seems that the formation of FeS is stimulated by excess-Fe(II). In turn, the excess-Fe(II) promote the dissolution of FeS and the formation of pyrite. Hence, the reaction kinetics appears to be controlled by the amount of excess-Fe(II).

3.5.3. Formation of secondary minerals

In the case of ferrihydrite, initially dissolved sulphide adsorbed only to the oxide surface and we observed no formation of new crystalline phase like FeS. Probably amorphous FeS were formed which may acted as FeS or pyrite "prototype" because the reflexes 0.284 nm and 0.32 nm in Fig. 3.8b are closed to the pyrite reflexes 0.27 nm and 0.31 nm. In the presence of lepidocrocite and goethite we observed the formation of mackinawite onto their surfaces. After 2 days the reaction changed in each experimental solution and $Fe(II)_{HCl}$ and S(0) (Fig. 3.2) were consumed due to the dissolution of the amorphous FeS and mackinawite (Hellige et al., 2010). After 14 days of reaction, pyrite was formed accompanied by traces of magnetite except for goethite (Fig. 3.10a, 3.11a, Hellige et al., 2010). Pyrite and magnetite was not anymore associated with the oxide surfaces. Here, magnetite was a by-product due to the high Fe(II) generation. Furthermore, in natural environments, pyrite formation is often associated

with magnetite (Qian et al., 2010) In the presence of ferrihydrite was more magnetite formed than in the other experiments which explained that the suspension was still black. The formation of magnetite in the experiment with ferrihydrite (eq. 2) and lepidocrocite (eq. 3) can be explained by the following reaction pathways (Hellige et al., 2010)

$$2\ Fe(OH)_3 + Fe^{2+} \rightarrow Fe_3O_4 + 2\ H_2O + 2\ H^+ \quad (2)$$

$$6\ \gamma\text{-FeOOH} + 3\ Fe^{2+} \rightarrow 3\ Fe_3O_4 + 6\ H^+ \quad (3)$$

As described in Hellige et al. (2010) the onset of mackinawite dissolution started after 72 hours in the experimental solution with lepidocrocite while S(0) and $Fe(II)_{HCl}$ decreased. TEM measurements showed the accumulation of sulphur and iron between the lepidocrocite crystals which could be consisted of FeS clusters (eq. 4). These FeS clusters may further converted into pyrite by polysulphides (eq. 5) (Luther, 1991; Rickard, 2006; Rickard and Morse, 2005; Schoonen and Barnes, 1991b; Wilkin and Barnes, 1996).

$$FeS_m \rightarrow FeS_{(aq)} \quad (4)$$

$$FeS_{(aq)} + S_n^{2-} \rightarrow [FeS\text{-}S_n]^{2-} \rightarrow FeS_2 + S_{n-1}^{2-} \quad (5)$$

The pyrite formation requires reduced sulphur. And if is not enough reduced sulphur available for the pyrite precipitation, partial re-oxidation of Fe(II) is required which leads to the formation of S(-I). Though, the formation of pyrite could be also occurring via the reaction of FeS with dissolved Fe^{2+}. Whether the pyrite formation occurs is unclear but it seems that the presence of excess-Fe(II) stimulate its formation and might serve as a readily reductant of S(-II) in FeS and by this trigger the FeS_2 formation. In addition, the equilibrium thermodynamic model showed that formation of pyrite occurs if larger amounts of excess-Fe(II) is formed (Fig. 3.1).

In the experimental solution with ferrihydrite, 26.4 % (=3.17 mmol L^{-1}) of the total iron is bound in pyrite (Table 3.3, run 24) detected by Mössbauer spectroscopy. After 14 days 2 mmol L^{-1} Fe(II) was extractable with HCl. So, totally 5.17 mmol L^{-1} of ferrihydrite was reduced by the initial sulphide concentration of 7.5 mmol L^{-1}. 6.34 mmol L^{-1} was bound in pyrite. Either S(0) nor dissolved sulphide could be detected after 14 days; hence ~15 % of sulphur could not be detetected while in the experimental solution with lepidocrocite (run 14) ~46 % of sulphur remained undetected (Hellige et al., 2010). Mössbauer spectroscopy suggests that pyritic Fe in the experimental solution with goethite (Table 3.3, run 21) made up

2 % of the total iron (=0.44 mmol L^{-1}). Together with 2 mmol L^{-1} of Fe that were extracted with HCl after 14 days a total ammount of 2.44 mmol L^{-1} of goehtite was reduced by the initial sulphide concentration of 6.7 mmol L^{-1} in run 21. However, only 1.58 mmol L^{-1} sulphur (0.88 mmol L^{-1} as pyrite S plus 1.5 mmol L^{-1} as S(0)) could be recovered after 14 days implying that a significant fraction of sulphur (~76 %) remained undetected. It seems that the recovery of sulphur depends on the mineral. With increasing crystallinity the rate of sulphur recovery decreased. Mössbauer spectroscopy results implies that the amount of excess-Fe(II) is proportional of the pyrite abundace which follows the order ferrihydrite > lepidocrocite > goethite.
Generally, the formation of magnetite and pyrite requires excess-Fe(II).

The TEM measurements after 2 hours and the Mössbauer samples after 1 hour and 24 hours indicated the reductive dissolution of ferrihydrite by dissolved sulphide and its transformation into more stable minerals which involves redox reactions including re-oxidation of Fe(II) and reduction of S(0). Fe(II) was formed during the reaction of ferrihydrite and dissolved sulphide which may associated to the ferrihydrite surfaces and acted here as catalyst for the transformation into more stable mineral phases. Ferrihydrite has metastable properties and their transformation into more thermodynamically stable species is affected by temperature, pH and anionic media (Liu et al., 2008). Liu et al. (2008) conducted batch experiments with ferrihydrite and Fe(II) under anoxic and abiotic conditions and suggested that the transformation is slow in the absence of catalysts like Fe(II). We observed the transformation of ferrihydrite to hematite (eq. 7) with goethite (eq. 6) being intermediary (Fig. 3.10) (Das et al., 2010; Liu et al., 2008; Liu et al., 2005) accompanied by the formation of magnetite (eq. 2).

$$Fe(OH)_3 + 2\,Fe^{3+} + 3\,H_2O \rightarrow 3\,\alpha\text{-}FeOOH + 6\,H^+ \quad (6)$$

$$Fe(OH)_3 + Fe^{3+} \rightarrow Fe_2O_3 + 3\,H^+ \quad (7)$$

During these formations, protons are released into solution (eq. 6, 7, 2) which may account for the significantly lower consumption of HCl compared to the other oxides (Fig. 3.4). Ferrihydrite belongs to the hexagonal system which is different from goethite which belongs to the orthorhombic system. Hematite belongs to the hexagonal crystallographic system and has a similar anionic framework (same stacking of close-packed anions) to ferrihydrite. Liu et al. (2009) proposed that the nucleation and growth of hematite involved a combination of

dehydration and rearrangement process which is facilitated by its structural resemblance to ferrihydrite. So, there is no simple relationship between the structures of goethite, hematite, and magnetite and the replacing mineral ferrihydrite which support their formation by dissolution-precipitation processes catalyst by Fe(II). Our data are consistent with that of Pederson et al. (2005) who observed the complete ferrihydrite transformation into new minerals by Fe(II) within 2 days. Furthermore, our results agree very well with the crystal growth concept which indicates that the size of particles increased when the kinetic of transformation was slower. In the case of ferrihydrite the transformation was rapid and thus, the new formed crystals become smaller (Fig. 3.10c).

In contrast to lepidocrocite no magnetite was formed in the beginning of the reaction of goethite with dissolved sulphide. The extent of magnetite precipitation depends on the Fe(II) concentration (Hansel et al., 2005; Pedersen et al., 2005). Hansel et al. (2005) observed the magnetite formation only at Fe(II) concentrations about 2 mM. Compared to lepidocrocite, goethite has a higher crystallinity and a lower surface area corresponding to a lower reaction velocity. Hence, only a minor fraction of goethite surface sites reacted with dissolved sulphide to Fe(II) and may be the Fe(II) concentration was not high enough to form magnetite. Furthermore, the adsorption of Fe(II) to lepidocrocite occurs only with an electron transfer while the adsorption to goethite occurs with or without an electron transfer (Hiemstra and van Riemsdijk, 2007). These assumptions explain why we did not observe the magnetite formation in the presence of goethite while we observed its formation in the case of lepidocrocite.

But after 14 days of reaction, hematite precipitated onto the goethite surface (Fig. 3.11d, eq. 8).

$$2\ \alpha\text{-FeOOH} \rightarrow Fe_2O_3 + H_2O \qquad (8)$$

The residual Fe(II) which was not bound in pyrite may be adsorbed to the goethite surface and their interaction causes in hematite precipitation due to an interfacial electron transfer by $Fe(II)_{ads}$-$Fe(III)_{oxide}$ (Fig. 3.11d). Hence, hematite was formed as a by-product of pyrite formation. Other investigators observed no transformation of goethite after the reaction with Fe(II) (Handler et al., 2009; Jang et al., 2008; Pedersen et al., 2005; Tamaura et al., 1983).

3.5.4. Conceptual model

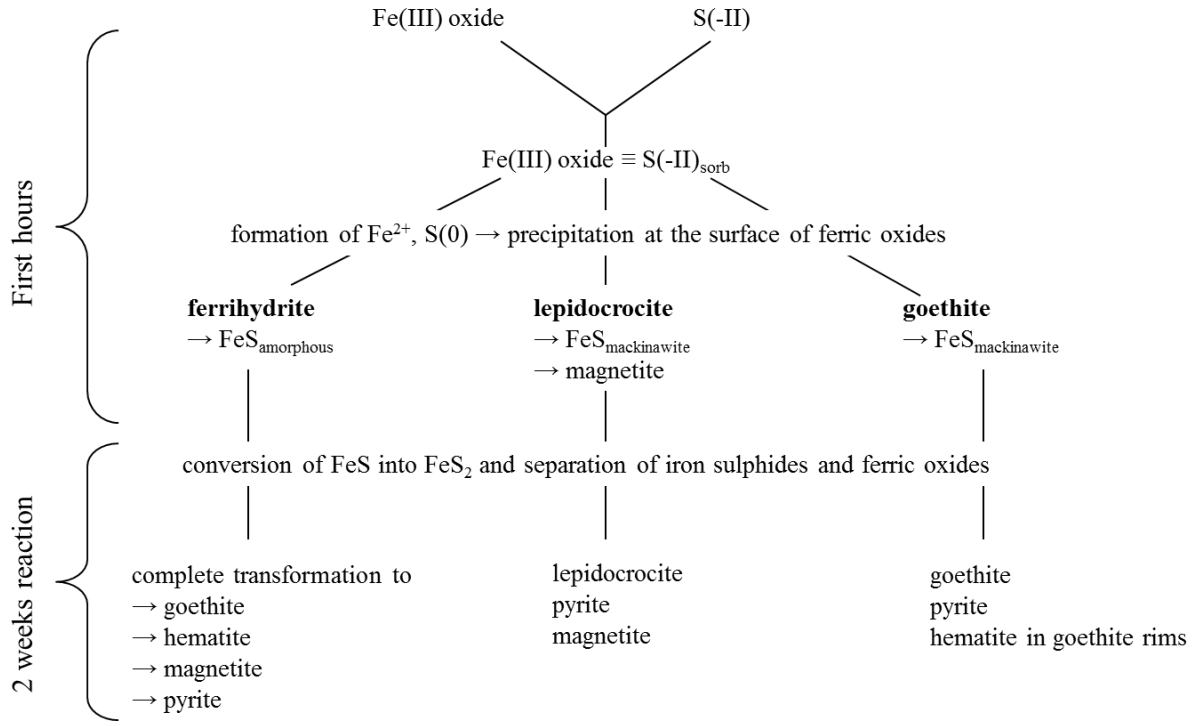

Fig. 3.12. Conceptual model for the reaction of ferric (hydr)oxides with dissolved sulphide at pH 7.

The secondary mineralization pathways in sulphide-rich systems are complex and involve an interplay between a number of geochemical factors and competing Fe(II)-induced mineralization pathways (Hansel et al., 2005). Based on our results, we suggest a simplified conceptual model of secondary mineralization pathways following the iron reduction of ferric (hydr)oxides by dissolved sulphide (Fig. 3.12). Initially, Fe(II) and S(0) were formed due to the rapidly adsorption of sulphide to the oxide surface. The reduced Fe(II) remained at the oxide surface and formed FeS. On a longer run, FeS was converted into pyrite via a reaction with polysulphides and excess Fe(II). The pyrite crystals consisted of nanocrystalline domains in all experiments. Except for the experimental solution of goethite, the formation of pyrite was accompanied by magnetite.

Despite the same reaction kinetics for ferrihydrite and lepidocrocite, the product pathway of both oxides differs. The lower solubility of goethite and lepidocrocite relative to ferrihydrite resulted in lower aqueous Fe(III) and aqueous Fe(II) concentration. Thus, we observed for both minerals only the pyrite formation, for lepidocrocite the magnetite formation as well, and the host minerals remained. Only small amounts of goethite were transformed to hematite. Within 2 weeks, due to re-equilibration reactions, ferrihydrite was transformed completely via dissolution-precipitation processes into new and more stable phases such as hematite,

magnetite, and pyrite. Only a minor amount of goethite was observed. The extent of transformation depends on the current ferric (hydr)oxide and the production of Fe(II).

The current work provides an improved understanding of the possible reaction pathways of ferric (hydr)oxides in sulphide-rich systems involved the interaction of Fe(II) with the oxide surface and with dissolved sulphide. The reductive dissolution of Fe(III) oxides and its transformation is controlled by the extent of excess-Fe(II) and their ability to accommodate Fe(II) in its bulk which decreases in the sequence ferrihydrite > lepidocrocite > goethite. In addition, the specific surface area decreases in the same order which implies, that in contrast to a low specific surface area, a high specific surface area is more able to S(-II) adsorption followed by electron transfer and excess-Fe(II) formation. Hence, the differences in specific surface area might additionally emphasize the differences between the three ferric (hydr)oxides regarding the tendency to form excess-Fe(II).

3.6. Acknowledgements

This research was funded by the Deutsche Forschungsgemeinschaft (DFG) and part of the priority program 580 “Electron Transfer Processes in Anoxic Aquifers” (PE 438/11-2). We thank Prof. Stefan Haderlein and Prof. Andreas Kappler, University of Tübingen for using their Mössbauer spectroscopic instrument. Furthermore, we thank the staff members of the Department of Hydrology, University of Bayreuth for help and support.

3.7. References

Canfield, D.E., Raiswell, R. and Bottrell, S., 1992. The reactivity of sedimentary iron minerals toward sulphide. *American Journal of Science*, **292**: 659-683.

Catalano, J.G., Fenter, P., Park, C., Zhang, Z. and Rosso, K.M., 2010. Structure and oxidation state of hematite surfaces reacted with aqueous Fe(II) at acidic and neutral pH. *Geochimica Et Cosmochimica Acta*, **74(5)**: 1498-1512.

Cornell, R.M. and Schwertmann, U., 1996. *The iron oxides: Structure, Properties, Reactions, Occurence and Uses.* Wiley-VCH Verlag GmbH, Weinheim, New York, Basel, Cambridge, Tokyo, 573 pp.

Das, S., Hendry, M.J. and Essilfie-Dughan, J., 2010. Transformation of two-lone ferrihydrite to goethite and hematite as a function of pH and temperature. *Envion. Sci. Technol.*

Dos Santos Afonso, M. and Stumm, W., 1992. Reductive Dissolution of iron(III) (hydr)oxides by hydrogen sulfide. *Langmuir*, **8**: 1671-1675.

Ferdelman, T.G., Church, T.M. and Luther, I.G.W., 1991. Sulfur enrichment of humic substances in a Delware salt marsh sediment core. *Geochemica et Cosmochemica Acta*, **55**: 979-988.

Fonselius S., Dyrssen D. and Yhlen B., 1999. *Determination of hydrogen sulphide.* In: Grasshoff K., Kremling K. and Ehrhardt M. (Editors), Methods of Seawater Analysis. Wiley-VCH, Weinheim, New York, Chichester, Brisbane, Singapore, Toronto, pp. 91-108.

Handler, R.M., Beard, B.L., Johnson, C.M. and Scherer, M.M., 2009. Atom Exchange between Aqueous Fe(II) and Goethite: An Fe Isotope Tracer Study. *Environmental Science & Technology*, **43(4)**: 1102-1107.

Hansel, C.M. et al., 2003. Secondary mineralization pathways induced by dissimilatory iron reduction of ferrihydrite under advective flow. *Geochim. Cosmochim. Acta*, **67(16)**: 2977-2992.

Hansel, C.M., Benner, S.G., Nico, P. and Fendorf, S., 2004. Structural constraints of ferric (hydr)oxides on dissimilatory iron reduction and the fate of Fe(II). Geochim. *Cosmochim. Acta*, **68(15)**: 3217-3229.

Hansel, C.M., Benner, S.G. and Fendorf, S., 2005. Competing Fe(II)-induced mineralization pathways of ferrihydrite. *Environ. Sci. Technol.*, **39**: 7147-7153.

Hellige, K., Pollok, K., Larese-Casanova, P., Behrends, T. and Peiffer, S., 2010. Pathways of ferrous iron mineral formation upon sulfidation of lepidocrocite surfaces. *submitted to Geochemica et Cosmochemica Acta*.

Hiemstra, T. and VanRiemsdijk, W.H., 1996. A surface structural approach to ion adsorption: The charge distribution (CD) model. *Journal of Colloid and Interface Science*, **179(2)**: 488-508.

Hiemstra, T. and van Riemsdijk, W.H., 2007. Adsorption and surface oxidation of Fe(II) on metal (hydr)oxides. *Geochimica Et Cosmochimica Acta*, **71(24)**: 5913-5933.

Jang, J.H., Mathur, R., Liermann, L.J., Ruebush, S. and Brantley, S.L., 2008. An iron isotope signature related to electron transfer between aqueous ferrous iron and goethite. *Chemical Geology*, **250(1-4)**: 40-48.

Jeon, B.H., Dempsey, B.A., Burgos, W.D. and Royer, R.A., 2001. Reactions of ferrous iron with hematite. *Colloids and Surfaces a-Physicochemical and Engineering Aspects*, **191(1-2)**: 41-55.

Jeon, B.H., Dempsey, B.A. and Burgos, W.D., 2003. Kinetics and Mechanisms for Reactions of Fe(II) with Iron (III) Oxides. *Envion. Sci. Technol.*, **37**: 3309-3315.

Liu, H., Wei, Y. and Sun, Y., 2005. The Formation of hematite from ferrihydrite using Fe(II) as a catalyst. *Journal of Molecular Catalysis A: Chemical*, **226**: 135-140.

Liu H., Guo H., Li P. and Wei Y., 2008. The transformation of ferrihydrite in the presence of trace Fe(II): The effect of the anionic media. *Journal of Solid State Chemistry*, **181**: 2666-2671.

Liu H., Guo H., Li P. and Wei Y., 2009. Transformation from δ-FeOOH to hematite in the presence of trace Fe(II). *Journal of Physics and Chemistry of Solids*, **70**: 186-191.

Luther, I.G.W., 1991. Pyrite synthesis via polysulfide compounds. *Geochemica et Cosmochemica Acta*, **55**: 2839-2849.

Pedersen, H.D., Postma, D., Jakobsen, R. and Larsen, O., 2005. Fast transformation of iron oxyhydroxides by the catalytic action of aqueous Fe(II). *Geochimica Et Cosmochimica Acta*, **69(16)**: 3967-3977.

Pedersen, H.D., 2006. *The transformation of Fe(III) oxides catalysed by Fe^{2+} and the fate of arsenate during transformation and reduction of Fe(III) oxides*, Technical University of Denmark, Kgs. Lyngby, 1-71 pp.

Peiffer, S., Dos Santos Afonso, M., Wehrli, B. and Gächter, R., 1992. Kinetics and mechanism of the reaction of H_2S with lepidocrocite. *Environ. Sci. Technol.*, **26(12)**: 2408-2413.

Peiffer, S., 1994. *Reaction of H_2S with Ferric Oxides - Some Conceptual Ideas on Its Significance for Sediment-Water Interactions.* In: L.A. Baker (Editor), Environmental Chemistry of Lakes and Reservoirs. Advances in Chemistry Series. Amer Chemical Soc, Washington, pp. 371-390.

Peiffer, S. and Gade, W., 2007. Reactivity of ferric oxides toward H_2S at low pH. *Environ. Sci. Technol.*, **41**: 3159-3164.

Poulton, S.W., Krom, D.M. and Raiswell, R., 2004. A revised scheme for the reactivity of iron (oxyhydr)oxide minerals towards dissolved sulfide. *Geochim. Cosmochim. Acta*, **68(18)**: 3703-3715.

Pyzik, A.J. and Sommer, S.E., 1981. Sedimentary iron monosulphides: kinetics and mechanism of formation. *Geochim. Cosmochim. Acta*, **45**: 687-698.

Qian, G., Brugger, J., Skinner, W.M., Chen, G.R. and Pring, A., 2010. An experimental study of the mechanism of the replacement of magnetite by pyrite up to 300 degrees C. *Geochimica Et Cosmochimica Acta*, **74(19)**: 5610-5630.

Rickard, D., 1974. Kinetics and mechanism of the sulfidation of goethite. American *Journal of Science*, **274**: 941-952.

Rickard, D., 1975. Kinetics and Mechanism of Pyrite Formation at Low Temperatures. *American Jounal of Science*, **275**: 636-652.

Rickard, D.T. and Morse, J.W., 2005. Acid volatile sulfide (AVS). *Mar. Chem.*, **97(3-4)**: 141-197.

Rickard, D., 2006. The solubility of FeS. *Geochimica Et Cosmochimica Acta*, **70(23)**: 5779-5789.

Schoonen, M.A.A. and Barnes, H.L., 1991b. Reactions Forming Pyrite and Marcasite from Solution .2. Via FeS Precursors Below 100-Degrees-C. Geochimica *Et Cosmochimica Acta*, **55(6)**: 1505-1514.

Schwertmann U. and Cornell R. M., 2000. *Iron oxides in the laboratory: Preparation and characterization.* Wiley-VCH Verlag GmbH, Weinheim, New York, Basel, Cambridge, Tokyo, 188 pp.

Silvester, E. et al., 2005. Redox potential measurements and Mossbauer spectrometry of Fe-II adsorbed onto Fe-III (oxyhydr)oxides. *Geochimica Et Cosmochimica Acta*, **69(20)**: 4801-4815.

Tamaura, Y., Ito, K. and Katsura, T., 1983. Transformation of γ-FeO(OH) to Fe_3O_4 by Adsorption of Iron(II) Ion on γ-FeO(OH). *J. Chem. Soc. Dalton Trans.* **(2)**: 189-194.

Tamura H., Goto K., Yotsuyanagai T. and M., N., 1974. Spectrophotometric determination of iron(II) with 1,10-phenanthroline in the presence of large amounts of iron(III). *Talanta*, **21**: 314-318.

Tronc, E., Belleville, P., Jolivet, J.P. and Livage, J., 1992. Transformation of Ferric Hydroxide into Spinel by Fe(II) Adsorption. *Langmuir*, **8(1)**: 313-319.

Wilkin, R.T. and Barnes, H.L., 1996. Pyrite formation by reactions of iron monosulfides with dissolved inorganic and organic sulfur species. *Geochimica Et Cosmochimica Acta*, **60(21)**: 4167-4179.

Williams, A.G.B. and Scherer, M.M., 2004. Spectroscopic evidence for Fe(II)-Fe(III) electron transfer at the iron oxide - water interface *Envion. Sci. Technol.*, **38**: 4782-4790.

4. Intrinsic rate constants for the abiotic oxidation of sulphide by various ferric (hydr)oxides

Planned submission to Environmental Science and Technology

Katrin Hellige[1] and Stefan Peiffer[1]

[1]Department of Hydrology, University of Bayreuth, Universitätsstraße 30, D-95445 Bayreuth, Germany

4.1. Abstract

The reaction between synthetic ferric (hydr)oxides and H_2S was studied under flow-through conditions at pH 4 and 7. Therefore, we developed a fluidized-bed reactor to investigate initial reaction kinetics with a constant oxidation rate of H_2S over the experiment period. The concentration of Fe(III) solids regarding the surface area was equal for each mineral and so, the different ferric (hydr)oxides could be compared with each other. The formation of the main products Fe(II) and S(0) was decoupled which suggested that the formation was non-stoichiometric during the reaction. We explained these differences of Fe(II):S(0) ratios with different lattice stabilities. In the presence of ferrihydrite and lepidocrocite, the adsorption of Fe(II) was accompanied with the uptake into the bulk crystal which led to high Fe(II):S(0) ratios. Contrary, the adsorption of Fe(II) onto the goethite surface occurred without an electron transfer and resulted in low Fe(II):S(0) ratios. These different Fe(II) conditions may influence the redox potential of the reactor suspension. That conditions in turn affect semiconducting properties of Fe(III) oxides and thus, their reactivity.

The reaction rate coefficient k_{obs_H2S} and $k_{obs\_Fe(II)}$ normalized to the surface area suggested that the reactivity of Fe(III) (hydr)oxides decreased in the order ferrihydrite > lepidocrocite > goethite and followed a second order rate law. k_{obs_H2S} increased with pH and specific surface area.

We proposed that the reactivity is largely controlled by the adsorption and electron properties of the Fe(III) solid phase and by the specific variations of the generated Fe(II).

Keywords: ferric (hydr)oxides, dissolved sulphide, kinetics, reductive dissolution, coordination chemistry, surface-chemistry, mechanism

4.2. Introduction

Ferric (hydr)oxides are widely distributed in natural environments such as aquifers or marine sediments, solids, and freshwater sediments. In these environments, ferric (hydr)oxides play a major role in abiotic and biotic reactions as reductants and oxidants, in electron transfer reactions, and in the (re)cycling of elements *(1-4)*. Due to their high surface area they are efficient scavengers for trace metals, organic compounds and ferrous iron which may be released to solution during their reductive dissolution *(5)*. The prominent abiotic reductant of ferric (hydr)oxides is H_2S which may form during the sulphate reduction by microorganisms in anoxic environments *(6)*. The major reaction products are S(0) and Fe(II) *(7,8)*. These two species contribute to formation of FeS or FeS_2 and contribute to the storage of sulfur in sediments *(6,9,10)*. Hence, the reductive dissolution of ferric (hydr)oxides by H_2S is highly relevant for the cycling of sulfur *(10,11)*.

The mechanisms and kinetics of the abiotic dissolution of ferric (hydr)oxides have been studied in detail for a number of reductants including H_2S, ascorbate, and fructose *(4,7,9,12-17)*. The interaction between ferric (hydr)oxides and dissolved sulphide is surface controlled *(18)* and depends on factors like mineralogy, crystallinity, specific surface area, grain size, and the concentration of reductants and oxidants. The various ferric (hydr)oxides have a wide variation in reactivity. Minerals with a lower degree of crystal order (hydrous ferric oxides and lepidocrocite) are reactive on a time scale of minutes to hours while the more ordered minerals such as goethite, magnetite, and hematite are reactive on a time-scale of tens of days *(6,14)*. Furthermore, Al substitution in ferric (hydr)oxides *(14)* or the adsorption of sulphate to the Fe(III) (hydr)oxide surface *(7)* may affect their reactivity. Generally, the initial Fe(III) (hydr)oxide reduction rate is denoted as a function of the oxide surface area with a first order dependency and the reactivity decreases in the order of 2-l ferrihydrite > 6-l ferrihydrite > lepidocrocite > goethite > hematite *(14-16)*. Other investigators who determined the reactivity of ferric (hydr)oxides by their reduction with ascorbic acid suggested that crystal properties have a significant effect on the reactivity *(15,16)*.

The rate of the reaction between dissolved sulphide and ferric (hydr)oxides is regarded to be proportional to the surface species >FeSH *(13)*

$$R = k_{intr} \{>FeSH\} \quad (1)$$

where k_{intr} denotes the intrinsic rate constant for this reaction. Eq. 1 qualitatively accounts for the rate dependency on pH *(13,19)* as well as the rate maximum at pH 7 *(13)*. At this pH or

greater, the reaction is accompanied by FeS precipitation which may trap S(-II) and by this prevent its oxidation by Fe(III). In a previous study, we have demonstrated that the formed Fe(II) formed through the reaction of sulphide with ferric (hydr)oxides has a profound influence on the overall reaction pathways and electron transfer mechanisms at circumneutral pH *(8,20)*. Hence, the kinetic studies carried out as initial-rate batch experiments are not suitable to study intrinsic rate constants under these conditions. To overcome these problems we have performed flow-through experiments to investigate the reactivity of various various ferric (hydr)oxides with respect to H_2S at pH 4 and 7. We used various synthetic Fe(III) (hydr)oxides with a broad range of crystallinity and different surface properties in order to their influence on the reaction kinetics. The concentration of the solid Fe(III) phases was chosen to obtain the same total concentration of surface area (approximately 24 m^2 L^{-1}). Thus, in the initial phase of reaction the Fe(III) surface concentration is equal for all experiments so that the different ferric (hydr)oxides can be compared with each other and the reaction becomes independent from the specific surface area but influenced by surface and crystal properties of each oxide.

4.3. Materials and methods

All solutions were prepared with distilled water and bubbled with N_2 to remove oxygen. All reagents were of analytical grade.

4.3.1 Ferric (hydr)oxides

Synthetic 6-line ferrihydrite and goethite were synthesized following the recipes given in ref *(21)*. Lepidocrocite was prepared according to ref *(22)*. Additionally, synthetic lepidocrocite (Bayferrox 943) and goethite (Bayferrox 920 Z) were purchased from Lanxess (Leverkusen, Germany). To remove ions like sulphate from Bayferrox oxides surface, 1 mol L^{-1} of it was suspended in 0.01 mol L^{-1} $NaNO_3$ and the pH was adjusted to 10 with NaOH. After 4 days of shaking the Bayferrox solution was washed and freeze-dried. The Bayferrox lepidocrocite is contaminated with goethite *(23)*.

The ferric (hydr)oxides were characterized using X-ray diffractometry (XRD), scanning electron microscopy (SEM), and transmission electron microscopy (TEM). XRD and TEM measurements showed pure Fe(III) (hydr)oxides. Surface area was measured by multi-point BET-N_2 (Brunauer, Emmett and Teller) method (Gemini 2375 Surface Area Analyzer). The

point of zero charge (pH_{pzc}) was determined for every mineral using the method of ref *(24)* (Table 4.1).

Table 4.1. Characterization of commercial and synthesized iron minerals.

	Commercial Fe(III) minerals		Synthesized Fe(III) minerals		
	Lepidocrocite	**Goethite**	**6-l Ferrihydrite**	**Lepidocrocite**	**Goethite**
Multi-point BET-N_2 (m^2 g^{-1})	17.34	9.12	140	169.9	27.02
Particle size (µm)	0.2-0.4	0.6-0.9	–	0.2-0.6	0.7-1.5
pH_{pzc}	–	7.5	7.1	6.85	7.4

4.3.2. Experimental Set-up

Flow-through experiments with synthetic and commercial ferric (hydr)oxides in excess and dissolved sulphide were performed at pH 4 and 7 at room temperature. The solid concentration of the various Fe(III) (hydr)oxides was chosen to obtain the same total concentration of surface area as approximately 24 m^2 L^{-1}. The initial conditions for each Fe(III) mineral and pH are shown in Table 4.2. All reactions were conducted in a 250-mL glass vessel with ports for sampling and removals, pH electrode and temperature (see supporting information: Fig. S. 1). The reaction solution was stirred with a Teflon-coated stirring bar at constant rate. The sulphide stock solution of 150 to 340 µmol L^{-1} was stored in gas-tight aluminized PP/PE-bags (Tesseraux Spezialverpackungen GmbH, Bürstadt). To adjust the pH to 4 0.01 M Na-acetate/acetic was added to the sulphide stock solution. The pH of 7 was established using 0.015 M PIPES (piperazine-N,N'-bis{2-ethanesulfonic acid},dipotassium salt) buffer and NaOH. The H_2S containing carrier solution flow through the reactor continuously with a flow of 0.003 L min^{-1}. After the reactor was completely filled with the carrier solution, wet ferric (hydr)oxide was injected through a septum with a syringe. The syringe was flushed three times with the reactor solution after injection of the Fe(III) oxide.

Samples were taken periodically for the determination of dissolved Fe(II), dissolved S(-II), dissolved sulphate, acid extractable Fe(II), total Fe, and total S(0). The samples were taken at the outflow and from the inside reaction solution through the septum. Before each run the concentration of dissolved sulphide were determined in the stock solution, in the inside of the reactor, and at the outflow of the reactor.

4.3.3. Chemical analyses

The iron species were determined after addition of HCl using the phenanthroline method of ref *(25)*. Dissolved Fe(II) ($Fe(II)_{diss}$) was measured on filtered (0.45 µm) samples, while total iron ($Fe(III)_{TOT}$) was measured on unfiltered samples. After the extraction of the solid phase bound Fe(II) ($Fe(II)_{HCl}$) with 0.5 N HCl, the solution was filtered and Fe(II) was determined. Dissolved sulphide ($S(-II)_{diss}$) was determined photometrically by methylene blue method of ref *(26)* after filtration. Elemental sulphur (S(0)) of the solid phase was measured by High Performance Liquid Chromatography (HPLC, Beckman) combined with UV detection (Detector 168, Beckman) after extraction with methanol. Therefore 300 µL unfiltered sample was suspend in 1200 µL methanol. After 1 h equilibration time the solution was filtered and stored at 4°C until measurement. Dissolved sulphate (SO_4^{2-}) was determined turbidimetrically after ref *(27)*. The method is not very sensitive with a detection of 10 µmol L^{-1}.

Table 4.2. Initial conditions for each run.

Run no.	Mineral	pH	Runtime (hours)	Mineral concentration (mmol L^{-1})	Surface area (m^2 L^{-1})	Initial sulphide concentration (µmol L^{-1})
14	Ferrihydrite	4	5.88	2.0	25.6	189
16	Ferrihydrite	4	7.52	2.0	26.2	218
15	Lepidocrocite	4	9.87	1.7	26.0	254
18	Lepidocrocite	4	7.28	2.3	34.3	253
10	Goethite	4	7.53	9.2	22.0	235
11	Goethite	4	7.01	10.0	24.0	240
12	Goethite	4	5	15.5	37.3	153
13	Goethite	4	7.52	8.7	20.8	152
20	Bayferrox Lepidocrocite	4	7.28	13.6	21.1	254
21	Bayferrox Lepidocrocite	4	7.27	21.7	33.5	236
17	Bayferrox Goethite	4	7.27	32.9	26.0	186
19	Bayferrox Goethite	4	7.27	29.6	24.7	243
4	Ferrihydrite	7	7	2.1	27.0	184
7	Ferrihydrite	7	7.52	1.9	24.4	332
3	Lepidocrocite	7	6.5	1.8	27.1	343
6	Lepidocrocite	7	7.52	1.0	15.6	297
2	Goethite	7	7.51	13.3	31.9	275
8	Goethite	7	7.53	12.7	30.6	296
22	Bayferrox Lepidocrocite	7	7.27	13.1	20.3	242
23	Bayferrox Lepidocrocite	7	7.26	15.4	23.8	227
1	Bayferrox Goethite	7	6.59	29.8	24.5	320
5	Bayferrox Goethite	7	7.77	21.6	17.7	284
9	Bayferrox Goethite	7	7.51	31.7	26.0	244

4.3.4. Data evaluation

The reductive dissolution of ferric (hydr)oxides by dissolved sulphide can be described operationally by a second order kinetic law with respect to the surface area and initial dissolved sulphide concentration *(3,13,18)*

$$R_{obs} = \frac{dc(H_2S)}{dt} = k_{obs\_H2S}\, c(H_2S)\, A \qquad (2)$$

where R_{obs} is the observed oxidation rate of H_2S (mol L^{-1} min^{-1}), k_{obs_H2S} is the rate constant for the oxidation of sulphide (L m^{-2} min^{-1}), $c(H_2S)$ the initial concentration of H_2S (mol L^{-1}), and A the concentration of surface area of Fe(III) mineral added (m^2 L^{-1}).

In order to evaluate the experimental data with respect to k_{obs_H2S}, we have developed a quantitative model for the time course of the concentration of H_2S in the flow-through reactors. The model is based on the mass-balance for H_2S in a linear flow through reactor *(28)* and can be written as

$$\frac{dc(H_2S)}{dt} = c(H_2S)_{initial}\frac{Q}{V} - c(H_2S)_{reactor}\frac{Q}{V} - k_{obs\_H2S}\, c(H_2S)_{reactor}\, A(t) \qquad (3a)$$

$$= c(H_2S)_{initial}\, k_w - (c(H_2S)_{reactor}\,(k_w + k_{obs\_H2S}\, A(t))) \qquad (3b)$$

where $c(H_2S)_{initial}$ is the initial H_2S concentration (mol L^{-1}), $c(H_2S)_{reactor}$ is the concentration in the reactor (mol L^{-1}), k_w is the specific flow rate with $k_w = \frac{Q}{V}$. Q is the flow rate of the H_2S carrier solution (0.003 L min^{-1}) and V is the volume of the reactor (0.25 L), k_{obs_H2S} is the unknown, and $A(t)$ is the specific surface area of ferric (hydr)oxide (m^2 L^{-1}) depending on time. $A(t)$ was explicitly derived for each time step as

$$A(t) = A_s\, c(Fe(III)_t \qquad (4)$$

in which A_s is the specific surface area (m^2 g^{-1}) and $c(Fe(III)_t$ is the solid Fe(III) concentration in suspension at a certain time step (g L^{-1}). $Fe(III)_t$ was calculated by the following equation

$$c(Fe(III)_t) = c(Fe(III))_{initial}\, e^{-kt} \qquad (5)$$

where $c(Fe(III))_{initial}$ is the initial concentration of Fe(III) added ($m^2\ L^{-1}$), $k_{Fe(III)}$ is the rate constant for the consumption of Fe(III) in the reactor (min^{-1}), t is the time (min). $k_{Fe(III)}$ was derived from the slope of the (natural) logarithm of numbers of the moles of consumed Fe(III).

Equation 3b can be integrated to *(28)*

$$c(H_2S) = c(H_2S)_{initial}\, e^{-k^*t} + c^{\infty}\,(1-e^{-k^*t}) \qquad (6)$$

with $k^* = k_w + k_{obs\_H2S}\, A(t)$ and $c^{\infty} = \frac{k_w}{(k_w + k_{obs\_H2S} A(t))} \cdot c(H_2S)_{initial}$.

The parameter k_{obs_H2S} was estimated by non-linear parameter fitting using the statistic software CoHort.

In similar approach the rate constants for the formation of Fe(II) ($k_{obs\_Fe(II)}$) during the reaction of ferric (hydr)oxides with dissolved sulphide were derived after the following equation

$$c(Fe(II)) = k_{obs\_Fe(II)}\, c(H_2S)\, \frac{A(t)}{k_w}\,(1 - e^{(-k_w t)}) \qquad (7)$$

4.4. Results

4.4.1. Evolution of sulphur and iron species during reaction

In the following we will demonstrate the chemical speciation during the reaction using the example of lepidocrocite. Additional ferric (hydr)oxides are given in supporting information (Fig S2-S9). Fig. 4.1 and 4.2 shows the typical temporal development of sulphur and ferrous iron during the reductive dissolution of lepidocrocite by dissolved sulphide at pH 4 and 7, respectively. The main products were S(0), dissolved Fe(II) and acid extractable Fe(II) which is consistent with previous studies *(7-9,14)*. In each experiment, these species built up fast in the beginning of the experiment, followed by a slower decrease. Sulphate could not be detected in any experiment.

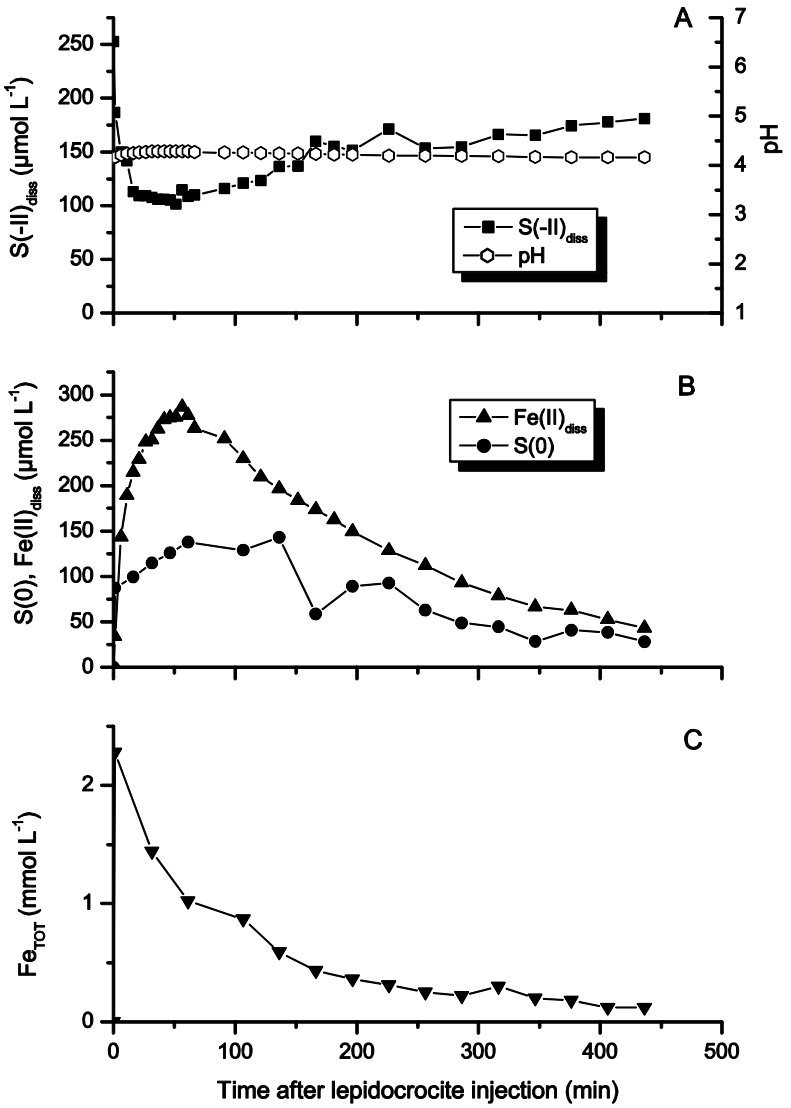

Fig. 4.1. The experimental outcome of the reaction between H_2S and lepidocrocite at pH 4 (run 18). Time zero corresponds to the addition of lepidocrocite. The evolution of dissolved sulphide during the reaction with lepidocrocite is shown in (A). The main products total S(0) and dissolved Fe(II) were monitored during the reaction (B). (C) shows the evolution of total Fe during the reaction.

Fig. 4.1 shows the reaction between lepidocrocite (A_s = 34 m^2 L^{-1}, c = 2.3 mmol L^{-1}) and dissolved sulphide (c = 253 µmol L^{-1}) at pH 4. The addition of lepidocrocite leads to a rapid drop of dissolved sulphide with a minimum of 109 µmol L^{-1} after approximately 60 minutes. At the same time, the pH increased slightly from 4.15 to 4.28 and started to decrease again after 100 minutes to a value of 4.16. The main products were dissolved Fe(II) and S(0) that formed immediately. The concentration of dissolved Fe(II) had a maximum at 280 µmol L^{-1} and S(0) at 140 µmol L^{-1} after 60 minutes with a stoichiometric Fe(II):S(0) ratio of 2:1.

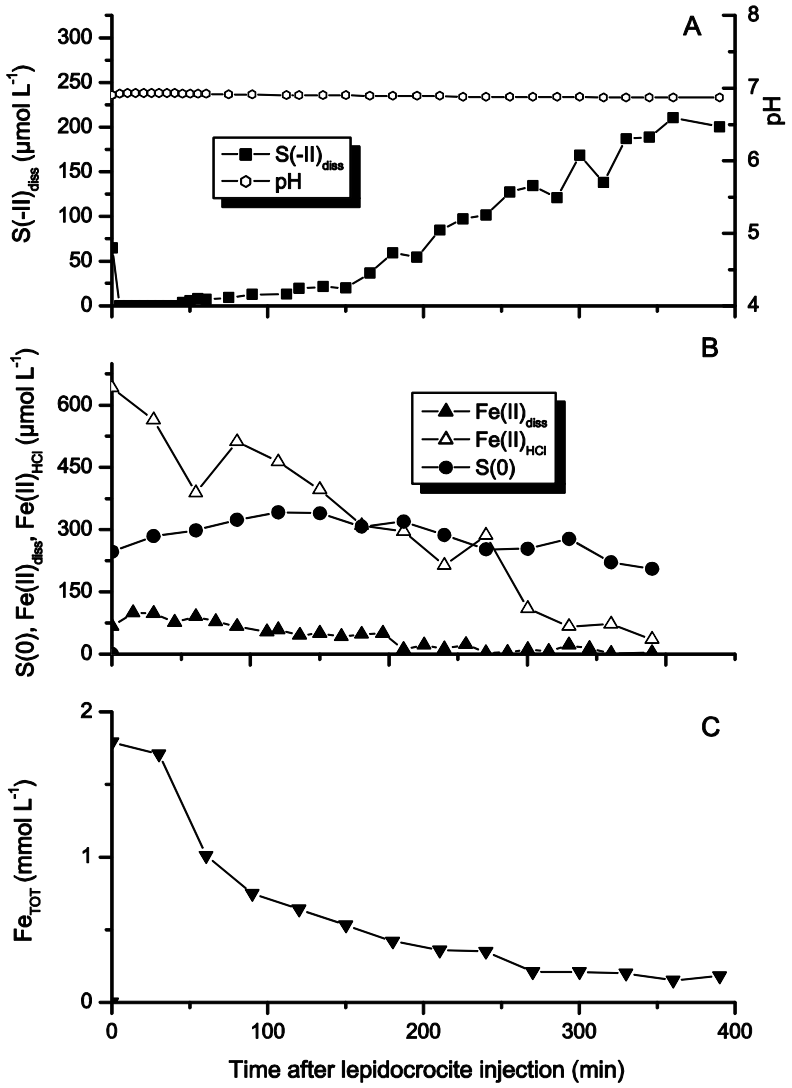

Fig. 4.2. Experimental outcome of the reaction of H_2S and lepidocrocite at pH 7 (run 3). Time zero corresponds to the addition of lepidocrocite. (A) shows the evolution of dissolved sulphide during the reaction with lepidocrocite. The main products total S(0), $Fe(II)_{HCl}$, and dissolved Fe(II) were monitored during the reaction (B). (C) displays the evolution of total Fe during the reaction.

At pH 7, immediately after the addition of lepidocrocite (A_s = 27.1 m^2 L^{-1}, c = 1.8 mmol L^{-1}), dissolved sulphide (c = 343 µmol L^{-1}) was consumed almost completely and started to increase again after 40 minutes (Fig. 4.2). Simultaneously, the pH increased from 6.90 to 6.93 and achieved a value of 6.87 toward the end of the experiment. Contrary to the experiments performed at pH 4, the solution turned black after the addition of lepidocrocite to the reactor solution. Within the first 5 minutes of the reaction dissolved Fe(II) and acid extractable Fe(II) achieved a maximum concentration of 99 µmol L^{-1} and 642 µmol L^{-1}, respectively. S(0) increased slower to approximately 340 µmol L^{-1}. $Fe(II)_{aq}$ and S(0) species remained stable for 150 minutes while $Fe(II)_{HCl}$ started to decrease after 5 minutes.

4.4.2. Rates of H_2S oxidation and Fe(II) dissolution

The simulated H_2S concentration correspond well to the measured H_2S concentration which implies that the surface complexation model for the oxidation rate of H_2S underlying the simulations is valid throughout the entire experimental time span (Fig. 4.3). The calculated Fe(II) concentration correspond well to the measured Fe(II) concentration at pH 4. At pH 7 the calculated Fe(II) concentration does not fit to the measured Fe(II) concentration due to some interferences at this pH. However, product formation did not lead to interferences which makes the flow-through reactor a suitable tool to investigate particularly the initial reaction kinetics.

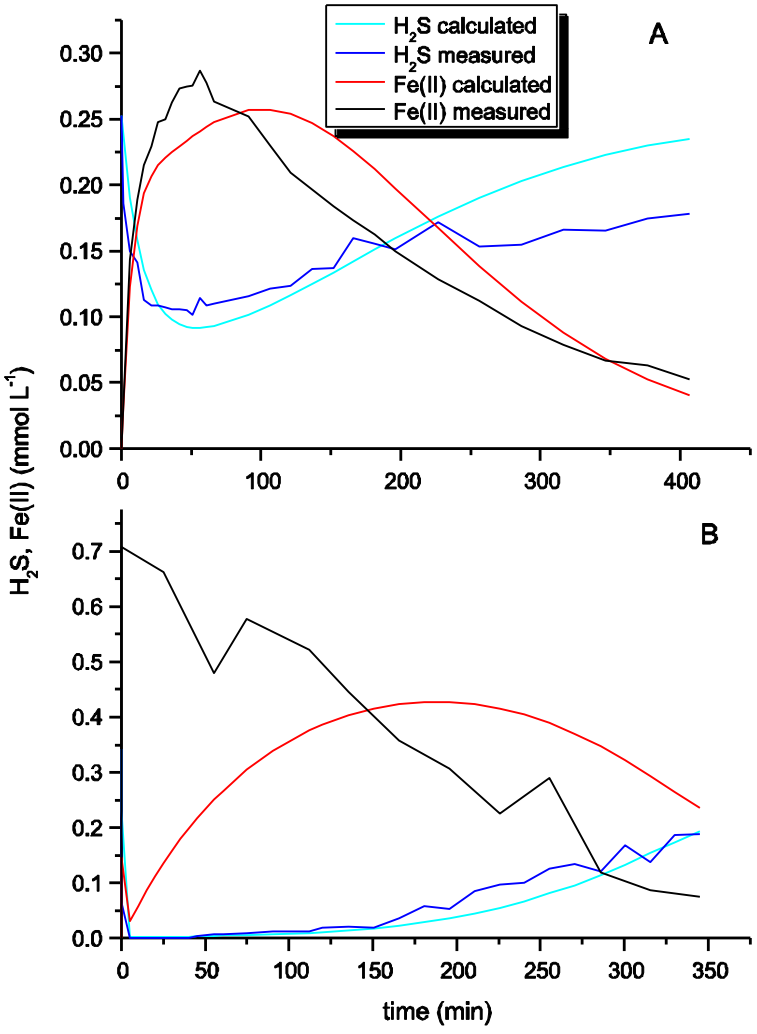

Fig. 4.3. The modeled H_2S and Fe(II) concentration and measured H_2S and Fe(II) concentration for the reductive dissolution of lepidocrocite at pH 4 (A, run 18) and at pH 7(B, run 3).

The pH dependency of Fe(III) (hydr)oxide reactivity is well-established and occurs due to the formation of different surface species and due to the changes in the speciation of the dissolved

reactant *(13,29)*. The observed reaction rate constants k_{obs_H2S} and $k_{obs\_Fe(II)}$ showed a strong pH dependency and also varied between the minerals over two orders of magnitude for pH 4 and for pH 7 over three magnitudes. The reactivity coefficient $k_{obs\_(H2S)}$ and $k_{obs\_Fe(II)}$ normalized to the surface area decreases in the order ferrihydrite > lepidocrocite > goethite > Bayferrox lepidocrocite > Bayferrox goethite and ranged between 10^{-3} to 10^{-4} L min^{-1} m^{-2} for pH 4 (Table 4.3) while at pH 7 the reductive dissolution decrease in the sequence ferrihydrite ~ lepidocrocite > Bayferrox lepidocrocite > goethite ~ Bayferrox goethite and ranged between 10^{-1} to 10^{-3} L min^{-1} m^{-2} for pH 7 (Table 4.4). The reactivity coefficients k_{obs_H2S} and $k_{obs\_Fe(II)}$ suggest that the oxidation of sulphide and the formation of Fe(II) occurred at the same rate at both pH.

Bayferrox lepidocrocite is contaminated with goethite which explains the lower k_{obs_H2S} and $k_{obs\_Fe(II)}$ compared to synthetic lepidocrocite.

Table 4.3. The observed reaction constants k_{obs} for the oxidation of sulphide and the formation of Fe(II) at pH 4. k_{obs} is derived in terms of A.

Mineral	Run	k_{obs_H2S} ($L\ min^{-1}\ m^{-2}$)	Standard deviation (H_2S) ($L\ min^{-1}\ m^{-2}$)	$k_{obs\_Fe(II)}$ ($L\ min^{-1}\ m^{-2}$)	Standard deviation (Fe(II)) ($L\ min^{-1}\ m^{-2}$)
Ferrihydrite	14	2.14×10^{-3}	3.07×10^{-2}	7.39×10^{-3}	7.72×10^{-1}
Ferrihydrite	16	5.05×10^{-3}	2.04×10^{-2}	1.64×10^{-2}	3.89×10^{-1}
Lepidocrocite	15	8.00×10^{-4}	1.24×10^{-2}	1.57×10^{-3}	4.64×10^{-2}
Lepidocrocite	18	1.50×10^{-3}	2.02×10^{-2}	3.45×10^{-3}	3.20×10^{-2}
Goethite	10	9.89×10^{-4}	6.63×10^{-2}	1.34×10^{-3}	1.16×10^{-1}
Goethite	11	1.03×10^{-3}	2.10×10^{-2}	1.36×10^{-3}	7.73×10^{-2}
Goethite	12	4.23×10^{-4}	1.96×10^{-2}	9.10×10^{-4}	3.28×10^{-2}
Goethite	13	1.40×10^{-3}	3.78×10^{-2}	1.49×10^{-3}	3.86×10^{-2}
Bayferrox Lepidocrocite	20	4.53×10^{-4}	7.46×10^{-2}	4.92×10^{-4}	9.91×10^{-2}
Bayferrox Lepidocrocite	21	2.06×10^{-4}	2.09×10^{-3}	4.21×10^{-4}	1.02×10^{-3}
Bayferrox Goethite	17	1.62×10^{-4}	9.91×10^{-3}	1.30×10^{-4}	4.38×10^{-4}
Bayferrox Goethite	19	5.79×10^{-4}	1.69×10^{-2}	2.17×10^{-4}	7.40×10^{-4}

Table 4.4. The observed reaction constants k_{obs} for the oxidation of sulphide and the reductive formation of Fe(II) at pH 7. k_{obs} is derived in terms of A.

Mineral	Run	k_{obs_H2S} ($L\ min^{-1}\ m^{-2}$)	Standard deviation (H_2S) ($L\ min^{-1}\ m^{-2}$)	$k_{obs\_Fe(II)}$ ($L\ min^{-1}\ m^{-2}$)	Standard deviation (Fe(II)) ($L\ min^{-1}\ m^{-2}$)
Ferrihydrite	4	3.70×10^{-1}	1.17×10^{-2}	7.42×10^{-1}	2.51×10^{-2}
Ferrihydrite	7	1.98×10^{-2}	4.46×10^{-2}	8.94×10^{-2}	6.60×10^{-1}
Lepidocrocite	3	8.85×10^{-2}	3.84×10^{-2}	1.47×10^{-1}	9.22×10^{-1}
Lepidocrocite	6	2.12×10^{-1}	2.69×10^{-2}	1.98×10^{-1}	2.50×10^{-1}
Goethite	2	4.86×10^{-3}	3.56×10^{-2}	3.24×10^{-3}	1.11×10^{-1}
Goethite	8	5.03×10^{-3}	6.24×10^{-2}	2.84×10^{-3}	9.43×10^{-2}
Bayferrox Lepidocrocite	22	2.32×10^{-2}	7.83×10^{-3}	3.07×10^{-2}	6.53×10^{-2}
Bayferrox Lepidocrocite	23	2.31×10^{-2}	8.48×10^{-3}	3.56×10^{-2}	1.05×10^{-1}
Bayferrox Goethite	1	7.90×10^{-3}	1.27×10^{-2}	7.08×10^{-3}	1.78×10^{-2}
Bayferrox Goethite	5	3.04×10^{-3}	2.94×10^{-2}	1.66×10^{-3}	1.26×10^{-2}
Bayferrox Goethite	9	2.16×10^{-3}	2.10×10^{-2}	2.79×10^{-3}	1.46×10^{-2}

4.5. Discussion

4.5.1. Electron balance during reaction

The reaction between lepidocrocite and dissolved sulphide could be divided into three steps. In the initial phase, the majority of dissolved sulphide was rapidly consumed due to a pre-equilibrium phase with respect to the sulphide adsorption at the oxide surface *(18)*. In a second step, the H_2S concentration remained constant until the reduction of ferric (hydr)oxides stopped followed by the third step, the increase of H_2S.

This reaction is described by the surface complexation model proposed by ref *(18)*. According to this surface controlled reaction, the sum of Fe(II) phases should be double the concentration of sulphide oxidized, consistent with the conservation of electrons during the oxidation of sulphide to elemental sulphur *(14)*.

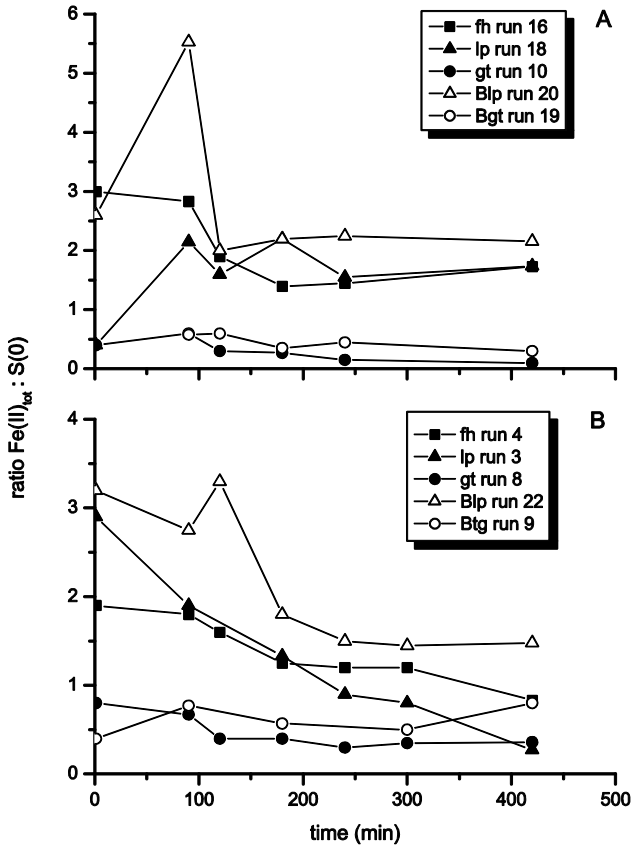

Fig. 4.4. Ratios of $Fe(II)_{tot}$:S(0) for ferrihydrite (fh), lepidocrocite (lp), goethite (gt), Bayferrox lepidocrocite (Blp), and Bayferrox goethite (Bgt) at pH 4 (A) and pH 7 (B) (Table S 1, S 2).

The ratios of $Fe(II)_{tot}$:S(0) during the reaction of ferric (hydr)oxides and dissolved sulphide at pH 4 and pH 7 are shown in Fig. 4.4 (Supporting information: Table S 1, S 2). The data show some scatter which is probably due to some analytical uncertainty. However, some general patterns can be derived.

The initially ratios of $Fe(II)_{tot}$:S(0) were >2 for ferrihydrite and the both lepidocrocites and the ratio of 2:1 was achieved between 30 to 100 minutes after starting the experiment (Table S 1, S 2). The ratio of $Fe(II)_{tot}$:S(0) for the both goethites ranged between 0.3 to 1 at both pH (Fig. 4.4). These observations suggest that the formation of S(0) and Fe(II) was decoupled.

At each point of time, the formation of S(0) was higher than the formation of Fe(II) phases for goethite compared to lepidocrocite and ferrihydrite where the formation of Fe(II) was more than double the S(0) formation. In a previous study *(20)* we observed the same non-stoichiometric ratios of Fe(II):S(0) which we explained by different lattice stabilities of the Fe(III) (hydr)oxides and by the surface complexation model. That is, first the adsorption of dissolved sulphide to the oxide surface which resulted in the formation of S(-I) and Fe(II). At pH 7 the most of the formed Fe(II) is associated to the Fe(III) oxide surface which leads to an electron transfer between the structural Fe(III) and the adsorbed Fe(II) *(30-32)*. The recycled

Fe(III) at the surface is then available to oxidize an additional S(-II) ion or S(-I) ion. These interactions lead to excess-Fe(II) formation in the presence of ferrihydrite and lepidocrocite *(20)*. The extent of excess-Fe(II) formation increases in the sequence goethite < lepidocrocite < ferrihydrite *(20)* which implies that a higher specific surface area emphasizes the formation of Fe(II). Furthermore, at circumneutral pH the precipitation of FeS occurs which trap S(-II) and thus, prevent its further oxidation which leads also to high Fe(II):S(0) ratios in the case of ferrihydrite and lepidocrocite.

But in the presence of goethite, the adsorption of Fe(II) may occurs with or without an electron transfer *(33)*. So, the Fe(II) remained at the goethite surface without an electron transfer and occupied the surface sites and so, prevent the further oxidation of S(-II) and S(-I). These processes may explain the observed low Fe(II):S(0) ratios in the reactor suspensions with goethite. Significantly, the underestimation of Fe(II) occurs at pH 4 as well as at pH 7. Another study *(32)* investigated the reaction of different hematite surfaces with Fe(II) at pH 3 and pH 7 and observed that the structural transformations of hematite by Fe(II) are generally independent of pH but vary with crystallographic plane of hematite. They found out that the reaction between Fe(II) and hematite occurs at acidic pH values as well. This could be an explanation for the observed low concentrations of Fe(II) at pH 4 in the presence of goethite.

The differences of $Fe(II)_{tot}$:S(0) ratios implies that the Fe^{2+} detachment kinetic from Fe(III) (hydr)oxide surfaces control their reactivity and thus, the detachment of Fe^{2+} is the rate limiting step *(9,14,18)*. These desorption kinetics are influenced by the thermodynamic stability of the Fe(III) solid phase.

Similar observations were made in previous studies *(8,9,12-14)*. At circumneutral pH the dominant oxidized sulphur product was S(0) and a part of reduced iron was bound to the solid phase FeS while a larger proportion remained at the oxide surface with or without an electron transfer. These different conditions of Fe^{2+} are attributed to the different ratios of $Fe(II)_{tot}$:S(0) which may influence the redox potential of the reactor suspension and therefore the reactivity of the ferric (hydr)oxides.

4.5.2. Variables controlling reactivity

The results have demonstrated that the reactivity of Fe(III) oxides decreases in the sequence ferrihydrite > lepidocrocite > goethite follow a second rate order (Table 4.3, 4.4). The reactivity order follows the dissolution order of Fe(III) (hydr)oxides and is reverse to the order of the degree of crystallinity of ferric (hydr)oxides *(34)*. Additionally, with increasing

specific surface area the reactivity of the Fe(III) (hydr)oxides increases. These observations are consistent with the findings of investigators who determined the reactivity of various ferric (hydr)oxides towards dissolved sulphide or ascorbic acid *(7,14-16,18).* Some of these studies suggest a pseudo-first order reaction with respect to the initial dissolved sulfide concentration *(3,13,16).* Other studies determined a reaction order of 1.5 for total dissolved sulphide during the formation of FeS *(12)* or a reaction order of 0.5 due to some interferences between Fe(II), H_2S, and the surface at pH 7.5 *(14).* Prior studies suggest that the reactivity is largely controlled by the surface properties and sulphide concentration *(3,9,13,18,35)* while recent studies suggest that the crystallographic properties of ferric (hydr)oxides are the rate controlling step *(14,16).*

In our experiments, the solid concentration of the various ferric (hydr)oxides was chosen to obtain the same total concentration of surface area as approximately 24 $m^2\ L^{-1}$. Thus, in the initial phase of reaction the surface concentration is equal for all experiments. As the model fit demonstrates we have constant reaction conditions over the experiment period (Fig. 4.3). So, the different ferric (hydr)oxides can be directly compared with each other and the reaction is independent from the specific surface area but influenced by surface and crystal properties of each oxide.

The mineral reactivity can be related to thermodynamic considerations (free energy). The dependency of the reductive dissolution of ferric (hydr)oxides on free energies has been stressed by several authors *(4,7,14,18).* We calculated the free energies for the following reactions

$$2\ FeOOH + H_2S + 4\ H^+ \rightarrow S(0) + 2\ Fe^{2+} + 4\ H_2O \quad (8)$$

$$2\ Fe(OH)_3 + H_2S + 4\ H^+ \rightarrow S(0) + 2\ Fe^{2+} + 6\ H_2O \quad (9)$$

$$2\ FeOOH + 2\ H_2S + 4\ H^+ \rightarrow S(0) + Fe^{2+} + FeS + 4\ H_2O \quad (10)$$

$$2\ Fe(OH)_3 + 2\ H_2S + 4\ H^+ \rightarrow S(0) + Fe^{2+} + FeS + 6\ H_2O \quad (11)$$

The free energy values used for eq. 8-11 are listed in Table 4.5. It is commonly assumed that at pH 4 all Fe(II) is present as aqueous Fe^{2+}. But the study of ref *(32)* found out that there are also interactions between Fe(II) and the structural Fe(III) at lower pH. At pH 7 there are complications due to the formation of FeS and the continued association of Fe(II) with the oxide surface. The free energy of associated Fe(II) to the oxide surface were not available from the literature. Hence, only the formation of FeS and dissolved Fe^{2+} are considered.

Table 4.5. G_f° **values of the three ferric (hydr)oxides used in eq. 8-11.**

	G_f° (kJ mol^{-1})	Reference
Ferrihydrite ($Fe(OH)_3$)	-711	*(36)*
Lepidocrocite (γ-FeOOH)	-480.1	*(37)*
Goethite (α-FeOOH)	-490.6	*(38)*
$FeS_{amorphous}$	-21.3	*(39)*

To compare the minerals among each other, the intrinsic rate constants k_{intr} for the oxidation of sulphide normalized to the surface species were estimated after the following equation *(7)*

$$R_{obs} = k_{intr}\, \beta_{FeOH,ox}\, \alpha_{H2S}\, S_{TOT}\, A_s\, c(FeOOH)\, c(H_2S)_{tot}\, K_{Ads} \qquad (12)$$

where R_{obs} is the observed reaction rate (mol L^{-1} min^{-1}), k_{intr} is the intrinsic rate coefficient for the oxidation of H_2S (min^{-1}) $\beta_{FeOH,ox}$ is the fraction of surface sites >FeOH, which depends on both surface charge and the intrinsic acidity constants of the respective oxide (-),α_{H2S} is the protolysis coefficient of the species H_2S (-), S_{TOT} is the site density (3.75*10^{-6} mol m^{-2}), A_s is the specific surface area (m^2 g^{-1}), $c(FeOOH)$ is the concentration of the oxide (g L^{-1}), $c(H_2S)_{tot}$ is the initial concentration of H_2S in the reactor solution, and K_{Ads} is the adsorption constant ($10^{2.82}$ L mol^{-1}).

Setting eq. 12 equal to eq. 2, one obtains

$$k_{obs} = k_{intr}\, \beta_{FeOH,ox}\, \alpha_{H2S}\, S_{TOT}\, K_{Ads} \qquad (13a)$$

$$k_{intr} = \frac{k_{obs}}{\beta_{FeOH,ox}}\, \alpha_{H2S} S_{TOT} K_{Ads} \qquad (13b)$$

$\beta_{FeOH,ox}$ was calculated by using PHREEQC described in supporting information.

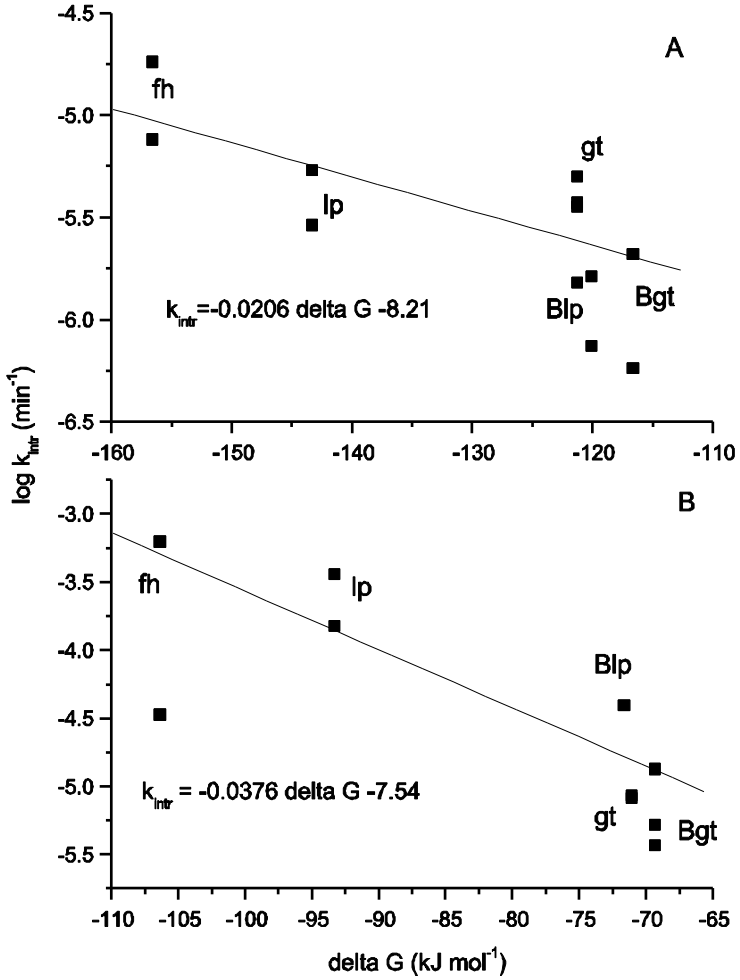

Fig. 4.5. Relationship between the logarithm of intrinsic rate constant k and the free energies for the reactions of the ferrihydrite (fh), lepidocrocite (lp), goethite (gt), Bayferrox lepidocrocite (Blp), and Bayferrox goethite (Bgt) with dissolved sulphide at pH 4 (A, eq. 8-9) and pH 7 (B, eq. 10-11).

Fig. 4.5 displays a significant relationship between the intrinsic rate constant k_{intr} and the free energies. For both pH the intrinsic reaction coefficients decrease with increasing free energies which implies that k_{intr} increases at more negative ΔG values *(14,18)*. Comparison of Fig. 4.5A and 4.5B showed that the reactivity at pH 7 are stronger influenced by free energy than at pH 4.

However, there are a number of uncertainties inherent in the derivation of Fig. 4.5. The weakest influence may arise from $\beta_{FeOH,ox}$ due to its low variation between the Fe(III) (hydr)oxides (Supporting information: Table S 3). Also, the validity of K_{Ads} is unknown. The value was derived as fitting parameter in a study of H_2S and hematite *(18)* and may bear uncertainty in itself. Moreover K_{Ads} may reflect a mean adsorption constant integrating over different crystal faces. The relative importance of each of these species may vary significantly *(33)*. Also the calculation of free energies is associated with severe uncertainties particularly since the role of the redox potential of surface associated Fe(II) is not understood (see section

4.5.1.). The observed ratios of $Fe(II)_{tot}$:S(0) implies that Fe(II) inhibit the reactivity of goethite while the association of Fe(II) to the ferrihydrite and lepidocrocite surface seems to be accelerate their reductive dissolution by dissolved sulphide. So, the reactivity of Fe(III) (hydr)oxides is largely control by mineral properties. Association of Fe(II) with the oxide surface or even uptake in bulk structure may affect conduction band bending and significantly affect the energies of the conduction band and thus, the semiconducting properties *(40)*. Large differences in energy between the donor and acceptor levels resulted in a slow electron transfer as in the presence of goethite *(41)*. This means, that the reactivity of ferric (hydr)oxides are influenced by their adsorption properties and the electron properties and accordingly by the dynamics of Fe(II). Thus, the formed Fe(II) and its further reaction to FeS or its interaction with the oxide surface control the reaction between ferric (hydr)oxides and dissolved sulphide.

Research is required to identify the mineral specific variation in reactivities also in quantitative terms such as the Fe(II) variations of Fe(III) oxides.

4.6. Acknowledgements

This study was carried out with financial support from the Deutsche Forschungsgemeinschaft (DFG) and was part of the priority program 580 “Electron Transfer Processes in Anoxic Aquifers” (PE 438/11-2). We thank Jutta Eckert for help and support in the lab.

4.7. References

(1) Jacobsen, R.; Postma, D. Redox zoning, rates of sulfate reduction and interactions with Fe-reduction and methanogenesis in a shallow sandy aquifer, Romo, Denmark *Geochim. Cosmochim. Acta* **1999**, 63, 137-151.

(2) Stumm, W.; Sulzberger, B. The Cycling of Iron in Natural Environments - Considerations Based on Laboratory Studies of Heterogeneous Redox Processes *Geochim. Cosmochim. Acta* **1992**, 56, 3233-3257.

(3) Yao, W.; Millero, F. J. Oxidation of hydrogen sulfide by hydrous Fe(III) oxides in seawater *Mar. Chem.* **1996**, 52, 1-16.

(4) Roden, E. E. Fe(III) oxide reactivity toward biological versus chemical reduction *Environ. Sci. Technol.* **2003**, 37, 1319-1324.

(5) Pedersen, H. D.; Postma, D.; Jakobsen, R.; Larsen, O. Fast transformation of iron oxyhydroxides by the catalytic action of aqueous Fe(II) *Geochim. Cosmochim. Acta* **2005**, 69, 3967-3977.

(6) Canfield, D. E.; Raiswell, R.; Bottrell, S. The reactivity of sedimentary iron minerals toward sulphide. *American Journal of Science* **1992**, 292, 659-683.

(7) Peiffer, S.; Gade, W. Reactivity of ferric oxides toward H_2S at low pH *Environ. Sci. Technol.* **2007**, 41, 3159-3164.

(8) Hellige, K.; Pollok, K.; Larese-Casanova, P.; Behrends, T.; Peiffer, S. Pathways of ferrous iron mineral formation upon sulfidation of lepidocrocite surfaces *submitted to Geochemica et Cosmochemica Acta* **2010**.

(9) Pyzik, A. J.; Sommer, S. E. Sedimentary iron monosulphides: kinetics and mechanism of formation Geochim. Cosmochim. Acta **1981**, 45, 687-698.

(10) Rickard, D. Kinetics and Mechanism of Pyrite Formation at Low Temperatures American Jounal of Science **1975**, 275, 636-652.

(11) Berner, R. A. Sedimentary pyrite formation *American Journal of Science* **1970**, 268, 1-23.

(12) Rickard, D. Kinetics and mechanism of the sulfidation of goethite *American Journal of Science* **1974**, 274, 941-952.

(13) Peiffer, S.; Dos Santos Afonso, M.; Wehrli, B.; Gächter, R. Kinetics and mechanism of the reaction of H_2S with lepidocrocite *Environ. Sci. Technol.* **1992**, 26, 2408-2413.

(14) Poulton, S. W.; Krom, D. M.; Raiswell, R. A revised scheme for the reactivity of iron (oxyhydr)oxide minerals towards dissolved sulfide *Geochim. Cosmochim. Acta* **2004**, 68, 3703-3715.

(15) Postma, D. The Reactivity of Iron-Oxides in Sediments - a Kinetic Approach *Geochim. Cosmochim. Acta* **1993**, 57, 5027-5034.

(16) Larsen, O.; Postma, D. Kinetics of reductive bulk dissolution of lepidocrocite, ferrihydrite, and goethite *Geochim. Cosmochim. Acta* **2001**, 65, 1367-1379.

(17) Lovley, D. R.; Phillips, E. J. P.; Lonergan, D. J. Enzymatic Versus Nonenzymatic Mechanisms for Fe(III) Reduction in Aquatic Sediments *Environmental Science & Technology* **1991**, 25, 1062-1067.

(18) Dos Santos Afonso, M.; Stumm, W. Reductive Dissolution of iron(III) (hydr)oxides by hydrogen sulfide *Langmuir* **1992**, 8, 1671-1675.

(19) Yao W.; Millero F. J. Oxidation of hydrogen sulfide by hydrous Fe(III) oxides in seawater *Mar. Chem.* **1996**, 52, 1-16.

(20) Hellige, K.; Pollok, K.; Larese-Casanova, P.; Behrends, T.; Peiffer, S. The influence of structural properties of ferric hydroxides 6-line ferrihydrite, lepidocrocite, and goethite on reaction pathways with sulphide *unpublished* **2010**.

(21) Schwertmann U.; Cornell R. M. *Iron oxides in the laboratory: Preparation and characterization*; Wiley-VCH Verlag GmbH: Weinheim, New York, Basel, Cambridge, Tokyo, **2000**.

(22) Gupta S. K.; *Über die Phosphat-Elimination in den Systemen HPO-γ-FeO(OH) und HPO-FeCl und die Eigenschaften von Klärschlamm-Phosphat.* Dissertation Thesis, Universität Bern: Bern, **1976**; 138pp.

(23) Buchholz, A. *Redox reactions and phase transformation processes at iron mineral surfaces studied by compound specific isotope analysis.* Dissertation Thesis, Geowissenschaftliche Fakultät; Eberhard Karls Universität Tübingen: Tübingen, **2009**; 145pp.

(24) Chongxuan, L.; Zachara, J. M.; Strickland, J. Kinetics of reductive dissolution of hematite by bioreduced anthraquinone-2,6-disulfonate *Environ. Sci. Technol.* **2007**, 41, 7730-7735.

(25) Tamura H.; Goto K.; Yotsuyanagai T.; M., N. Spectrophotometric determination of iron(II) with 1,10-phenanthroline in the presence of large amounts of iron(III) *Talanta* **1974**, 21, 314-318.

(26) Fonselius S.; Dyrssen D.; Yhlen B. Determination of hydrogen sulphide. In *Methods of Seawater Analysis*; Grasshoff K., Kremling K., Ehrhardt M., Eds.; Wiley-VCH: Weinheim, New York, Chichester, Brisbane, Singapore, Toronto, **1999**; pp 91-108.

(27) Tabatabai M. A. A rapid method for determination of sulfate in water samples *Environ. Letters* **1974**, 7, 237-243.

(28) Imboden, D. M.; Koch, S. *Systemanalyse- Einführung in die mathematische Modellierung natürlicher Systeme*; Springer, **2004**.

(29) Poulton, S. W. Sulfide oxidation and iron dissolution kinetics during the reaction of dissolved sulfide with ferrihydrite *Chemical Geology* **2003**, 202, 79-94.

(30) Williams, A. G. B.; Scherer, M. M. Spectroscopic evidence for Fe(II)-Fe(III) electron transfer at the iron oxide - water interface *Envion. Sci. Technol.* **2004**, 38, 4782-4790.

(31) Handler, R. M.; Beard, B. L.; Johnson, C. M.; Scherer, M. M. Atom Exchange between Aqueous Fe(II) and Goethite: An Fe Isotope Tracer Study *Environmental Science & Technology* **2009**, 43, 1102-1107.

(32) Catalano, J. G.; Fenter, P.; Park, C.; Zhang, Z.; Rosso, K. M. Structure and oxidation state of hematite surfaces reacted with aqueous Fe(II) at acidic and neutral pH *Geochim. Cosmochim. Acta* **2010**, 74, 1498-1512.

(33) Hiemstra, T.; van Riemsdijk, W. H. Adsorption and surface oxidation of Fe(II) on metal (hydr)oxides *Geochim. Cosmochim. Acta* **2007**, 71, 5913-5933.

(34) Cornell, R. M.; Schwertmann, U. *The iron oxides: Structure, Properties, Reactions, Occurence and Uses*; Wiley-VCH Verlag GmbH: Weinheim, New York, Basel, Cambridge, Tokyo, **1996**.

(35) Wang, F.; Chen, J.; Forsling, W. Surface properties of natural aquatic sediments *Wat. Res.* **1997**, 31, 1796-1800.

(36) Majzlan, J.; Navrotsky, A.; Schwertmann, U. Thermodynamics of iron oxides: Part III. Enthalpies of formation and stability of ferrihydrite (similar to $Fe(OH)_3$), schwertmannite (similar to $FeO(OH)_{3/4}(SO4)_{1/8}$), and ε-Fe_2O_3 *Geochim. Cosmochim. Acta* **2004**, 68, 1049-1059.

(37) Majzlan, J.; Grevel, K. D.; Navrotsky, A. Thermodynamics of Fe oxides: Part II. Enthalpies of formation and relative stability of goethite (alpha-FeOOH), lepidocrocite (gamma-FeOOH), and maghemite (gamma-Fe_2O_3) *American Mineralogist* **2003**, 88, 855-859.

(38) Navrotsky, A.; Mazeina, L.; Majzlan, J. Size-driven structural and thermodynamic complexity in iron oxides *Geochim. Cosmochim. Acta* **2008**, 72, A673-A673.

(39) Anderko, A.; Shuler, P. J. A computational approach to predicting the formation of iron sulfide species using stability diagrams *Computers & Geosciences* **1997**, 23, 647-658.

(40) Sherman, D. M. Electronic structures of iron(III) and manganese(IV) (hydr)oxide minerals: Thermodynamics of photochemical reductive dissolution in aquatic environments *Geochim. Cosmochim. Acta* **2005**, 69, 3249-3255.

(41) Xu, Y.; Schoonen, M. A. A. The absolute energy positions of conduction and valence bands of selected semiconducting minerals *American Mineralogist* **2000**, 85, 543-556.

Appendix: Supporting Information

Intrinsic rate constants for the abiotic oxidation of sulfide by various ferric (hydr)oxides

Planned submission to Environmental Science and Technology

Katrin Hellige[1] and Stefan Peiffer[1]

[1]Department of Hydrology, University of Bayreuth, Universitätsstraße 30, D-95445 Bayreuth, Germany

Experimental set-up

The fluidized bed reactor (Fig. S 1) was developed to determine the reaction rates of various Fe(III) (hydr)oxides. The glass frit was added to prevent the export of the Fe(III) (hydr)oxide particles. The Teflon-coated stirring bar was kept in a frame to prevent the mechanical pulverization of the Fe(III) (hydr)oxide particles.

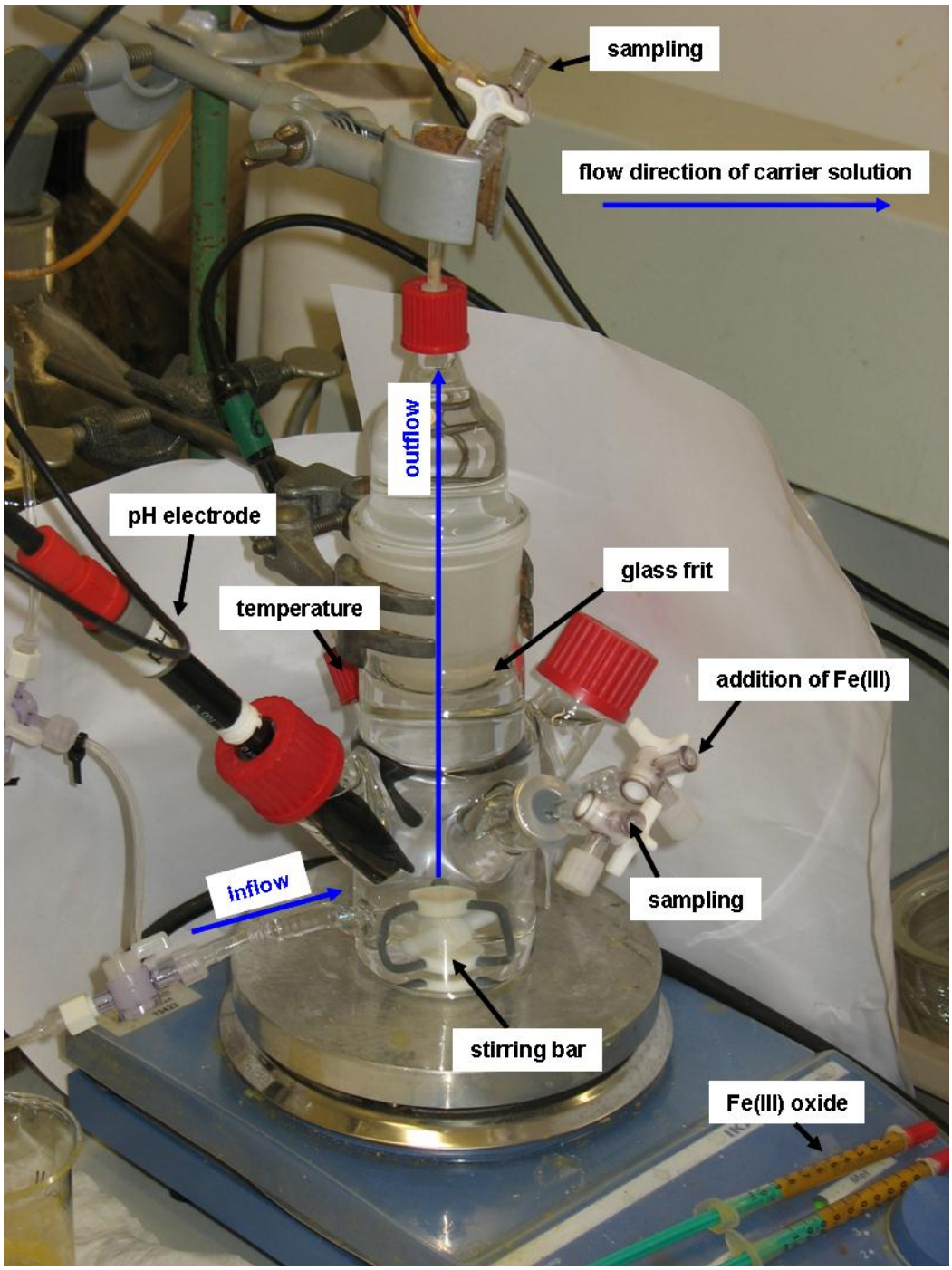

Fig. S 1. Experimental set-up.

Reaction of Fe(III) oxides with H_2S

The evolution of sulphur and iron species during the reaction of various ferric (hydr)oxides with dissolved sulphide at pH 4 and pH 7 (Fig. S2-S9):

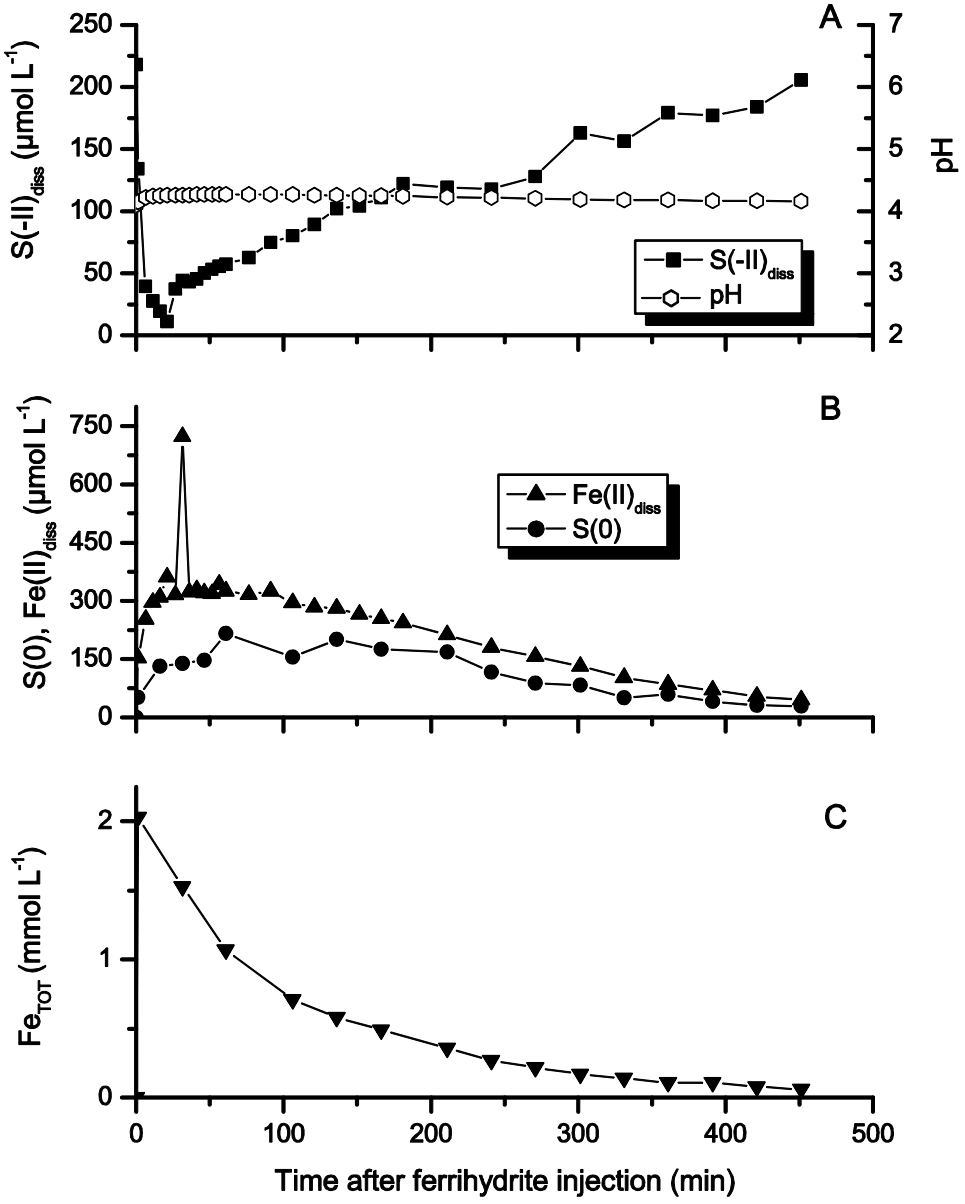

Fig. S 2. Ferrihydrite, pH 4 (Run 16).

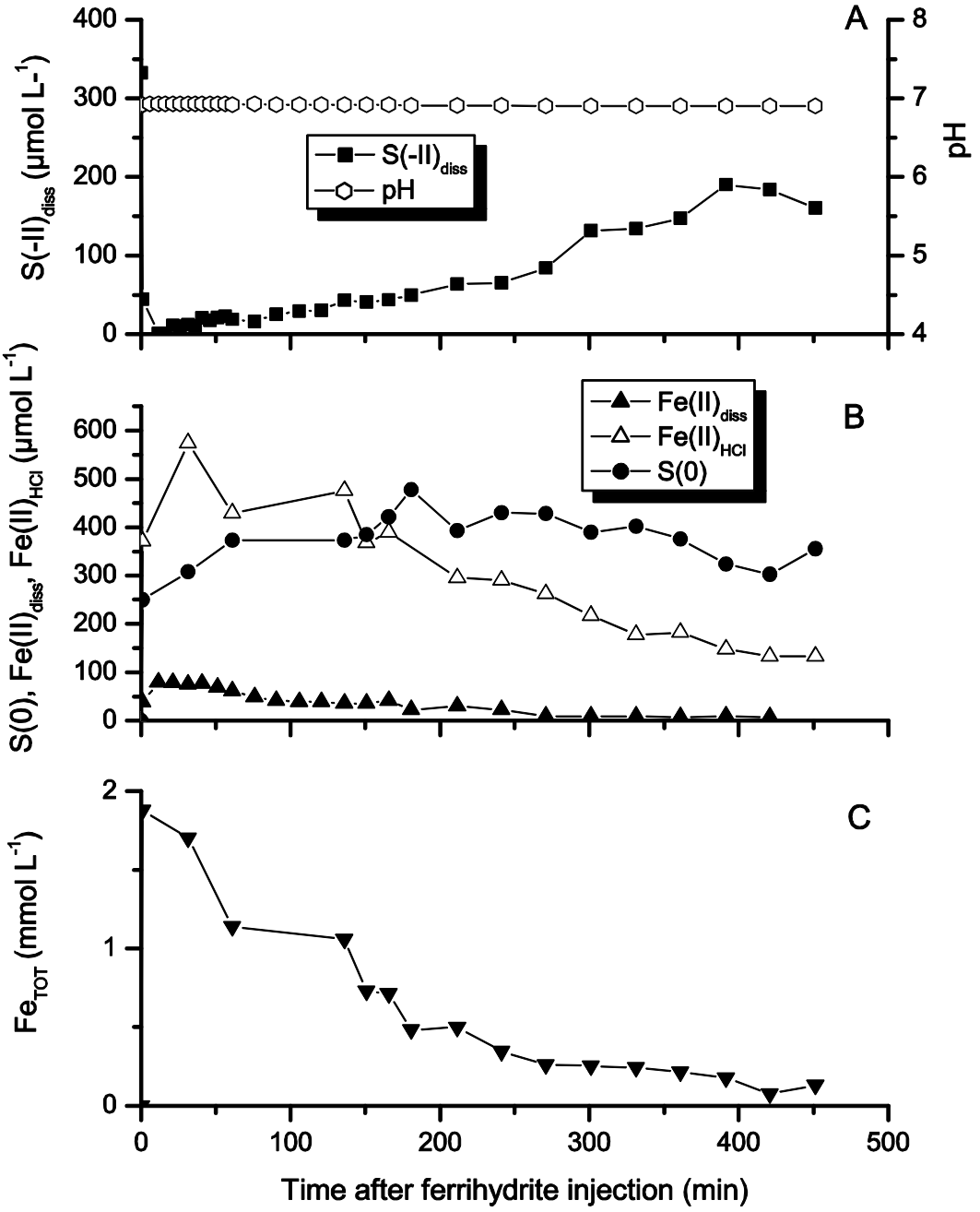

Fig. S 3. Ferrihydrite, pH 7 (Run 7)

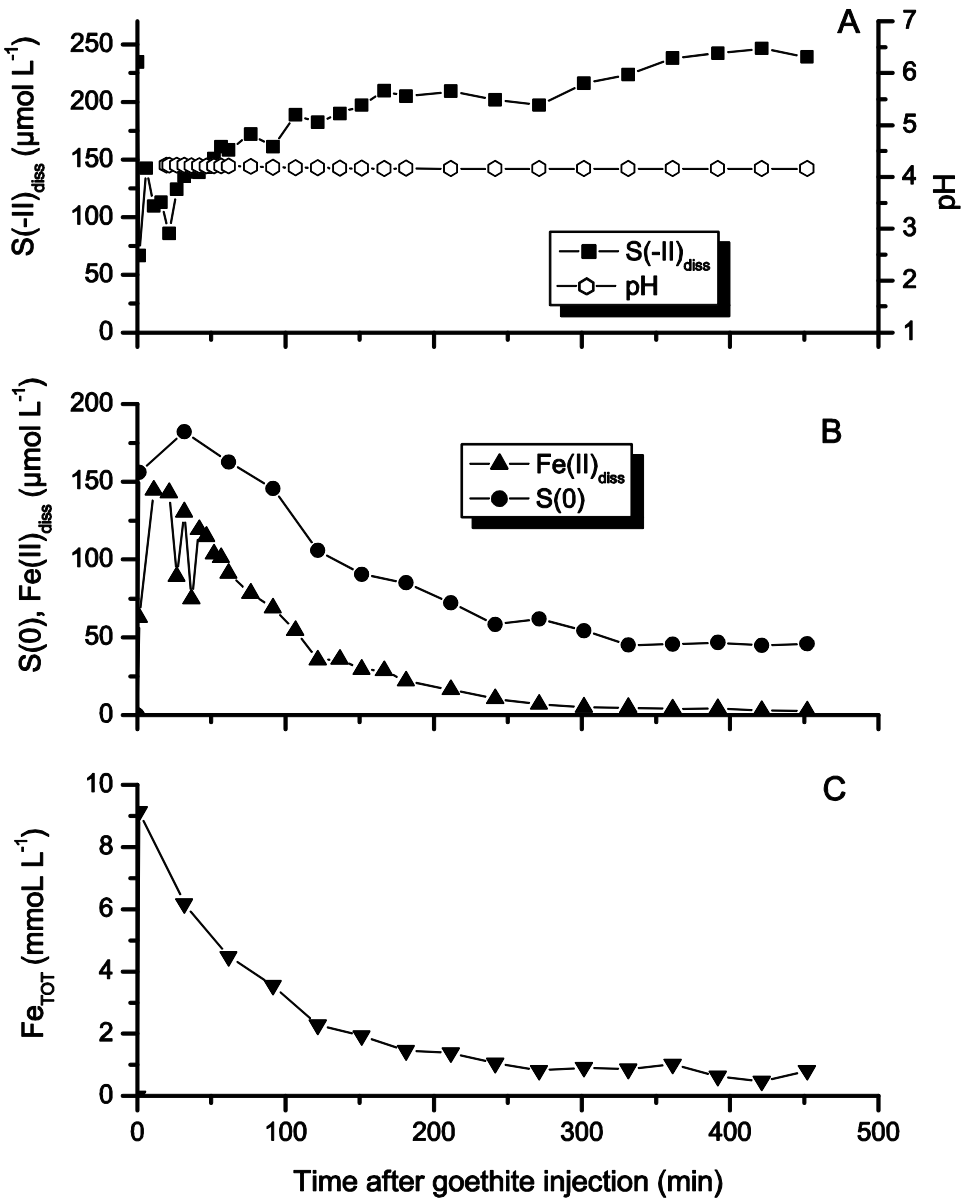

Fig. S 4. Goethite, pH 4 (Run 10)

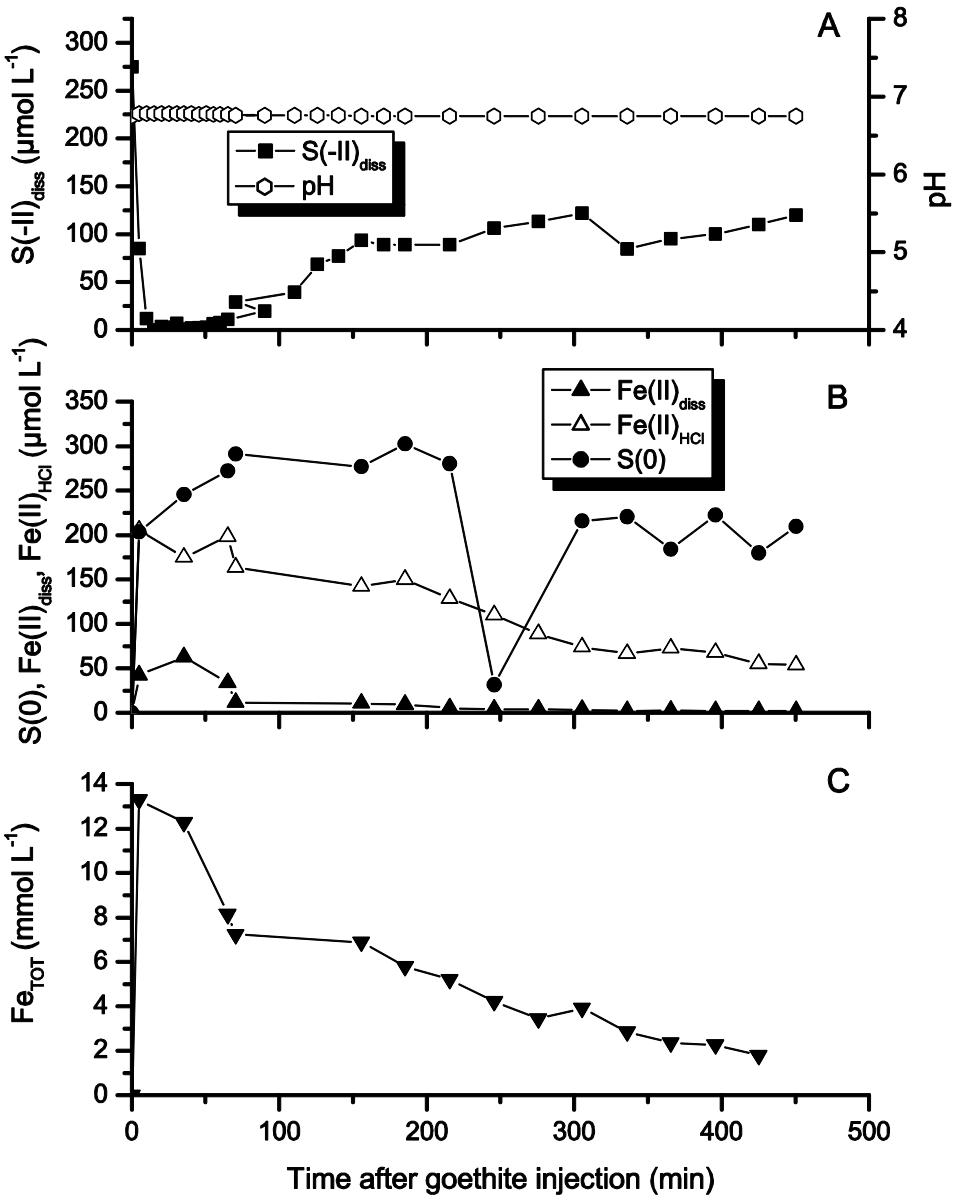

Fig. S 5. Goethite, pH 7 (Run 2).

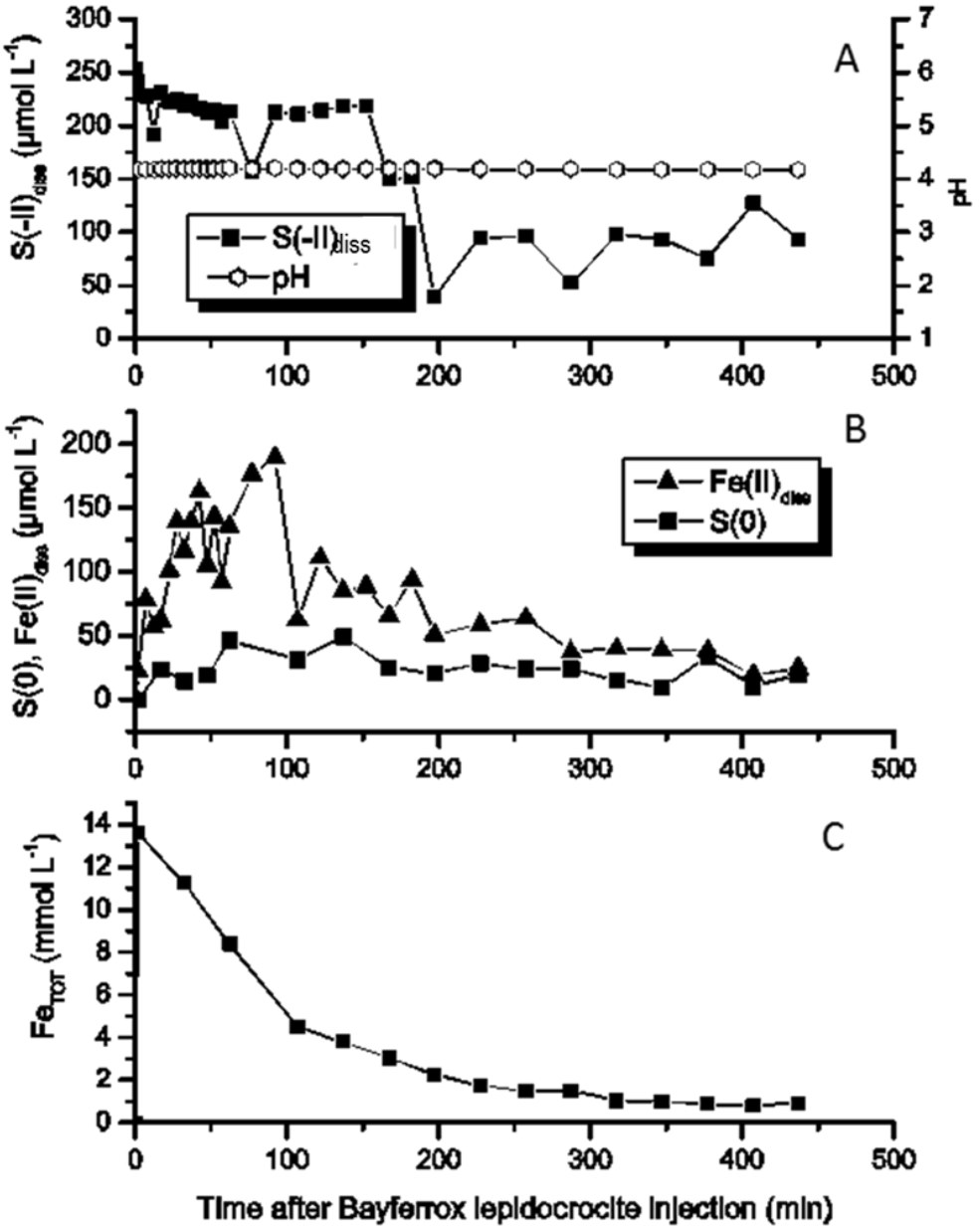

Fig. S 6. Bayferrox Lepidocrocite, pH 4 (Run 20).

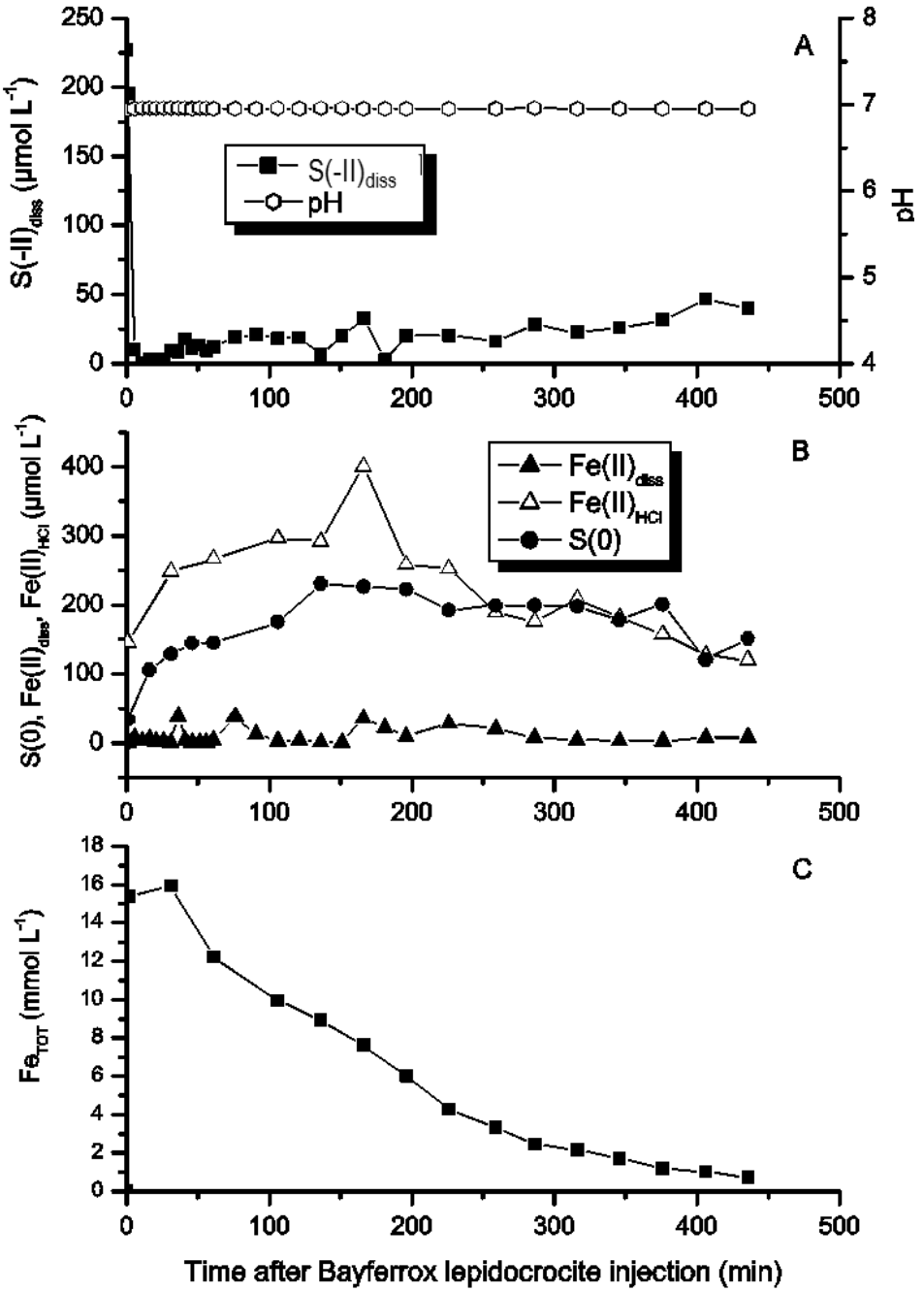

Fig. S 7. Bayferrox Lepidocrocite, pH 7 (Run 23)

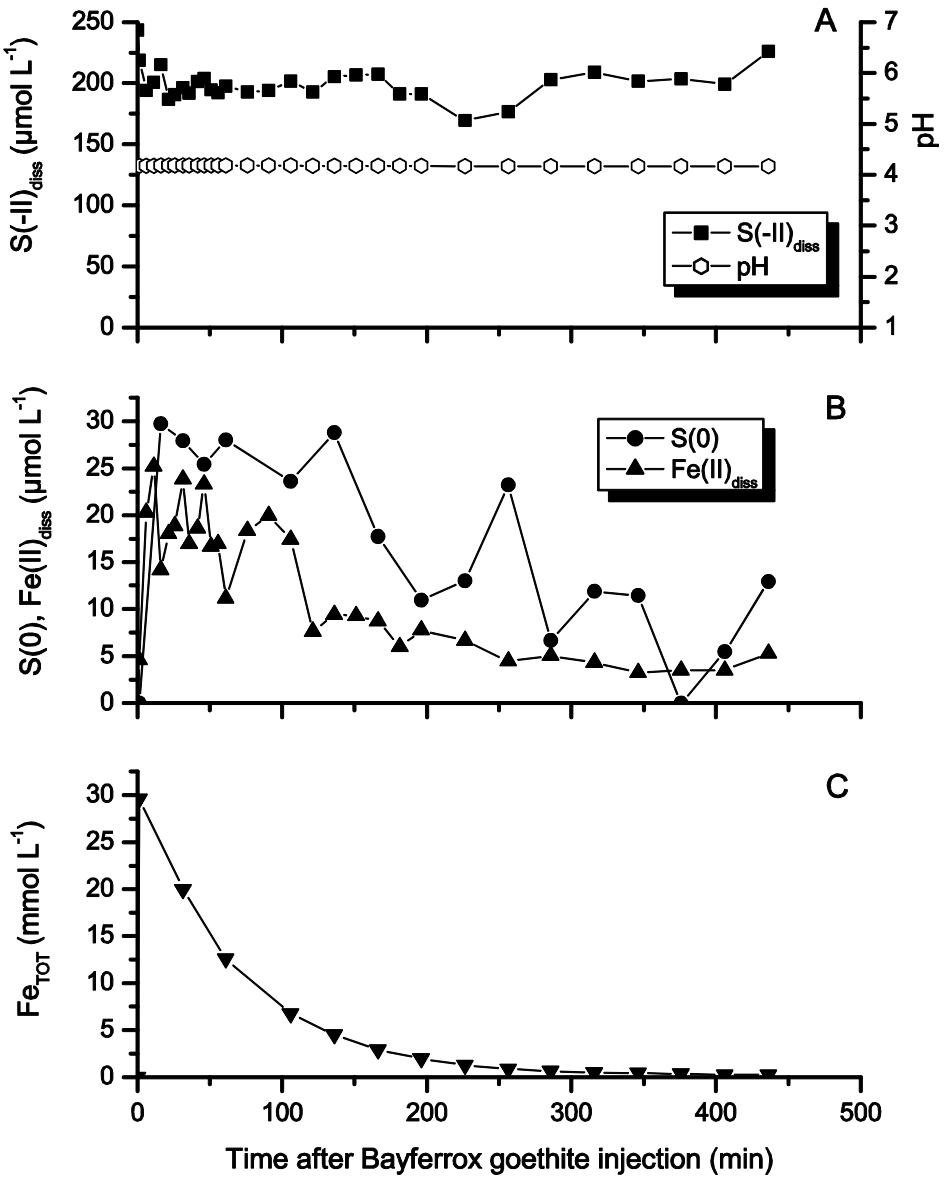

Fig. S 8. Bayferrox Goethite, pH 4 (Run 19)

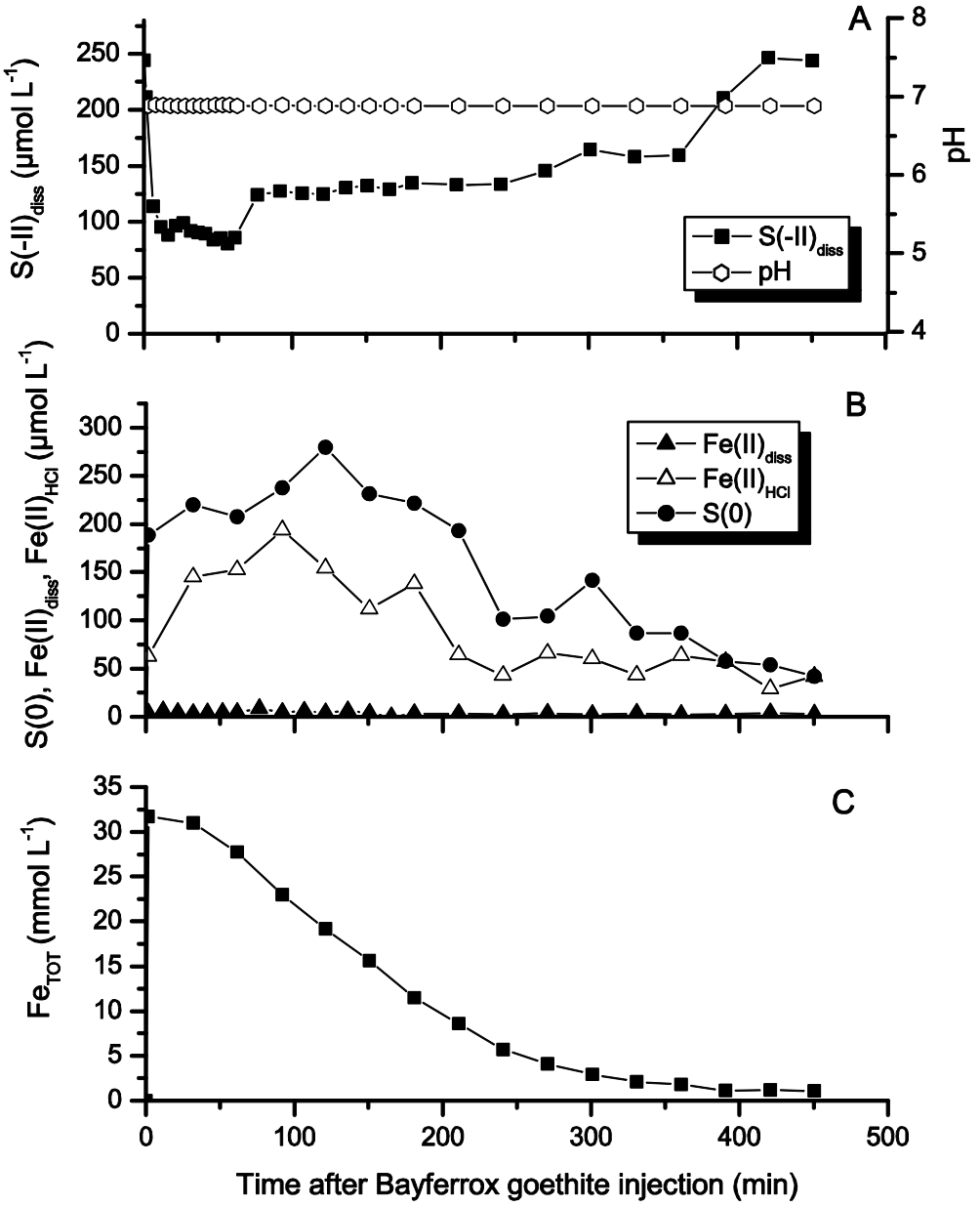

Fig. S 9. Bayferrox Goethite, pH 7 (Run 9)

Table S 1. Ratios of $\Delta Fe(II)_{tot}$:$\Delta S(0)$ for all minerals for each point of time during the reaction of ferric (hydr)oxides and dissolved sulphide at pH 4.

	$\Delta Fe(II)_{tot}$:$\Delta S(0)$						
Time	**Ferrihydrite**	**Lepidocrocite**	**Goethite**		**Bayferrox Lepidocrocite**		**Bayferrox Goethite**
(min)	**Run 16**	**Run 18**	**Run 10**	**Run 11**	**Run 20**	**Run 21**	**Run 19**
1	3	0.4	0.4	0.2	2.6	13	
15	2.4	2.2				1	0.4
30	5.2	2.2	0.7	1.2	8	1.7	0.7
45	2.2	2.2			5.6	1.5	0.8
60	1.5	2	0.6	1	3	1.4	0.4
75			0.5				
90				0.7			
105	1.9	1.8	0.3		2	1	0.6
120		1.4		0.6			
135	1.4	1.4	0.3		1.8	1.2	0.3
150				0.7			
165	1.4	3	0.3		2.6	1.3	0.4
180			0.2	0.7			
195		1.7			2.4	0.9	0.5
210	1.3		0.2	0.7			
225		1.4			2.1	2.1	0.4
240	1.6		0.1	0.6			
255		1.8			2.7	1.1	0.2
270	1.8		0.1	0.6			
285		1.9			1.6	0.5	0.4
300	1.6		0.1	0.8			
315		1.8			2.6	0.6	0.3
330	2.1		0.1	0.6			
345		2.3			4	0.6	0.2
360	1.4		0.1	0.8			
375		1.5			1.2	1.2	
390	1.7		0.1	0.7			
405		1.4			1.8	0.4	0.4
420	1.8		0.1	0.7			
435		1.5			1.2	2	0.3

Table S 2. Ratios of $\Delta Fe(II)_{tot}$:$\Delta S(0)$ for all minerals for each point of time during the reaction of ferric (hydr)oxides and dissolved sulphide at pH 7. Fe(II) consisted of the sum of dissolved Fe(II) and acid extractable Fe(II).

	$\Delta Fe(II)_{tot}$:$\Delta S(0)$										
Time	**Ferrihydrite**		**Lepidocrocite**		**Goethite**		**Bayferrox Lepidocrocite**		**Bayferrox Goethite**		
(min)	**Run 4**	**Run 7**	**Run 3**	**Run 6**	**Run 2**	**Run 8**	**Run 22**	**Run 23**	**Run 1**	**Run 5**	**Run 9**
1	1.9	1.6	2.9	1.6		0.8	3.2	4.3		0.7	0.4
5					1.2				0.5		
30	1.9	2.1	2.3	1.3	1	0.8	2.8	1.9	0.5	1.2	0.7
60	1.9	1.3	1.6	1.1	0.9	0.7	2.7	1.9	0.4	0.7	0.8
90	1.6		1.8		0.6	0.5		1.7	0.3	0.5	0.8
105							3.3	1.3			
120	1.6		1.5			0.4			0.3	0.4	0.6
135		1.4		1			1.7	2			
150	1.5	1	1.3	0.8	0.6	0.4				0.4	0.5
165		1		0.8			1.9				
180	1		1.2	0.6	0.5	0.4			0.2		0.6
195							1.4	1.2		0.4	
210	1.2	0.8	1	0.4	0.5	0.3			0.2		0.4
225							1.6	1.5		0.3	
240	1.2	0.7	0.8	0.6		0.3			0.2		0.5
255							1.5	1.1		0.4	
270		0.6	1.1	0.3		0.4			0.2		0.7
285							1.4	0.9		0.3	
300	1.2	0.6	0.5	0.3	0.4	0.3			0.2		0.4
315							1.4	1.1		0.4	
330	0.9	0.5	0.3	0.3	0.3	0.3			0.2		0.5
345							1.6	1		0.3	
360	0.8	0.5	0.3		0.4	0.4			0.1		0.8
375							2.6	0.8		0.2	
390	0.8	0.5	0.2	0.3	0.3	0.5			0.1		1
405							0.9	1.1		0.3	
420	0.8	0.5		0.3	0.3	0.3					0.6
435							0.9	0.8		0.2	
450		0.4		0.3	0.3	0.3					1.1
465										0.2	

The intrinsic rate constant

The intrinsic rate coefficient was calculated for each Fe(III) oxide by using eq. 13b. The fraction of reactive surface sites $\beta_{FeOH,ox}$ was simulated by PHREEQC and by $\{FeOH\}_{tot}$ and pK_a values at pH 4 and 7. Table S 3 shows the values for the calculation of $\beta_{FeOH,ox}$.
$\{FeOH\}_{tot}$ can be written as

$$\{FeOH\}_{tot} = S_{tot}\, A_s\, c(FeOOH) \qquad (14)$$

where S_{tot} is the site density ($3.75*10^{-6}$ mol m^{-2}), A_s is the specific surface area ($m^2\ g^{-1}$) and *c(FeOOH)* is the concentration of the oxide ($g\ L^{-1}$). The values of $\{FeOH\}_{tot}$ for each mineral at the given pH are listed in Table S 3.

The pK_{a1} and pK_{a2} values were calculated by using PHREEQC according the following equation

$$pK_{a1}; pK_{a2}(\text{oxide}) = pH_{pzc}(\text{oxide}) \pm \left(\frac{1}{2}(pK_{a2}(\text{PHREEQC}) - pK_{a1}(\text{PHREEQC})\right) \qquad (15)$$

$$= pH_{pzc} \pm 0.82$$

The simulated pKa values for each Fe(III) mineral are listed in Table S 3.

Table S 3. Used values for the estimation of $\beta_{FeOH,ox}$. The pK_a values were also estimated by using PHREEQC and eq. 15.

	Synthesized oxides			Commercial oxides (Bayferrox)	
	Ferrihydrite	**Lepidocrocite**	**Goethite**	**Lepidocrocite**	**Goethite**
specific surface area (multi point BET-N_2) ($m^2\ g^{-1}$)	140	169.9	27.02	17.34	9.12
pH_{pzc}	7.1	6.85	7.4	6.85	7.5
pK_{a1}	6.28	6.03	6.58	6.03	6.68
pK_{a2}	7.92	7.67	8.22	7.67	8.32
$\beta_{FeOH,ox}$ pH 4	0.717	0.734	0.689	0.734	0.676
$\beta_{FeOH,ox}$ pH 7	0.768	0.768	0.767	0.768	0.767
$\{FeOH\}_{tot}$ (mol L^{-1})	$9.61*10^{-5}$	$9.56*10^{-5}$	$7.8*10^{-5}$	$7.8*10^{-5}$	$8.89*10^{-5}$
mass ($g\ L^{-1}$)	0.18	0.15	0.77	1.2	2.6

Table S 4 shows the calculated k_{intr} values.

Table S 4. Used values for Fig. 4.5.

Oxide	Run no.	pH	k_{intr} (min^{-1})	log k_{intr} (min^{-1})	ΔG° (kJ mol^{-1})
Ferrihydrite	14	4	6.77E-06	-5.11	-156.75
Ferrihydrite	16	4	1.93E-05	-4.73	-156.75
Lepidocrocite	15	4	3.00E-06	-5.53	-143.5
Lepidocrocite	18	4	5.18E-06	-5.26	-143.5
Goethite	10	4	3.81E-06	-5.44	-121.4
Goethite	11	4	3.38E-06	-5.42	-121.4
Goethite	12	4	1.39E-05	-5.81	-121.4
Goethite	13	4	4.47E-06	-5.29	-121.4
Bayferrox Lepidocrocite	20	4	7.79E-07	-5.78	-120.23
Bayferrox Lepidocrocite	21	4	1.91E-07	-6.12	-120.23
Bayferrox Goethite	17	4	1.59E-06	-6.23	-116.79
Bayferrox Goethite	19	4	8.89E-07	-5.67	-116.79
Ferrihydrite	4	7	7.16E-04	-3.19	-106.5
Ferrihydrite	7	7	1.42E-04	-4.46	-106.5
Lepidocrocite	3	7	1.70E-04	-3.81	-93.49
Lepidocrocite	6	7	5.09E-04	-3.43	-93.49
Goethite	2	7	8.60E-06	-5.07	-71.22
Goethite	8	7	9.38E-06	-5.05	-71.22
Bayferrox Lepidocrocite	22	7	4.41E-05	-4.39	-71.77
Bayferrox Lepidocrocite	23	7	4.34E-05	-4.39	-71.77
Bayferrox Goethite	1	7	3.69E-05	-4.86	-69.5
Bayferrox Goethite	5	7	5.36E-06	-5.27	-69.5
Bayferrox Goethite	9	7	3.88E-06	-5.42	-69.5

5. Conclusion

The primary goal of this study was to establish a generalized kinetic model for the abiotic anaerobic H_2S oxidation by ferric (hydr)oxides in the pH range of 4 to 7. In particular the main objectives were (i) the determination of the reaction rate coefficients of various ferric (hydr)oxides towards dissolved sulphide with regard to different pH and their influencing factors, (ii) identify the processes occurring at the ferric (hydr)oxide surfaces by chemical analysis, spectroscopy and microscopy measurements, (iii) elucidate the role and dynamics of Fe^{2+} and its various species, and (vi) improve our understanding of the pathway of pyrite formation.

Batch experiments with various ferric minerals and dissolved sulphide suggested that the reaction progress was highly dynamic and occurs at different reaction rates with pyrite as the final product. On the basis of wet chemistry the reaction of Fe(III) oxides with dissolved sulphide could be divided into three phases: (i) dissolved sulphide was rapidly consumed and S(0) and acid extractable Fe(II) were generated, (ii) a continuous but slower formation of S(0) and acid extractable Fe(II), and (iii) decrease of acid extractable Fe(II) and S(0) due to the formation of pyrite. The reactivity of the used Fe(III) oxides decreased in the order of ferrihydrite ~ lepidocrocite > goethite whereby dissolved sulphide was consumed within the first 15 minutes in the experimental solution of ferrihydrite and lepidocrocite. Goethite requires more than 5 hours to consume dissolved sulphide completely.

It could be shown that FeS was formed at the oxide surfaces in the first phase of reaction. In the case of lepidocrocite and goethite the FeS consisted of mackinawite while only amorphous FeS was formed in the experimental solution of ferrihydrite. TEM measurements revealed also an interfacial magnetite layer between mackinawite and lepidocrocite. The magnetite layer can be seen as an intermediate stage linking two reactions, the formation of mackinawite which reduces ferric iron at the lepidocrocite surface on one hand and the transport of electrons in the deeper regions of the lepidocrocite bulk crystal on the other hand. The electrons appeared to be transferred between lepidocrocite and mackinawite through magnetite as an interfacial layer acting as an “electron shuttle”. With proceeding reaction, TEM measurements indicated that mackinawite completely dissolved from the surface of lepidocrocite while the precipitation of pyrite occurred separated from the lepidocrocite surface, as well as, for the other minerals. The pyrite formation is coupled to mackinawite

dissolution and probably accompanied by the formation of FeS clusters and polysulphides that serve as precursors. Although, the pyrite formation may also occurred via a reaction of FeS with dissolved Fe^{2+}. The exact pathway of the pyrite formation in this study could not be clarified. Concluding, the kinetics of precursor formation from reductive dissolution of ferric (hydr)oxides by hydrogen sulfide and the subsequently pyrite formation are kinetically decoupled.

This study has also demonstrated that the amount of excess-Fe(II) differed for each mineral which depends on their electron transfer properties and on their ability to accommodate Fe(II) within the structure. The production of excess-Fe(II) was more facilitated for ferrihydrite and lepidocrocite due to their higher specific surface area compared to goethite. When dissolved sulphide was completely consumed, the system evolution and the type and concentrations of secondary minerals being formed dependent on the amount of excess-Fe(II) and on the reactivity of the remaining Fe(III) (hydr)oxide phase. This means, that the lower solubility of goethite and lepidocrocite relative to ferrihydrite resulted in lower aqueous Fe(III) and aqueous Fe(II) concentration. Thus, we observed for both minerals only the pyrite formation, for lepidocrocite the magnetite formation as well and the host minerals remained. Only small amounts of goethite were transformed to hematite. Within 2 weeks, ferrihydrite was transformed completely via dissolution-precipitation processes into new and more stable phases such as hematite, magnetite, and pyrite.

The geochemical reaction sequences of the processes for the different ferric (hydr)oxides occurred at different reaction kinetics based on different sulphide sources (dissolved S(-II), FeS). The extent of transformation depends on the current ferric (hydr)oxide and the production of excess-Fe(II). Furthermore, the presence of excess-Fe(II) seems to stimulate pyrite formation.

The mechanisms for the reductive dissolution of ferric (hydr)oxides towards dissolved sulphide have been studied in detail (Canfield et al., 1992; Dos Santos Afonso and Stumm, 1992; Peiffer et al. 1992; Peiffer and Gade, 2007; Poulton et al., 2004; Pyzik and Sommer, 1981; Yao and Millero, 1996). These studies were carried out as batch experiments and determined an initial rate for the reaction, while the surface properties of Fe(III) oxides were considered constant. Contrary, in the current study a flow-through reactor was developed in which initial conditions at every point in time and the reaction coefficients k_{obs} are determined by the decrease of the surface area in the reactor.

The experiments showed that the mineral reactivity decreased in the sequence ferrihydrite > lepidocrocite > goethite following a second order rate law. k_{obs} for the oxidation of sulphide (k_{obs_H2S}) and the formation of Fe(II) ($k_{obs\_Fe(II)}$) increased with pH and specific surface area and it seems, that minerals with a lower crystal degree and a higher surface area are more reactive than minerals with a higher crystal degree. Furthermore, it could be shown, that there is a relationship between k_{intr} for the oxidation of sulphide and free energy of the Fe(III) solid phase.

The flow-through experiments validate the results of the batch experiments and showed also the decoupled formation of Fe(II) and S(0) during the reaction. This decoupling can be explained by the surface complexation model. That is, first the adsorption of dissolved sulphide to the Fe(III) (hydr)oxide surfaces which resulted in the formation of Fe(II) and S(-I). At circumneutral pH, Fe(II) remained at the surface while S(-I) is released into solution. In the presence of ferrihydrite and lepidocrocite, the Fe(II) interact with the structural Fe(III) which lead to an electron transfer between them. The new Fe(III) surface is then available to oxidize another S(-II) or S(-I) ion. Due to this incorporation of Fe(II) into the bulk crystal, Fe(II) is formed in excess. Results suggested, that Fe(II) accelerate the reductive dissolution of ferrihydrite and lepidocrocite by dissolved sulphide. Although, goethite behaved differently; the adsorption of Fe(II) occurred without an electron transfer. Fe(II) seems to be inhibiting the reactivity of goethite.

The Fe(II) which is either associated with the oxide surface or incorporated into the bulk crystal may affect the redox potential of the reaction suspension, which in turn, affects the semiconducting properties of Fe(III) oxides and thus, their reactivity. Hence, the reactivity depends on different lattice stabilities of the Fe(III) solid phases and on the dynamics of Fe(II). Thus, the formed Fe(II) and its further reaction to FeS or its interaction with the oxide surface control the reaction of ferric (hydr)oxides and dissolved sulphide.

However, these results are a major simplification compared to what happens in a natural environment, where often a significant part of the iron oxide present is reduced (Larsen and Postma, 2001; Postma, 1993). In natural sediments, the most reactive ferric (hydr)oxides will be removed resulting in changes in the mineralogy and the particle size distribution of the remaining pool of ferric (hydr)oxides. Furthermore, the reactivity of ferric (hydr)oxide reduction will decrease, and is in natural environments affected by intrinsic reactivity, the effectiveness of the reducing agent, and by microbial catalysis (Postma, 1993). Thus, experiments with natural sediments consisting of various ferric (hydr)oxides are important, as

well as, experiments with ferric (hydr)oxides in the absence and presence of iron reducing bacteria. As such, understanding the factors influencing the reductive dissolution of ferric (hydr)oxides by dissolved sulphide provides a framework for further flow-through experiments to predict the reductive dissolution of ferric (hydr)oxides in natural systems and to establish a generalized kinetic model. Furthermore, secondary mineralization pathways in sulphide-rich systems are complex and involve an interplay between a number of geochemical factors and competing Fe(II)-induced mineralization pathways. Therefore further investigations on the reaction of ferric (hydr)oxides and dissolved sulphide are necessary; e.g. the influence of organic matter should be further investigated. Furthermore, research is required to identify the mineral specific variation in reactivities also in quantitative terms such as the Fe^{2+} variations of Fe(III) oxides.

The current work provides an improved understanding of the possible reaction pathways of ferric (hydr)oxides in sulphide-rich systems involved the interaction of Fe(II) with the oxide surface and with dissolved sulphide. The study imply, that in aqueous systems enriched with iron and periodically formation of sulfide (e.g. movement of the capillary fringe in ground waters, inundation of coastal plains), ferric hydroxides may undergo “charging” with reduced substances that may lead to pyrite (and magnetite) formation, even in the absence of dissolved sulfide. Furthermore, the understanding of pyrite formation kinetics in these environments under these conditions is related to the nature of FeS clusters species, their transformation into precursor substances for pyrite precipitation, and their physical behaviour in terms of aqueous solubility and diffusivity. Also the dynamics and nature of Fe^{2+} species are related to the pyrite formation and contribute to the understanding of kinetics of pyrite formation.
As illustrated in the introduction, ferric (hydr)oxides can adsorb potential contaminants such as arsenic, phosphate, uranium, removing them from the hydrosphere and biosphere. As such, knowledge of the stability of ferric (hydr)oxides are important for containing these contaminants. For example, the reaction sequences in the batch experiments have implications for the retention of toxic metals by adsorption on nanocrystalline mackinawite. These toxic metals may get mobilized by further reaction to pyrite.

5.1. References

Canfield D. E., Raiswell R. and Bottrell S., 1992. The reactivity of sedimentary iron minerals toward sulphide. *American Journal of Science*, **292**: 659-683.

Dos Santos Afonso, M. and Stumm, W., 1992. Reductive Dissolution of iron(III) (hydr)oxides by hydrogen sulfide. *Langmuir*, **8**: 1671-1675.

Larsen, O. and Postma, D., 2001. Kinetics of reductive bulk dissolution of lepidocrocite, ferrihydrite, and goethite. *Geochimica Et Cosmochimica Acta*, **65(9)**: 1367-1379.

Peiffer, S., Dos Santos Afonso, M., Wehrli, B. and Gächter, R., 1992. Kinetics and mechanism of the reaction of H_2S with lepidocrocite. *Environ. Sci. Technol.*, **26(12)**: 2408-2413.

Peiffer, S. and Gade, W., 2007. Reactivity of ferric oxides toward H_2S at low pH *Environ. Sci. Technol.*, **41**: 3159-3164.

Postma, D., 1993. The Reactivity of Iron-Oxides in Sediments - a Kinetic Approach. *Geochimica Et Cosmochimica Acta*, **57(21-22)**: 5027-5034.

Poulton S. W., Krom D. M. and Raiswell R., 2004. A revised scheme for the reactivity of iron (oxyhydr)oxide minerals towards dissolved sulfide. *Geochim. Cosmochim. Acta*, **68(18)**: 3703-3715.

Pyzik, A.J. and Sommer, S.E., 1981. Sedimentary iron monosulphides: kinetics and mechanism of formation. *Geochim. Cosmochim. Acta*, **45**: 687-698.

Yao, W. and Millero, F.J., 1996. Oxidation of hydrogen sulfide by hydrous Fe(III) oxides in seawater. *Mar. Chem.*, **52**: 1-16.

Contribution to the different studies

Study 1

Pathways of ferrous iron mineral formation upon sulfidation of lepidocrocite surfaces

K. Hellige	55 %	Laboratory work, Manuscript preparation
K. Pollok	15 %	TEM analysis, Discussion of results
P. Larese-Casanova	5 %	Mössbauer spectroscopy analysis, Discussion of results
T. Behrends	5 %	Concept, Discussion of results, Manuscript preparation
S. Peiffer	20 %	Concept, Discussion of results, Manuscript preparation

Study 2

The influence of structural properties of ferric hydroxides 6-line ferrihydrite, lepidocrocite, and goethite on reaction pathways with sulphide

K. Hellige	55 %	Laboratory work, Manuscript preparation
K. Pollok	15 %	TEM analysis, Discussion of results
P. Larese-Casanova	5 %	Mössbauer spectroscopy analysis, Discussion of results
T. Behrends	10 %	Concept, Discussion of results, Manuscript preparation
S. Peiffer	15 %	Concept, Discussion of results, Manuscript preparation

Study 3

Intrinsic rate constants for the abiotic oxidation of sulfide by various ferric hydroxides

K. Hellige	85 %	Laboratory work, Manuscript preparation
S. Peiffer	15 %	Concept, Discussion of results, Manuscript preparation

The studies are based on each other. Hence, study 2 will be submitted when the first study is accepted and the third study will be submitted when the first ones are accepted.

Erklärung

Hiermit erkläre ich, dass ich diese Arbeit selbstständig verfasst und keine anderen als die angegebenen Quellen und Hilfsmittel verwendet habe. Ich erkläre ferner, dass ich an keiner anderen Hochschule als der Universität Bayreuth ein Promotionsverfahren begonnen und diese oder eine gleichartige Doktorprüfung endgültig nicht bestanden habe.

Bayreuth, 15. Dezember 2010

Danksagung

Ich möchte mich bei allen herzlich bedanken, die mich während meiner Doktorandenzeit unterstützt haben und auf die eine oder andere Art am Entstehen dieser Arbeit beteiligt waren. Besonderen Dank gilt dabei:

Stefan Peiffer, für die Vergabe des Themas, die Unterstützung, die Diskussionen und für die vielen Korrekturen.
Thilo Behrends, für das große Interesse an Eisen und Schwefel und für die Unterstützung über all die Jahre trotz der Entfernung. Danke auch für die herzliche Aufnahme in Utrecht und Grenoble.

Kilian Pollok und Philip Larese-Casanova, für die Unterstützung der TEM bzw. Mössbauer Spektroskopie Messungen, der Interpretation der Daten, der Korrekturen und der regen Diskussion.

Danke auch an alle Mitarbeiter der Forschergruppe, für die netten Treffen an schönen Orten, den gemeinsamen Abenden, Konferenzen, Diskussionen etc.:
Stefan Haderlein, Andreas Kappler, Hans Richnow, Rainer Meckenstock, Christian Zwiener, Anke Schmidt für die Synthese und Charakterisierung der Fe-Oxide und der guten Zusammenarbeit, Iris Bauer, Stefan Feisthauer, Carsten Jobelius, Rita Kleemann.

Jutta Eckert, für die Unterstützung der Durchflussexperimente, die tollen Tipps, fürs S° messen, das Anschalten der Durchflussexperimente um sechs Uhr früh- danke. Martina Rohr, für die nette Zeit im Labor, das Benutzen des Abzugs und für die Unterstützung bei der Bestimmung der Ladungsnullpunkte der Eisenminerale. Heidi Zier und Martina Heider, für die Synthese der Fe-Oxide. Danke für die gute Zusammenarbeit und das Drumherum.

Martin Back- danke für die schöne Laborzeit und noch schönere Zeit neben dem Labor und für die herzliche Aufnahme in der Hydro am Anfang meiner Bayreuth-Zeit. Sabine Thüns, für die schöne Bürozeit (auch wenn wir einen schlechten Start hatten- am Ende ist’s immer schön!), für viele offene Ohren, für das gemeinsame Klettern und zu guter Letzt das (ausschweifende) abendliche Programm. Auch bedanke ich mich bei Svenja Bartsch und Uwe Kunkel für die schöne Bürozeit, die Unterstützung bei Vorträgen, der „PC-Hilfe“ etc. Uwe,

natürlich auch für das sportliche Rahmenprogramm, das Abendprogramm etc. Sven Frei, für die sportlichen Aktivitäten wie Klettern und Joggen etc. neben dem Laboralltag. Chris Shope, thanks for your valuable comments on an earlier version of the manuscript.
Auch allen anderen Hydros danke für die schöne Zeit im und neben dem Labor.

Meiner „Zweitfamilie“ den Fleckis- Sophie, Lina, Anke und Jan danke für die schönen, lustigen Stunden bei Euch und mit Euch und für Euer Vertrauen.
Dem größten Dank gilt meinen Eltern und meinem Opa für Ihre Unterstützung, das Vertrauen, die Hilfe und den Glauben über all die Jahre an mich.